The use of a novel alpha-synuclein binding aptamer in models of Parkinson's disease.

Katelyn Victoria Ventura

A thesis submitted to the Department of Neuroscience in partial fulfillment of the requirements for completion of the degree:
Doctor of Philosophy
in
Neuroscience

Carleton University
Ottawa, Ontario

Acknowledgements

The alpha-synuclein binding aptamer as well as the delivery vehicle in this research has been included in a Canadian & US patent (CA2018/051335 & US-2020-0325476-A1). The preparation, synthesis, and constitution were completed by our collaborators, Dr. Maria DeRosa and her team, which comprised Dr. Erin McConnell, PhD, Joshua Callaghan, MSc; Veron Hunt, MSc; Spencer Boisjoli, MSc; Dr. Anna Koudrina, PhD; Dr. Evan Monk, PhD. It is because of her team's participation and assistance with the synthesis that any of these experiments could be conducted.

I would like to thank my family, friends, members of the Department, and all of the colleagues I have had the pleasure of working with over the years. Without each and every one of you, I would not have had the emotional support, guidance, and/or expertise needed to complete this degree. I am also indebted to Dr. Hymie Anisman for his support and encouragement. Importantly, I would like to thank my supervisor, Dr. Matthew Holahan. Matt I am extremely grateful for your patience and support throughout the past decade, thank you.

This research was supported by grants from the Michael J Fox Foundation 9924 & 9924.01 and CIHR 162084 to Dr. Matthew Holahan and Dr. Maria DeRosa.

Dedication

I've heard my parents try to explain my dissertation to the rest of my family…..
I now understand why hearsay is not permissible in court

This is to you, mom and dad.
I'll explain my thesis once more when I'm home.

Table of Contents

Table of Figures

Table of Tables

List of Abbreviations:

0.2% Triton-X 0.01M phosphate buffered saline (PBS-TX)
1-methyl-4-phenyl-1,2,3,6-tetrahyropyridine (MPTP)
3,3'-Diaminobenzidine (DAB)
6-hydroxydopamine (6-OHDA)
Alpha-synuclein (asyn)
Analysis of Variance (ANOVA)
Animal Free Blocker (AFB)
Avidin-biotinylated complex (ABC)
Base of support (BOS)
Blood brain barrier (BBB)
Bovina Serum Albumin (BSA)
Brain derived neurotrophic factor (BDNF)
Catechol-O-methyltransferase (COMT)
Cerebrospinal fluid (CSF)
Central nervous system (CNS)
Dementia with Lewy bodies (DLB)
Dissociation constant (K_D)
Dopamine (DA)
Dopamine transporter (DAT)
Dulbecco's Modified Eagle's Medium Formulation (DMEM)
Enriched green fluorescent protein (eGFP)
Fetal Bovine Serum (FBS)
Flurodopa (F-dopa)
Gastrointestinal (GI)
Genomic DNA (gDNA)
Globus pallidus interna (GPi)
Globus pallidus externa (GPe)
International Business Machines (IBM)
Intraperitoneal (i.p.)
Irritable bowel-syndrome (IBS)
Leuchine-rich repeat kinase 2 (LRRK2)
Levodopa (l-DOPA)
Lewy bodies (LB)
Lewy body diseases (LBDs)
Lewy neurites (LN)
Medium spiny neuron (MSN)
Micro-brightfield (MBF)
Monoamine oxidase (MAO)
Movement disorder society (MDS)
Multiple system atrophy (MSA)
Multiplicity of Infection (MOI)
Non-amyloid-beta component (NAC)
Paraformaldehyde (PFA)
Parkinson's disease (PD)

Parkinson's disease with dementia (PDD)
Phosphate Buffered Saline (PBS)
Phosphate Buffered Solution (PB)
Phosphorylated alpha-synuclein (pAsyn)
Poly-D-Lysine (PDL)
Positron emission tomography (PET)
Quantification Cycle (Cq)
Quantitative polymerase chain reaction (qPCR)
Real time polymerase chain reaction (RT-PCR)
Relative Transgene expression (ΔCq)
REM sleep behaviour disorder (RBD)
Retinoic acid (RA)
Rotations per minute (RPM)
Single photon emission computed tomography (SPECT)
Soluble N-ethylmaleimide sensitive fusion attachment proteins (SNAP)
Soluble N-ethylmaleimide sensitive fusion attachment proteins to receptor (SNARE)
Standard error of the means (SEM)
Substantia nigra (SNc)
Substantia nigra pars compacta (SNpc)
Substantia nigra pars reticulata (SNpr)
Subthalamic nucleus (STN)
Systematic evolution of ligands by exponential enrichment (SELEX)
Transcranial sonography (TCS)
Transferrin receptor aptamer (TRA)
Transgenic (Tg)
Tris buffered saline (TBS)
United Kingdom Parkinson's disease society Brain Bank (UKPDSBB)
Unified Parkinson's Disease rating scale (UPDRS)
Vascular endothelial growth factor (VEGF)
Wild type (WT)

Abstract:

Parkinson's disease (PD) is characterized by a range of motor and non-motor behavioral deficits thought to occur because of the loss of dopaminergic neurons in the substantia nigra (SNc). It has been thought that the appearance of the disorder stems from elevated alpha-synuclein (asyn) protein expression, known to form Lewy body inclusions. The overarching theme of the current series of experiments comprised the evaluation of how increased asyn expression contributes to the development of PD, and whether these actions could be attenuated by a DNA sequence designed to inhibit asyn oligomer formation (i.e., an asyn binding aptamer). A better understanding of asyn protein accumulation and toxic aggregate formation might provide a therapeutic avenue with considerable clinical relevance, especially if tolerance does not develop to the effects of the treatment as it does with other therapeutic approaches. As such, we assessed a novel asyn binding aptamer within both *in vitro* and *in vivo* models of Parkinson's disease. *In vitro*, a single treatment with the asyn binding aptamer reduced levels of pAsyn, but multiple treatments unexpectedly had less noteworthy effects. Accordingly, the influence of the asyn aptamer was assessed in mice *in vivo*. It was demonstrated that the asyn aptamer could be detected in several brain regions and in the liver at various times following its administration. Ordinarily, in transgenic mice overexpressing the human A53T variant of asyn protein, the elevated expression of asyn protein occurs at about 5 months of age. Thus, transgenic mice of this age were treated with the asyn binding aptamer both acutely and repeatedly to detect asyn protein level changes. The aptamer reduced pAsyn levels compared to control wildtype animals. Indeed, Western blot analyses revealed that this was evident with respect to pAsyn and oligomer asyn in

response to both acute and repeated treatment conditions. These reductions in asyn conformations were evident in the more exterior and interior regions of the brain. Overall, the data have important preliminary implications for the development of asyn binding aptamer treatment strategies that target asyn processes in PD. To be sure, the asyn aptamer needs to be assessed further in other preclinically relevant models to determine the validity of the approach to halt or slow the progression of the disease.

Chapter 1:
General Introduction

Introduction

Parkinson's Disease

Parkinson's disease (PD) is the second most common neurodegenerative disorder affecting approximately 1.2% of people above the age of 40 and 4% of people over the age of 80 [1–5]. It is expected that this number will more than double, reaching 14.2 million in 2040 as a direct result of the ageing population [4,6]. PD is characterized by numerous symptoms, which include resting tremor, bradykinesia, rigidity, postural instability, and stooped posture, as well as non-motor features, such as cognitive and behavioural symptoms, sleep disorders, autonomic dysfunction, sensory dysfunction, and fatigue [7–9]. In recent years, new treatments addressing the motor and non-motor symptoms have been developed; however, no therapeutic currently available can slow the progression of the disease [8,10].

Parkinson first described Parkinson's syndrome in his Essay on the Shaking Palsy (1817), where he discussed the classic clinical features of neurodegenerative disorders [11]. However, it was the discovery of dopamine in the mammalian nervous brain and the subsequent dopamine neuronal loss within the substantia nigra pars compacta (SNpc) that fueled the understanding of this disorder [12]. The understanding that neurons in the SNpc formed the nigrostriatal pathway led to the discovery that replenishment of striatal dopamine through oral administration of the dopamine precursor L-3,4-dihydroxyphenylalanine (levodopa, l-DOPA) alleviates most of these motor symptoms [11].

Features of PD

Non-motor symptoms

Several non-motor symptoms are associated with Parkinson's disease, many of which arise before clinical diagnosis, perhaps being present ten years earlier. These non-motor symptoms comprise gastrointestinal dysfunction, constipation, hyposomia, and sleep disorders [13]. Gastrointestinal (GI) dysfunction involves almost all levels of GI system and may actually contribute to the development of motor and non-motor impairments [14]. The related constipation is characterized by colonic and anorectal symptoms, which may be related to lifestyle factors, particulary reduced fluid intake. Olfactory deficits are also prevalent amongst PD patients, with more than 90% reporting these symptoms [15]. Interestingly, the olfactory disturbances have been less commonly linked to familial PD, although they appear to be benign in familial cases linked to Leucine rich repeat kinase 2 (LRRK2) or parkin mutations and far more damaging in sporadic PD cases [16].

Sleep disorders, such as sleep fragmentation, REM sleep Behaviour Disorder (RBD), and complex paroxysmal nocturnal motor behavioural disorders, are also common in PD [13,17]. REM sleep behaviour disorders comprise individuals' acting out their dreams and display violent limb movements while fully asleep. The neurological reasons for this link are uncertain, although the affected nuclei in the brainstem are thought to play key roles in the development of this non-motor feature [16].

Motor Symptoms

A constellation of motor symptoms characterizes Parkinson's disease. As mentioned earlier, these comprise resting tremor, rigidity, postural instability, and

bradykinesia. The bradykinesia, which refers to slowness of movement, is the most common clinical feature of Parkinson's disease [18]. In general, it is a hallmark feature of basal ganglia disorders that involve difficulties with planning, initiating, and executing movement, as well as with performing sequential tasks [18]. The initial manifestation of bradykinesia consists of slowness in performing daily activities, slow movement, and lengthier reaction times [18]. Rigidity has also been associated with movement disorders and disturbances in the basal ganglia presenting as stiffness and difficulties in coordinating smooth movements. One of the most widely known motor symptoms linked to PD is a resting tremor [19]. Parkinson's disease patients often exhibit a 4-6 Hz resting tremor on one side of the body that typically manifests as a repetitive back-and-forth movement of any limb, or the jaw, head, or trunk, which occurs when that part of the body is not intentionally moving [19,20]. Together, these motor symptoms have been linked to circuit dysfunction of the direct and indirect nigro-striatal pathways.

Analysis of PD has most often focused on the degeneration of neurons within the SNpc. It is typically thought that neurodegeneration in PD originates in the synaptic terminals within the striatum and then progresses along the nigrostriatal pathway, ultimately affecting homeostasis and survival of dopamine (DA) cells [21]. In addition, there is ample reason to believe that multiple brain regions contribute to the symptomatology of the disorder. During the preclinical phase, which precedes degenerative loss, the expression levels of a range of proteins involved in synaptic transmission are altered in the prefrontal and cingulate cortex, which likely contribute to the non-motor symptoms presented [21].

Diagnosing PD

Diagnosis of the disease is challenging due to the similarities with other motor diseases involving the basal ganglia. Indeed, PD cannot be entirely determined until post-mortem assessment, when the disease can be confirmed through an autopsy [22]. As PD is a progressive neurodegenerative disorder, it often involves multiple follow-up sessions to track and monitor the course of the disease to be assured that symptoms are not attributable to other illnesses [22]. As mentioned earlier, several motor and non-motor symptoms progress and develop as the disease worsens. The original clinical guidelines for diagnosing PD were implemented by Gibb and Lees (1988) with the United Kingdom PD Society Brain Bank and Gelb's criteria (UKPDSBB) [23]. This method entails a 3-step process. First, a clinician determines the presence of bradykinesia based on the level of muscle rigidity, resting tremors (4-6 Hz), and postural instability [23,24]. Next, possible explanations for Parkinsonian symptoms are evaluated, including familial and medical histories of the patient while also monitoring for the presence of new symptoms, such as oculogyric crises, supranuclear gaze palsy, or cerebellar signs related to balance [23]. Other indices comprising autonomic dysfunction, severe dementia, memory, and language disturbances, amongst other symptoms, are also evaluated [23]. Finally, an assessment is made to determine ‘supportive prospective positive criteria’ for PD whereby three or more of the following symptoms are present. These comprise unilateral onset, presence of resting tremor, progressive disorder, persistent asymmetry affecting the side of onset, and a positive response to l-DOPA [23]. One of the significant limitations of these original UKPDSBB diagnostic criteria was that they focus on the key

motor features of PD, such as bradykinesia and slow movement, and largely disregard the non-motor characteristics [24].

As an alternative to the UKPDSBB, the Movement Disorder Society (MDS) - Unified Parkinson's Disease Rating Scale (UPDRS) was introduced for use in clinical evaluations [24,25]. Since its introduction, this tool has been modified and adapted repeatedly but remains the major diagnostic instrument used by physicians. This approach has evolved to incorporate non-motor symptom manifestations, which is critical given that these features may arise years before the presentation of motor symptoms [24,25].

The UPDRS is separated into 4 parts that consider 65 items each ranked on a 0-4 scale (where 0 = normal, 1 = slight, 2 = mild, 3 = moderate, 4 = severe) [25]. Part I focuses on assessing non-motor symptoms, such as sleep disturbances, constipation, urinary problems, and cognitive impairment [25]. Part 2 assesses the motor disturbances based on how much they interfere with daily functions, whereas Part 3 involves the physician assessing motor impairments. Finally, Part 4 assesses dyskinesia, including the presence, duration, and ON/OFF fluctuations [25]. This tool also respects the assumption that the pathological process of PD may begin in non-dopaminergic structures of the brain and periphery, giving rise to the prodromal PD phase that represents the true initial stage of PD [24]. In essence, this diagnostic tool acknowledged the major shift in our understanding of PD, in which non-motor symptoms often predominate during the initial phase of PD. The assessment and monitoring of these non-motor manifestations could be key markers in identifying the prodromal/preclinical PD window.

As indicated earlier, it is typically thought that the manifestation of PD stems from the loss of dopaminergic neurons in the SNpc, leading to a loss of dopamine terminals but not degeneration in the striatum [11,26]. Imaging studies confirmed that 60% of these dopamine neurons degenerate and approximately 80% of dopamine depletion is required prior to the presentation of frank Parkinsonian motor symptoms [11,27]. Although other cells undergo degeneration, the dopaminergic cell loss is far more pronounced [11]. The loss of dopaminergic neurons in the SNc results in decreased dopamine release from the synaptic terminals in the dorsal striatum, ultimately leading to a loss of function in the nigrostriatal pathway. The loss of striatal dopamine triggers a range of motor symptoms, including bradykinesia, resting tremor, postural instability, and rigidity, which explains why PD is characterized as a movement disorder. In contrast, non-dopaminergic neuronal degeneration has been linked to the non-motor symptoms of PD, such as cognitive decline and autonomic dysfunction [28]. While these features can precede the motor symptoms, they can still play a significant role late in disease progression [28].

Beyond the cell loss, individuals must also present proteinaceous inclusions, termed Lewy bodies, that are often found in surviving neurons. These Lewy bodies comprise intraneuronal deposits of lipids and proteins, principally composed of a small acidic protein, alpha-synuclein (asyn), which contributes to degeneration [7,29]. Specifically, misfolded and aggregated forms of asyn, together with limited expression of parkin, ubiquitin, and other proteins, form Lewy bodies [30]. These Lewy bodies (LB) and Lewy neurites (LN), a smaller, axonally located form of Lewy body, are present throughout the brain parenchyma and are found in the soma and dendrites of neurons

[31]. Several diseases related to LBs have been identified, collectively referred to as Lewy body diseases (LBDs). These comprise a group of disorders that include Parkinson's disease (PD), PD with dementia (PDD), and dementia with Lewy bodies (DLB) [32]. Worldwide, these diseases affect more than 5 million people and are predominantly characterized by the progressive accumulation of the protein asyn, as well as by the degeneration of the neocortical, limbic, and nigral-striato pathways [33,34].

The preclinical components of PD entail separate subcategories: Preclinical, Prodromal, and ultimately Clinical PD [35]. The Preclinical PD component is characterized by neurodegenerative Lewy pathology, during which clinical symptoms are not present [35]. Thereafter, during the prodromal phase, patients present with early symptoms that are not sufficiently pronounced for clinical diagnosis [35]. Finally, the Clinical PD phase reflects the point at which a clinical diagnosis can be made based on the presence of classical motor signs [35]. This is the turning point from the pre-diagnostic phase to the progressive stages of PD. Unfortunately, current technologies that are used in tracking motor deficits still leave researchers struggling to differentiate between the different pre-diagnostic subcategories in PD patients. It is expected that advances in these technologies will allow for the differentiation of motor deficits during the early pre-diagnostic stages of PD, particularly among individuals with known risk factors.

As with many neurodegenerative illnesses, the motor symptoms of PD develop with years of cellular degeneration, as do the non-motor symptoms that precede these. There are five progressive stages of PD that describe the development of the illness following a clinical diagnosis. Prior to the clinical diagnosis of PD, there is a period

during which motor and non-motor symptoms are present, although they may not be sufficiently marked to warrant a PD diagnosis [2]. This preclinical period is nonetheless thought to be of particular importance as it might represent a window of opportunity for therapeutic interventions to prevent the progression of the disease. At present, the available treatments target PD symptoms as no therapies effectively slow the disease progression. It was suggested that at the time of clinical diagnosis, the disease pathology is too advanced to intervene with neuroprotective treatments even if they should become available [35].

A staging model for PD was introduced that focused on the predictable spreading pattern of asyn [36,37]. According to this model, a progressive process occurs wherein specific nuclei and neuronal types within the brainstem promote the development of Lewy pathology, advancing upward as severity and clinical manifestations of PD increase [38]. It was possible to identify cell types that were particularly vulnerable to Lewy pathology, notably projection neurons with long, thin, unmyelinated or poorly myelinated axons that were especially susceptible to the development of inclusions [37,38]. In contrast, subcortical projection neurons with long, sturdy, myelinated axons appeared to be resistant to Lewy pathology [38].

According to a model proposed by Braak [37], Lewy pathology begins when an environmental insult in the form of a bacteria enters the body and subsequently gains access to the central nervous system (CNS), where it spreads trans-synaptically from one vulnerable brain region to the next [38]. A “dual-hit” hypothesis was further offered in which it was suggested that an unknown pathogen (virus or bacterium) in the gut could be responsible for the initiation of sporadic PD [36,38]. Simply put, these PD cases were

hypothesized to originate from two locations: the neurons within the nasal cavity and the neurons within the gut [36,37]. These two routes may help explain the involvement of the olfactory structures in the early stages of Lewy pathology and why patients often complain about the loss of smell in the years preceding a clinical diagnosis [15]. Additionally, the gastric route involvement may account for the early non-motor symptoms, such as constipation, Irritable Bowel Syndrome (IBS) symptoms, and gastric dysfunctions [38].

The Lewy pathology is hypothesized to spread according to specific patterns via the olfactory tract and vagus nerve, toward and within the CNS [37]. The Braak model suggested that two independent processes are associated with the development of Parkinson's disease. At an early stage, PD is characterized by lesions in the olfactory bulb and anterior olfactory nucleus [39,40]. Concurrently, the Lewy pathology (toxic asyn aggregates) originates in the brainstem and advances rostrally, though it remains unclear if the brainstem is the first site affected in the disease process [38]. One of the fundamental underpinnings of Braaks' hypothesis is that asyn spreads through the vagal nerve and the dorsal motor nucleus of the medulla oblongata, and from there towards the substantia nigra and eventually to the neocortex [36].

In a subsequent stage, pathology spreads to the lower raphe nuclei, the magnocellular portions of the reticular formation, and the locus coeruleus [39,41]. Thereafter, pathology extends to the midbrain, profoundly affecting the SNpc [39,42]. Pathology subsequently spreads to the cortex [39], wherein the mesocortex is affected while the neocortex is not [37,39,42]. In this case, pathology reaches the neocortex

through prefrontal neocortex and then advancing to the pre-motor areas, the primary sensory areas, and the primary motor field [39,42].

One of the significant foundations of Braak's model of Lewy pathology and the "dual-hit" hypothesis rests on how asyn can spread from neuron to neuron. One suggestion had been that asyn acts in a prion-like manner [36,43]. This view of the underlying pathology holds that misfolded asyn is an infectious protein that spreads by forming a toxic template that seeds misfolding for nearby asyn protein, turning a healthy protein into one that is toxic, which then triggers Lewy pathology [36,44]. *In vitro* research by Kumari *et al.*, (2021) showed that when the positively charged N-terminal domain of monomeric asyn is near the negatively charged C-domain of fibril asyn a hydrostatic bond is formed [44]. This interaction leads to the partial unfolding of monomeric asyn (due to the lowered pH) by the C-terminal tail of asyn fibrils formed [44]. This unraveling exposes the NAC region of monomeric asyn and triggers aggregation [44].

Evidence supporting the prion-like nature of asyn stems from the observation of Lewy body pathology in grafted embryonic neurons that were transplanted into the putamen of human PD patients [38,45,46]. Post-mortem autopsies performed in these patients revealed that ~10-20 years following the graft transplantation, asyn positive Lewy body-like inclusions were observable on the grafted dopamine neurons [46,47]. It was unexpected to see inclusions in such "young neurons", which suggested that PD progression may be mediated by a prion-like process [47]. Moreover, in animal studies, an intracerebral injection of exogenous asyn induced a progressive asyn immunoreactive staining pattern, further supporting the view that asyn pathology propagates through a

prion-like process [48]. To be sure, this does not exclude the involvement of other mechanisms, such as chronic inflammation promoted by microglia that could contribute to neurodegenerative diseases [49].

Imaging and Potential Biomarkers

Currently, definitive biological or imaging markers for the detection of PD are unavailable so that the diagnosis of the disorder, as mentioned earlier, is made based on stringent clinical criteria [50]. Radiotracer imaging with single-photon emission computed tomography (SPECT), positron emission tomography (PET), and transcranial sonography (TCS) have all been used to differentiate patients with PD from healthy individuals [35]. New approaches have also been developed to confirm dopamine loss at the striatal level. These new tools include flurodopa (F-dopa) positron emission tomography (F-dopa-PET) and dopamine transporter (DAT) imaging with radionucleotide tracers through single-photon emission tomography (DAT-SPECT) [35,50]. Fluorodopa is an analog of l-DOPA and can be used to assess the integrity of the nigrostriatal pathway, whereby a PET scan is used in conjunction with this tracer to identify abnormalities [35]. Assessment using SPECT revealed that clinical diagnosis in a PD patient is accompanied by a 40-50% reduction in tracer binding within the SNc and further decline of striatal binding in the years following initial diagnosis amounting to about 11.2% [35]. An alternative to these procedures is TCS, in which hyperechogenicity in the SNc can be detected [35]. Using this procedure, it was observed that among patients with mild PD symptoms, 91% sensitivity and 82% specificity could be achieved [35,51]. As impressive as these various procedures have been, they are still considered

investigative and are used to confirm or support a clinician's diagnosis but are not routinely used to form a diagnosis.

Basal Ganglia Pathways in relation to PD

Overall, PD is considered a disorder of the motor cortex. As previously mentioned, cells within the SNc degenerate, in turn disrupting the circuitry involved in controlling movement. The basal ganglia comprises the substantia nigra, striatum, globus pallidus, and the subthalamic nucleus [52], which projects to the pre-motor cortex, thereby formulating a specific movement blueprint, that is acted on by the motor cortex [53]. The basal ganglia is involved in both positive and negative action selection (i.e., to act or not act) [53]. In PD, there are multiple symptoms relating to initiating movement (bradykinesia) and preventing involuntary movements (tremors). These motor symptoms exhibited by PD patients are attributable to disturbances in the direct and indirect pathways, which will be presented in greater detail in the section that follows.

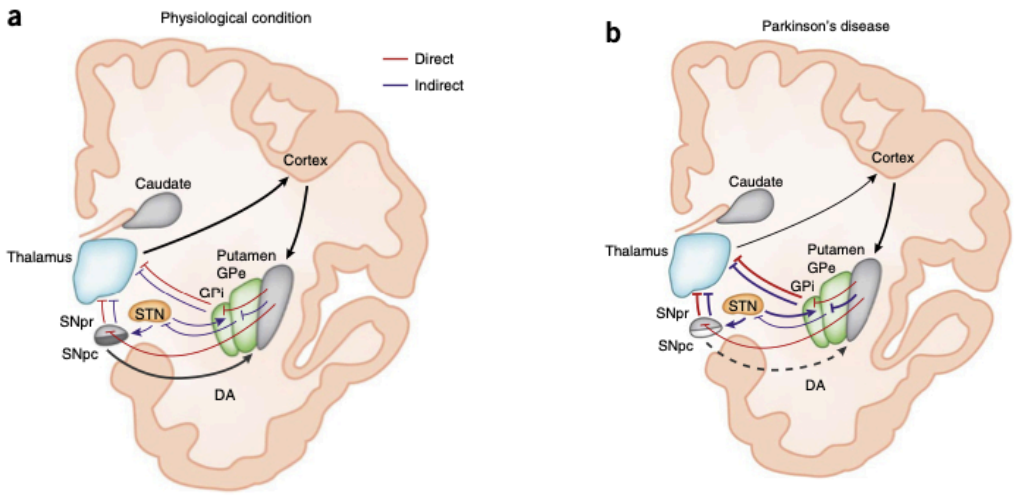

Figure 1: Schematic representation of the direct/indirect pathway classical model in the physiological condition and in Parkinson's disease *(***a**) In the physiological condition, DA

arising from the SNpc is thought to activate D1-expressing striatal MSNs of the direct pathway (red lines) and to inhibit D2-expressing striatal neurons of the indirect pathway (blue lines). The output nuclei globus pallidus internal (GPi) and SNpr project to the thalamus, which in turn sends efferents that complete the cortico-basal ganglia-thalamo-cortical loop. (**b**) In Parkinson's disease, degeneration of nigral neurons reduces DA receptor stimulation in striatal MSNs. The imbalance between direct and indirect pathways results into abnormal activation of output nuclei and over- inhibition of thalamic neurons projecting to the cortex. *Figure and Figure Caption taken from* [54]

Figure 1 depicts the neuronal connections associated with motor movements, particularly the direct and indirect pathways that have been implicated in Parkinson's disease. Among PD patients, dopamine neurons of the SNc are particularly vulnerable to degeneration, resulting in fewer projections to the striatum, leading to impaired neuronal functioning within the basal ganglia [55], [52]. This loss of functioning disturbs the pathways involved in motor movements and contributes to the hallmark resting tremor characteristic in PD patients.

To understand the role of dopaminergic neurons in movement, it is important to identify first how they behave in a healthy individual. The multiple components of the basal ganglia work in conjunction with one another with the help of the thalamus and motor cortex to both coordinate movements and to inhibit movements. This is accomplished by the direct and indirect pathways originating from the basal ganglia [56].

The direct pathway stems from the motor cortex, where it projects to the striatum through excitatory glutamatergic neurons (see Figure 1). Cortical activation initiates a release of glutamate, in turn, activating medium spiny neurons (MSNs) that are

GABAergic cells carrying inhibitory actions on neurons of the substantia nigra pars reticulata (SNpr) that are also GABAergic [54]. In turn, inhibiting the SNpr leads to the disinhibition of the thalamus through glutamatergic neurons that receive input from the SNpr and project to the cortex [54]. From the thalamus, excitatory pathways connect with the motor cortex, where synapses exist with neurons in the brainstem and spinal cord, thereby enabling voluntary movement [54,56].

Paralleling the direct pathway, activation of straito-pallidal MSNs project indirectly to the SNpr by means of the globus pallidus pars externa (GPe) and the subthalamic nucleus (STN), thereby inhibiting the inhibitory neurons of the globus pallidus externa (GPe) [54]. This results in disinhibition of the glutamatergic neurons of the subthalamic nucleus. The increased discharge of these excitatory STN neurons then activate the SNpr GABAergic neurons that project to the thalamus [54]. Activation of this pathway results in decreased activity and suppression of motor movements [54,56]. The dopaminergic neurons from the SNpc play a major role in both pathways, and it is these dopaminergic neurons that project to the striatum, forming the nigrostriatal pathway [57].

The differential motor actions between the direct and the indirect pathways are attributable to the different dopamine receptors located on the neurons within the striatum. The D1 and D2 receptors respond differently when stimulated by dopamine. Specifically, when dopamine binds to the D1 receptors of the direct pathway it results in increases in initiating voluntary movements. In contrast, when dopamine binds to the D2 receptors involved in the indirect pathway, there is an increase in disinhibition of the thalamus resulting in an increase in unwanted motor movements [56]. As previously mentioned, up to 70% of dopaminergic neurons in the SNpc are lost in PD patients, thus

leading to the collapse in the functioning of the nigrostriatal pathway, culminating in striatal dopamine receptors becoming hyposensitive [54,56]. Excessive indirect pathway activity is hypothesized to supress GPe firing, increasing STN activity, and driving an increase in GPi-mediated thalamic activity and increases in unwanted motor movements[54]. At the same time, this loss of dopamine, leads to decreased direct pathway firing and the disinhibition of GPi neurons resulting in suppression of the thalamus and cortex leading to difficulty initiating motor movements [56,58]. Ultimately, an imbalance between the two pathways at the striatal level is thought to be fundamental in the expression of Parkinsonian symptoms.

Environmental & Additional Risk Factors

Numerous risk factors contribute to the development and progression of PD, and it has been maintained that the disorder develops as a result of multiple hits. According to this multi-hit perspective, the onset and progression of the disease involves the collective contribution of psychological, inflammatory, and chemical challenges, which may also be linked to interactions with genetic factors [59]. In this regard, the possibility has been entertained that the factors contributing to PD exist on a spectrum with familial links that result in early PD diagnosis at one end and purely environmental impacts at the other. The most prominent contributions to PD might thus consist of the interactive effects of genetic vulnerability and environmental factors. Considering that not all genes associated with PD give rise to Parkinsonian symptoms speaks to the fundamental role of environmental influences in the provocation and progression of the disease [59,60]. In the multi-hit model of PD, the primary "hit" could entail genetic dispositions (mutations in

SNCA, LRRK2, and *DJ-1*), whereas chemical, inflammatory, and psychological challenges additively or synergistically serve as further hits that shape the evolution of the pathology [61].

Substantial evidence has pointed to certain environmental factors imposing a significant risk for the development of Parkinson's disease. For instance, pesticide exposure through occupations such as farming, as well as rural living, and pesticide-contaminated well water have been associated with the development of the disorder [35,62]. Of these pesticides, particular attention has focused on the contribution of rotenone and paraquat (which are structurally similar to 1-methyl-4-phenyl-1,2,3,6-tetrahyropyridine (MPTP), an illicit compound that causes Parkinsonism in consumers), which have been used to create animal models of Parkinson's disease [35].

Earlier animal models of PD employed a neurotoxic compound, 6-hydroxydopamine (6-OHDA), that was rapidly taken up by DA neurons and shown to induce rapid pathological impacts that mimic the neuroinflammation and DA loss; however, these toxicant models cannot effectively reproduce synucleinopathies, non-motor symptoms, and even the progressive nature of Parkinson's disease [63]. This compound nevertheless produced sufficient dopamine loss to reliably elicit signs of a PD-like condition. Likewise, the highly toxic substance, MPTP can destroy neurons upon its conversion to the toxic metabolite MPP^+ that is known to occur within the lysosomes of astrocytes [64]. Astrocytes and serotonergic cells have MAO-B present, which contribute to the creation of the toxic metabolite that is subsequently delivered to DA nerve terminals through DAT, allowing for DA cell death within the SNc [64]. These models have not only been important in showing the involvement of dopamine in PD but have

also allowed for the analysis of multiple steps that contribute to the development of the disorder as well as factors that moderate its progression.

In addition to pesticides, head injury has also been considered a minor but significant risk factor for Parkinson's disease. Indeed, individuals who suffer from repeated head injuries (boxers, American football and rugby players) are at elevated risk of developing a range of neurodegenerative conditions, including Parkinsonism, dementia, and motor neuron disease. In contrast to these influences, several lifestyle factors were negatively related to Parkinson's disease. Curiously, this included smoking as well as caffeine and alcohol consumption, although the source for these protective effects have not been fully deduced [35,62].

The Genetics underlying PD

Parkinson's disease is often considered as either familial involving a genetic component or idiopathic where there is no known cause. Approximately 90-95% of PD cases are classified as being idiopathic [35]. Having a family history of PD increases the odds of PD developing by 300-450%, and up to 10% of patients report a family history of PD [35,62,65]. The genes involved in this disorder can encompass either autosomal dominant mutant genes, like mutations in *SNCA* and *LRRK2,* or autosomal recessive mutant genes, namely *DJ-1*, *Parkin*, and *Pink1* [21,29]. Mutations in *SNCA* and *LRRK2* genes have been linked to genetic PD cases and Lewy body Parkinson's Disease (LBPD) [21]. Both genes have received considerable attention and have been deemed as potentially fundamental to the development of familial PD. In the present investigation, the focus of the research was exclusively on a familial model, particularly involving an

A53T mutation of the *SNCA* gene to produce and influence asyn protein changes that foster PD-like pathology.

The asyn protein is a 140 amino acid residue encoded by the *SNCA* gene located on human chromosome 4 and is predominantly expressed in presynaptic sites of multiple neurotransmitter pathways within the CNS. Asyn has a ubiquitous distribution throughout many brain regions known to be involved in complex behaviours, but as indicated earlier asyn pathology does not impact all brain sites equally, instead selectively targeting vulnerable sites [37,55,66].

Although the focus of the present investigation is on the A53T mutation of *SNCA* gene, this should not be misinterpreted as implying less importance of other genetic contributions. In fact, a genetic mutation in the leucine-rich repeat kinase 2 (LRRK2) gene and specifically the G2019S mutation has been linked to PD and the accompanying inflammatory processes [67]. Not only has the G2019S mutation been associated with the familial form of PD, but it has also been implicated as a risk factor for the idiopathic form of the disease [66]. This mutation has been estimated to account for 1% of idiopathic PD cases and 4% of familial PD cases [66]. In addition, another mutation, that of *DJ*-1 related to the autosomal recessive inheritance of Parkinson's disease, has been identified [68]. Mutations in the *DJ-1* gene have been linked to early-onset PD, slow disease progression, and a good response to l-DOPA [68]. *DJ-1* knockout in mice resulted in reduced survival and increased vulnerability to oxidative stress in both *in vitro* and *in vivo* models [68].

Among the multiple genes related to PD, *SNCA* encoding for asyn remains the most likely culprit in the provocation of the disorder. Among other things, mutations in

the *SNCA* gene that encodes asyn causes autosomal dominant PD, suggesting that a gain of toxic function through increased asyn expression may underlie the pathogenesis in familial PD cases. Furthermore, several polymorphic variants at the *SNCA* locus affect the expression of asyn and are risk factors of sporadic Parkinson's disease.

Accumulated asyn, as already described, is the main component of LBs, and together with genome-wide association studies were linked to a central pathogenic role in both familial and sporadic PD [21]. One of the most notable genetic factors that might contribute to PD is the A53T mutation in the *SNCA* gene [69]. Two other point mutations on the *SNCA* gene, notably A30P and E46K, have also been described in families descending from Germany and Spain that exhibited a degree of hereditary Parkinson's disease [69,70]. Individuals with the A53T mutation where threonine is substituted for alanine at residue 53 in the *SNCA* gene developed a severe form of PD that was often accompanied by dementia [71,72]. Likewise, families with the E46K *SNCA* point mutation demonstrate features associated with Lewy Body Dementia (LBD). In contrast, individuals with the A30P mutation, where phenylalanine is substituted for alanine at residue 30 [72], exhibited late-onset PD, which is typically accompanied by mild dementia [71]. Duplications of the *SNCA* gene were accompanied by PD similar to that of the sporadic disorder for the age of onset as well as symptomatology [71,73]. It also appeared that triplication of *SNCA* was associated with a more severe phenotype, as well as an earlier age of onset and more prominent cognitive deficits [71,73]. In most cases of *SNCA* mutations (point mutations or gene multiplications), the disease initially presents as PD but develops a dementia sub-component later. It was suggested that an increase in protein levels rather than a change in asyn's properties were sufficient for PD to emerge

[73]. Together, these findings imply that increased levels of phosphorylated asyn, possibly attributable to increased *SNCA* dosage (duplication or triplication) or the modulated clearance of asyn expression is the key event responsible for the formation of LBs and Lewy neurites, which eventually leads to neuronal cell death [73].

SNCA/ alpha-synuclein

The preceding discussion has made it clear that asyn is a key player in relation to PD pathology [55,66], being the major protein component of LB and LN [74]. Ordinarily, asyn exists in tissue in an equilibrium of monomeric and oligomeric confirmations that are not prone to form fibrils under normal physiological conditions. However, asyn can undergo a change in conformation from monomeric to fibrillar, whereby disequilibrium can result in pathology. There is some debate regarding which conformations of asyn are responsible for toxicity in neurodegenerative diseases. In a healthy brain, asyn is found at the presynaptic terminal. In Lewy bodies and Lewy neurites, asyn is in an amyloid fibril conformation with a cross beta quaternary protein structure [75]. This protein is natively unfolded but in the presence of lipid-containing vesicles, can change from an alpha-helical structure to a beta-pleated sheet or amyloid structure found in the fibrils that make up Lewy bodies [76]. Lewy bodies and Lewy neurites composed of asyn are not solely related to PD as their presence extends to other synucleinopathies, including the Lewy-body variant of Alzheimer's disease, dementia with Lewy bodies, neurodegeneration with brain iron accumulation type 1, and multiple system atrophy (MSA) [72].

An important hypothesis underlying Lewy body formation is that asyn monomers become oligomers (protofibrils), which then combine into fibrils and aggregate to form

Lewy body inclusions [72,76]. Mutations in the *SNCA* gene directly affect the probability of asyn to misfold and form oligomers and/or fibrils. These mutations cause amino acid displacements and alter the configuration of the encoded protein. These mutations are associated with PD, as they disrupt the stabilized alpha-helical tetramers and produce excess monomers, thereby, disrupting the monomer: tetramer ratio [77–79]. Although conflicting opinions exist as to why this occurs, one view is that cells may package excess cytoplasmic debris into a less accessible and toxic form [76]. This occurs because monomers and oligomers are soluble, whereas the fibrils and Lewy bodies are insoluble within the neuronal cytoplasm [72].

Considerable controversy has surrounded the role of different states of asyn and their involvement in PD pathology, particularly as Lewy bodies could potentially take on both a neurotoxic and a protective function. Beyond this, it has been hypothesized that the protofibrillary states (oligomers) and not the fibrils or Lewy bodies themselves are damaging to DA neurons [80]. This is thought to be attributable to the fact that oligomers produce radical oxygen species, increases in intracellular calcium, decreases in synaptic activity and neuronal excitability, ultimately leading to cell death [80].

Asyn Conformations & Risk Factors

Several environmental and genetic risk factors have been identified in relation to Parkinson's disease. These have included oxidative stress, mitochondrial dysfunction, neuroinflammation, point mutations, genetic-related duplication or multiplication, and specific polymorphisms, which may cooperate to create ideal conditions for the development of the disorder [55,81]. These factors also act as determinants that could

influence the propensity of asyn toxicity [55]. As such, asyn may express its neurotoxic potential when soluble monomers initially form oligomers and then progressively combine to form small protofibrils and further aggregate in large, insoluble asyn fibrils that form Lewy bodies [55]. Ordinarily, asyn exists in a balance between its soluble and membrane-bound configurations. Acute triggers that cause accumulation and aggregation of asyn can occur, leading to overproduction of the protein, failure in the molecular system that cleaves misfolded forms, altered pH levels, oxidative stress, and mitochondrial overwork.

Additionally, many post-translational modifications increase the likelihood of conformational changes of alpha-synuclein. Analysis of LBs has been fundamental in identifying which post-translational modifications are associated with pathogenic forms of alpha-synuclein. Among these modifications is phosphorylation, which is likely the most widely studied modification since phosphorylation of serine residue 129 is thought to be the dominant form of this protein in Lewy bodies, and has been used as an indicator for monitoring PD progression [82,83] Under normal physiological conditions, only 4% of asyn is phosphorylated in the brain, but in LBs, the majority of asyn (90%) is phosphorylated [84]. However, it is uncertain whether phosphorylation of asyn impacts the fibrillation process.

The physiological function of asyn

Although soluble natively unfolded conformations of asyn are present throughout the brain and peripheral nervous system, their function is still not fully understood. Currently, there is strong agreement that one of the major functions of asyn is to promote

membrane curvature and to contribute to binding vesicles to the presynaptic membrane [85,86]. Under normal physiological conditions, asyn is thought to be involved in neurotransmitter release through interaction with vesicle fusion complexes as a way to facilitate transport, release, and reuptake of these neurotransmitters [87,88]. The first function described for asyn was to act as a chaperone protein and control exocytosis through the management of synaptic vesicle pools and trafficking [55]. This hypothesis stemmed from research showing that expression of human asyn led to the redistribution of SNAP REceptor (SNARE) proteins, a family of receptors that bind to soluble N-ethylmaleimide sensitive fusion attachment proteins (SNAP) to receptor (SNARE) proteins and regulate their assembly [89]. This results in an associated reduction in exocytosis and dopamine release in transgenic mice [89]. Although the mechanism underlying this redistribution remains uncertain, mutations in the *SNCA* gene led to functional changes of SNARE proteins [89]. Asyn's role in inhibiting exocytosis prevents the breakdown of complexes present on vesicle surfaces that are involved in fusion with the plasma membrane [86].

Under physiological conditions, asyn has been implicated as both a negative and a positive regulator of synaptic transmission [90]. As a positive regulator, asyn and other homologs support synaptic function and the release of synaptic vesicles by chaperoning the SNARE complex in presynaptic terminals [90]. Comparatively, loss of asyn function has been linked to enhanced vesicle release in dopaminergic terminals, suggesting that asyn normally functions to suppress vesicle release [90]. Overexpression of wild-type human asyn suppresses presynaptic transmission through depletion of the recycling and readily releasable pools of synaptic vesicles [90][91]. It should be noted that in addition

to SNARE, asyn interacts with other presynaptic proteins, including synapsin III and VMAT2, which could potentially influence vesicle release, thereby diminishing neurotransmitter reserves [90].

During exocytosis, synaptic vesicles form a fusion pore. This pore dilates before fully collapsing into the plasma membrane. It can also close prematurely during a "kiss-and-run" event that serves to immediately regenerate a vesicle [86,92]. As such, this might indicate that the regulation of the membrane curvature plays a role in the behaviour of the fusion pore [86,92]. However, to better understand the role of asyn, it is important to consider that overexpression of asyn accelerates the release event, reducing the time for pore dilation, affiliated peptide release, and also preventing pore closure [86]. In contrast, the loss of asyn produces the opposite effect, wherein the time to decay increases, as does the likelihood of pore closure [86]. Overall, it appears that asyn plays two roles, that of promoting dilation of the fusion pore (in both an endogenous and overexpression scenario) and inhibiting exocytosis [86].

Breaking down Asyn

Asyn being such a large constituent of LB and LN has strengthened the position that it can be an important target to untangle the molecular mechanisms and pathogenesis of Parkinson's disease. This interest resulted in the structure of asyn being identified with the hope of defining target regions that might be able to prevent toxic conformations of the protein. The primary structure of asyn can be separated into several components: the amino-terminal domain (N-terminal, residues 1-60), the central domain (NAC domain,

residues 61-95) and the carboxy-terminal domain (C-terminal domain, residues 96-140) [39].

The N-terminus contains the first 60 amino acids; the NAC domain-containing amino acids 61-95 are both parts of the binding domain of asyn and are responsible for asyn interactions with lipid membranes [39,79,93]. The single point mutations A30P, E46K, and A53T responsible for the familial form of PD are all present in this region, reinforcing the hypothesis that changes in the lipid-binding domain (N-terminus) may be connected to asyn pathology [39]. The N terminal domain also includes four repeats of the 11 amino acid alpha-helical lipid-binding motif (KTKEGV), which are crucial for enabling the formation of amphipathic alpha-helical structures upon interaction with lipid membranes [39,93]. The NAC (non-amyloid-Beta component) region encompasses the amino acid residues 61 to 95 that are hypothesized to be responsible for the initial intramolecular interactions that result in asyn misfolding and, ultimately, aggregation.

The final region of the protein constitutes the C-terminus, which includes 14 acidic residues and does not establish a defined secondary structure when in solution or when asyn is bound to membranes, as well as when it forms amyloid fibrils. The C-terminus is polar by nature and can interact with the hydrophobic region of a separate denatured protein, sharing its structural and functional resemblance with other molecular chaperones [55]. The appreciable flexibility of this protein also relies on the ability of asyn to auto-assemble and act as an intramolecular chaperone [55].

Alpha-synuclein and the gut

For decades there has been discussion of asyn pathology originating in the gut. Endoscopic biopsies from children with gastric and duodenal inflammation who had received intestinal allografts but later contracted norovirus exhibited asyn in the duodenum, which was positively correlated with the degree of inflammation present [94]. Since asyn was expressed during acute and chronic gastrointestinal infections and this protein can be promoted by immune cells, supports the view that asyn is involved in gut inflammatory processes [87]. Beyond this, it was speculated that after prolonged inflammation, toxic asyn might travel from the gut to the CNS, where it contributes to pathology.

Current Treatments:

Regrettably, as previously mentioned, a cure for PD is not currently available, and treatments primarily target the symptoms experienced by PD patients. The most commonly prescribed drug for PD symptoms is l-DOPA, known to be particularly effective for bradykinesia symptoms [95,96]. L-DOPA was first introduced as a treatment in 1961, where it was shown to reduce symptoms [97]. As knowledge and understanding of l-DOPA as a treatment evolved so had physician's abilities to manage complications associated with l-DOPA therapy [96]. L-DOPA therapy is not without its consequences, and it is known to induce motor complications and fluctuations with dyskinesias based on the dose and duration of the treatment [95,98]. Notably, these symptoms often arise approximately five years following l-DOPA therapy commencement. As such, many physicians recommend therapeutic strategies that delay the onset of l-DOPA therapy

thereby delaying the onset of l-DOPA-related motor complications. Given these known limitations, multiple strategies can be employed to limit l-DOPA-induced dyskinesias. Instead of requiring a reduction in l-DOPA dose, many drug therapies can improve dyskinesias by simply adding an adjuvant to the treatment regime [95].

Fortunately, in this regard, since 2014, seven new Parkinson's drugs have been developed to attenuate symptoms among individuals in whom other treatments are ineffective or that have lost their efficacy [54]. Of these newly developed drug therapies only one, Azilect, a monoamine oxidase (MAO) B inhibitor can be prescribed alone, though its efficacy is limited to early stages of PD [99]. All other newly developed pharmacological interventions are to be administered in conjunction with l-DOPA [98,99]. These different medications work in a variety of ways to improve l-DOPA delivery to the brain (decarboxylase inhibitors), by lowering levels of enzymes capable of breaking down levodopa or dopamine (catechol-O-methyltransferase inhibitors (COMT), MAO B inhibitors), by blocking adenosine to boost dopamine signalling (adenosine receptor antagonists), by mimicking the action of dopamine (dopamine agonists), or by rebalancing the dopamine: acetylcholine neurotransmitter reserves (anticholinergic medications) [98]. These medications work in various ways, but it is the combination of therapies which is tailored and changed throughout the disease course. Many of these drugs have been based on the growing understanding of the genetic contributions to PD development and progression.

Aptamers as therapeutics

Beyond the normal role of DNA as a storage molecule, it is also capable of behaving like a probe or recognition element and can be used to create sensors, antibodies, and even therapies [100]. When a DNA molecule is used to perform a function such as this, it is termed an aptamer. In effect, aptamers represent a unique technology, whereby their specific sequence of nucleotides can fold into 3-dimensional shapes capable of binding non-covalently and with high affinity and specificity to a target molecule [100,101]. In order to design an aptamer, a process known as Systemic Evolution of Ligands by Exponential enrichment (SELEX) is performed in which three main steps are followed; selection, partitioning, and amplification [101]. The selection stage involves incubating an oligonucleotide library with a target molecule, which may comprise a library of ~10^{16} different sequences [100]. Following incubation with the target protein, any unbound sequences are removed, and this process is repeated until the best binding species are identified.

Speaking of their therapeutic potential, various aptamers have been used in the treatment of different medical issues like age-related macular degeneration, heparin intolerances, as well as tumour-targeted treatments [102]. In fact, aptamers have played a particularly relevant role in the advancement of cancer therapies, and to date there are many aptamers in clinical trials [102]. The excitement surrounding these products may give rise to further advances in the treatment of other disorders.

Relevant models for the present investigation

SHSY-5Y cells as an asyn overexpression model

The SH-SY5Y cell line is a three times subcloned subline (first cloned to SH-SY, then to SH-S5Y, and finally to SH-SY5Y) of SK-N-SH cells, which were originally established from a metastatic bone tumour biopsy of a 4-year old female patient with a neuroblastoma of sympathetic adrenergic ganglial origin [103–105]. This cell line has been a widely used model for neuronal functioning due to the biochemical, structural, and functional similarities these cells possess when compared to neurons. This cell line is particularly relevant to PD research since the cells express tyrosine and dopamine-β - hydroxylase and thus synthesize dopamine and norepinephrine, respectively. Moreover, SHSY-5Y cells also express the dopamine transporter (DAT), a protein expressed specifically by dopamine neurons in the central nervous system [106].

Most noteworthy is that SH-SY5Y cells can proliferate in culture for extended periods without contamination, a key requirement of an *in vitro* cell line model. SHSY-5Y neuroblastoma cells can be differentiated to better mimic mature neurons through treatment with chemical agents, including retinoic acid (RA), phorbol esters, and specific neurotrophins, such as brain-derived neurotrophic factor (BDNF)[107]. Differentiation alters the cells so that they express cell neurites and adopt a more neuron-like phenotype [108,109]. When these cells are differentiated, they extend long, branched processes, exhibit decreased proliferation, and can even polarize [107]. Applying different chemical agents during the differentiation process may select for specific neuron subtypes, including adrenergic, dopaminergic, and cholinergic neurons [105,110]. Fully differentiated SHSY-5Y cells also exhibit numerous markers commonly expressed by

mature neurons. Additionally, a major benefit of differentiating SHSY-5Y cells is that this synchronizes the cell cycle so that the cell population under investigation is a homogenous one [109,111,112]. Consequently, the SHSY-5Y cell line has been widely used in experimental neurological studies, including analysis of neuronal differentiation, metabolism, and function related to neurodegenerative and neuroadaptive processes, neurotoxicity, and neuroprotection [105]. The SHSY-5Y cell line not only offers a powerful model for investigating neurodegenerative diseases but provides an inexpensive, robust, and uniquely consistent biochemical and physiological phenotype that is comparable between facilities and laboratories.

A53T-eGFP virus

As described earlier, mutations of the *SNCA* asyn gene have been associated with the familial forms of Parkinson's disease. The duplications, triplications, or missense mutations (e.g. A53T, A30P, or G46 L) of this gene that accompany familial forms of PD has supported the assumption that asyn plays a fundamental role in the pathogenesis of this condition [70,113,114]. For the purpose of the present investigation, an A53T-eGFP virus (graciously donated by Dr. David Park, uCalgary) that was designed to cause cells to overexpress asyn was used to infect SHSY-5Y cells. This serves as an *in vitro* model that produces levels of asyn overexpression seen in A53T transgenic animals. One of the many benefits of using cellular models for PD research is how quickly asyn overexpression develops *in vitro.* In these cell lines, overexpression is evident within approximately 24 hours post-infection, whereas, *in vivo* animal models, at least three months is required for increased levels of asyn to appear in the brain. This said, it could

be argued that an *in vivo* model rather than one based on cell lines is a closer approximation of the human Parkinson's disease. Of course, these approaches are not mutually exclusive of one another, and the model and cell lines can be complemented by *in vivo* analyses.

A53T transgenic murine model

The M83 line of mice expresses the mutant human A53T mutation in the *SNCA* gene (asyn) under the direction of the mouse prion protein promoter. This specific line of mice is commercially available through Jackson Labs (Jax, Catalog# 004479) and was created by Lee *et al*. [115]. These transgenic mice overexpress asyn and show a decrease in readily available vesicles and impaired recycling of synaptic vesicles following endocytosis, thereby producing a reduction in the size of the synaptic vesicle pool [91,116]. Additionally, excess asyn results in a reduction in dopamine reuptake and inhibits inter-synaptic trafficking of vesicles leading to a smaller reserve of pool of vesicles. This mouse line is a unique preliminary model where increased levels of asyn are present, hence providing ideal conditions to assess an aptamer designed to bind to asyn and with a high propensity to reduce oligomerization.

Aptamer to target alpha-synuclein

The aptamer used in the present investigation comprised a 66 base pair sequence of single-stranded DNA with a high binding affinity for the asyn protein, specifically in the monomer conformation. In addition to having a high binding affinity for asyn, additional selection criteria were introduced during the aptamer development process to prevent the oligomerization of the protein. To create this aptamer, the Systematic

Evolution of Ligands by EXponential enrichment (SELEX) technique was used as described earlier. The development of the aptamer for the present investigation was conducted by Dr. M DeRosa (Carleton University).

Modified liposomes as delivery vehicles

For the asyn binding aptamer to cross the blood-brain-barrier (BBB) *in vivo,* modified liposomes were used as a delivery vehicle. Using liposomes for this purpose has been under heavy scrutiny owing to inconsistent loading and delivery. The current use of our modified liposomes is not without shortcomings but expected modifications and improvements to liposome synthesis may enhance these delivery vehicles.

Significance statement and specific hypotheses

The present thesis is underpinned by one major theme, specifically that increased asyn expression contributes to the pathological development of PD, particularly through Lewy Body protein inclusions. A better understanding of asyn protein accumulation and toxic aggregate formation represents a major therapeutic avenue with considerable clinical relevance. In the sections that follow, I will discuss our work related to alpha-synuclein overexpression *in vitro* and *in vivo* using different preclinical models. Specifically, Study 1 focused on assessing a novel aptamer designed to bind to asyn monomers in a cellular model of PD. Study 2 then focused on assessing the distribution of the novel asyn binding aptamer in which the aptamer was determined in tissue through qPCR. Study 3 moves on to assess the aptamer in transgenic mice carrying the A53T human variant of the *SNCA* mutation to determine asyn protein level changes. Thereafter, the discussion turns to the therapeutic potential of an asyn binding aptamer by using *in*

vitro and *in vivo* overexpression models to evaluate its safety, distribution profile, and its ability to reduce asyn protein expression acutely and chronically.

It was hypothesized that:

(1) the asyn binding aptamer would reduce aggregate formation and reduce phosphorylated asyn in a cellular model of asyn over-expression;
(2) Our delivery vehicle would successfully transport the asyn binding aptamer into the brain, where it will be detected in different brain regions and would also be apparent within the liver owing to its intraperitoneal administration;
(3) in an *in vivo* model of asyn overexpression, reductions in toxic formations of asyn protein will be evident in multiple brain regions following both acute and repeated administration of the asyn binding aptamer.

Chapter 2:
Study 1: asyn binding aptamer in vitro using SHSY-5Y cells as a biological model

Introduction:

Initial *in vitro* experiments were conducted to evaluate asyn in a cellular context that might be relevant for the later analyses in a mouse model of Parkinson's disease. Specifically, the goal of these *in vitro* experiments was to administer, assess, and visualize cells in response to the asyn aptamer treatment. This provided the groundwork for subsequent *in vivo* assessments. In order to understand asyn protein in a cellular context, we initially investigated the protein using an enriched Green Fluorescent Protein (eGFP) tagged aav-virus with the common A53T mutation in the *SNCA* gene. This approach was used to induce an increase of asyn protein expression in the commonly used SHSY-5Y neuroblastoma cell line. To this end, the experiments;

(1.1) validated that an A53T-eGFP virus increases pAsyn protein levels compared to a control virus,

(1.2) assessed the asyn binding aptamer at different percentages using a Live vs Dead Cell Assay,

(1.3) evaluated a non-binding version of the asyn aptamer using the same Live vs Dead Cell assay,

(1.4) created an experimental model and visualized both phosphorylated-asyn (pAsyn) and filament asyn at a lengthy interval following transfection,

(1.5) determined the impact of 3 concentrations of aptamer (5 μM, 10 μM, 25μM) as a single or repeated treatment and evaluated changes in the fluorescent intensity of filament and pAsyn following these treatments, and

(1.6) assessed 5 μM and 10 μM asyn binding aptamer concentrations on changes in asyn protein levels (pAsyn and Oligo asyn) using Western blot analysis.

Materials and Methods

Cell growth and Differentiation

The initial SHSY-5Y cells, control-eGFP, and A53T-eGFP alpha-synuclein virus were generously donated by Dr. David Park. Cells were thawed at 37°C and added to a T-75 tissue culture flask with 10mL of warmed (37°C) growth medium (DMEM high glucose; Sigma Catalog# D6429), 10% inactivated Fetal Bovine Serum; GE catalog # SH30071.02, and 1% penicillin-streptomycin; Sigma Catalog #P4333). Cells were incubated at 37°C, 5% CO_2 and confluence was monitored. Cells were passaged in a T-75 tissue culture flask to a concentration of 5 x 10^4 cells/mL in 10mL of complete growth medium every 5-7 days once 80% confluence was reached.

Coating Coverslips

A single 12mm sterile glass coverslip was placed in each well of a 24-well plate. A solution containing 10ug/mL Poly-D-Lysine (PDL) (Sigma Catalog# P0296) (1:1000 stock) and 1.8 µg/mL laminin (1:1000 stock) was prepared in Ultra Pure Water (ThermoFisher Catalog# 10977015). The solution was mixed thoroughly prior to adding 500uL of PDL/laminin solution in each experimental well. All coverslips were submerged in the solution and incubated at 37^0C, 5% CO_2 for 2 hours. The solution was removed and wells were air dried in a Biohazard Safety Cabinet while cell suspensions were prepared.

Plating for Experimental Use

For experimental procedures, cells were plated at a concentration of 5 x 10^3 cells/mL in warmed (37˚C) growth medium in a sterile 24-well plate with a coated glass coverslip at the bottom of each experimental well. Forty-eight hours following plating, the cells were treated with 10uM solution of retinoic acid (RA) prepared in complete growth medium. Complete media with 10 μMol retinoic acid was replaced every 48 hours over 1 week (media changes 3 times in 7 days). Between media changes, experimental plates were incubated at 37˚C and 5% CO_2. These methods were consistent in the experiments that followed. Any differences in the procedure are described as necessary.

Statistical analyses

In each of the experiments the data were analyzed by analysis of variance (ANOVA) to determine whether group differences existed. Follow-up tests for significant main effects were conducted using Fisher's HSD post hoc analyses.

Experiment 1.1

Experimental Treatment groups

A validation experiment was conducted to confirm that the adeno-associated A53T-eGFP virus increased asyn protein compared to adeno associated control-eGFP virus in the SHSY-5Y cell line. To assess this, pAsyn protein levels were determined for the A53T virus (n=3) compared to the control virus (n=3).

Viral Transfection

Following a week of differentiation, cells were treated with eGFP control virus or an A53T-eGFP alpha-synuclein virus in DMEM (MOI of 3). The SHSY-5Y cells were incubated with 500uL of the virus solution at 37°C and 5% CO_2 for 24 hours. Twenty-four hours afterwards, the viral solution was removed and cells were then fixed with 4% paraformaldehyde for 15 minutes.

Fluorescent Staining SH-SY5Y cells

Cells were fixed in 4% paraformaldehyde for 15 minutes. Cells were then washed in phosphate buffered saline (PBS; pH 7.2) three times for a period of 5 min followed by a 30-min incubation in blocking solution containing 2% Bovine Serum Albumin (BSA) in 0.1% PBS-TX (500uL per well). Cells were then incubated with primary antibody (pAsyn (1:1000) AbCam #59264) in a solution containing 2% BSA in PBS for one hour. Cells were washed in PBS three times for a period of 5 min each and then reacted with a secondary antibody for the appropriate species (1:1000 Anti-rabbit Alexa 594) for 30 min in 2% BSA in 0.1M PBS. Cells were then washed for 5 min in Hoescht Buffer (1:12,000). Finally, cells were washed three times for a period of 5 min each and coverslips were mounted using fluoromount (Sigma; Catalog# F4680).

Microscopy and Image J analysis

The fluorescent signal was visualized with immunofluorescence microscopy using micro-brightfield (MBF) image acquisition software on a Zeiss LS560 microscope. At least 3 images were captured for each coverslip (3 technical replicates for all 3 biological

replicates) and Image J software was used to assess integrated density of pAsyn. An average for integrated density for pAsyn was calculated for each coverslip and compared across the two treatment groups.

Statistical Analysis

A t-test comparing the integrated density of pAsyn for the control-eGFP and A53T-eGFP virus revealed that a significant difference in mean integrated density between the groups, $t = 2.52$, $p = 0.033$. The analyses also revealed that comparable variances were present (Levene's test, $F = 2.88$, $p = 0.124$). Figure 2 shows a sample representation of cells treated with the (a) control-eGFP and (b) A53T-eGFP virus demonstrating staining for DAPI, each eGFP virus, and pAsyn and (c) compared the integrated density of pAsyn seen in differentiated SHSY-5Y cells.

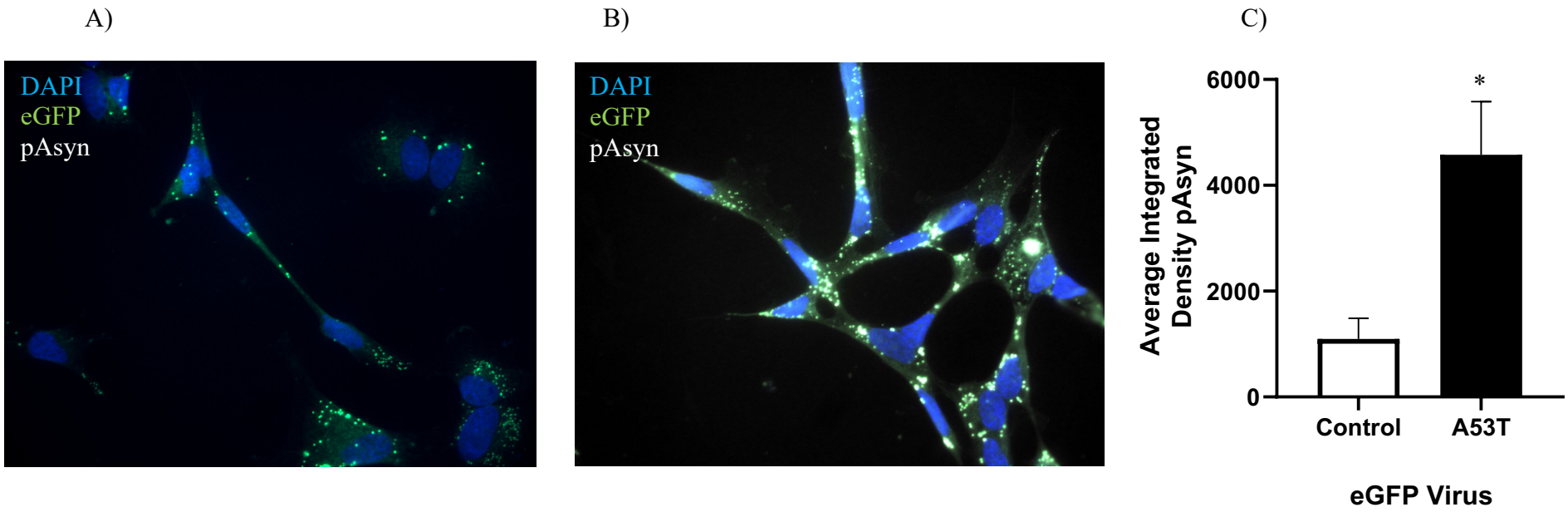

Figure 2: A) Depicts cells stained with DAPI (Blue), control-eGFP virus (Green), and pAsyn (White) 24 hours post viral infection B) Depicts cells stained with DAPI (Blue), the A53T-eGFP virus (Green), and pAsyn (White) 24 hours post viral infection. Images were taken at 63X using a Zeiss LS560 microscope C) Average Integrated Density for pAsyn in SHSY-5Y cells 24 hours post viral infection for the control and A53T-eGFP viruses

* = $p<0.05$

Experiment 1.2

It was important to assess cell viability following asyn binding aptamer treatment. To do so, cells were differentiated using retinoic acid in complete media as described earlier except that cells were plated at a concentration of 5 x 10^3 cells/mL in warmed (37˚C) growth medium in a sterile 96-well plate. The timeline for the varied steps in the procedure are provided in Figure 3.

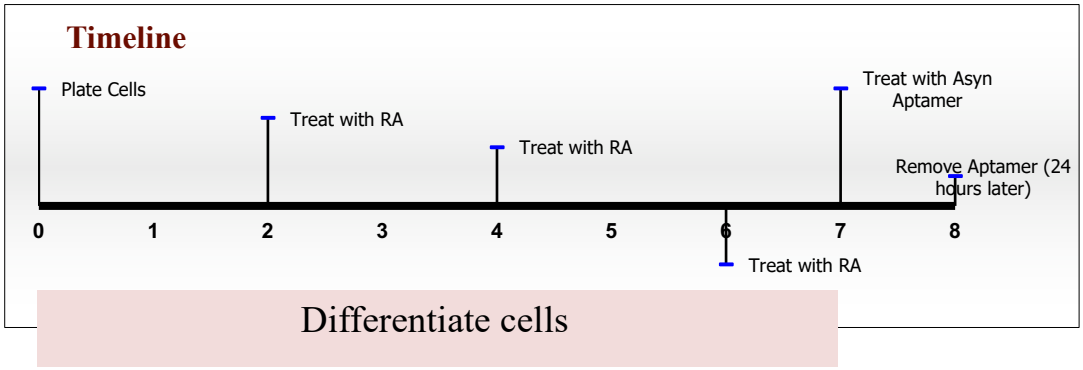

Figure 3: Experimental Timeline for Experiment 1.2
Experimental Day is depicted along the X-axis and RA= retinoic acid

Experimental Treatment groups

To assess the effect of the asyn aptamer on cell viability, multiple treatment percentages were assessed. The asyn aptamer generously provided by Dr. Maria DeRosa (Carleton University) was administered to differentiated SHSY-5Y cells at the following percentages: 0%, 5%, 10%, 15%, 30%, 45%, 60%, 100% (n = 3 per percentage) of the overall complete media solution and each was assessed in triplicate. The Asyn aptamer was 25 µM in concentration and modified with Cy5 for fluorescent detection purposes. Thus, the eight treatment groups comprised the 0% Asyn Aptamer Treatment (Control)

and the varying percentages of asyn binding aptamer treatment. Following differentiation, SHSY-5Y cells were treated with the asyn binding aptamer in complete media and incubated at 37˚C and 5% CO_2. Following 24 hours of incubation with the corresponding asyn aptamer treatment, cells were washed with complete media and incubated for 15 minutes. Live Cell Viability Reagent (Thermo Fisher, Catalog# R37609) was added to each well and cells were incubated at 37˚C and 5% CO_2 for 15 min.

Microscopy and Image J analysis

Images were taken using an Evos Floid microscope (ThermoFisher) and were assessed using Image J software. Output was exported and analyzed using SPSS Statistics 26 (IBM) and figures were created using Graph Pad Prism Version 5 (Le Jolla, CA).

Results

A one way ANOVA was conducted to compare the different percentages of asyn binding aptamer in complete media to assess how these altered the viability of the SHSY-5Y cells by use of a Live dead cell assay. The groups that received the asyn aptamer treatment at the 45%, 60%, and 100% doses were excluded from the analysis because there were no living cells visible (making the ratio of live to dead cells 0). The ANOVA of the percent dead cells as a function of the percentages of asyn aptamer administered, revealed a between group difference, $F_{(4,9)} = 970.59$ ($p < 0.001$). As indicated in Figure 4, it was apparent that cell death was elevated to a greater extent when 30% of asyn binding aptamer was included in the cell culture media. Indeed, at 30% asyn aptamer treatment, cell death was elevated by over 400%.

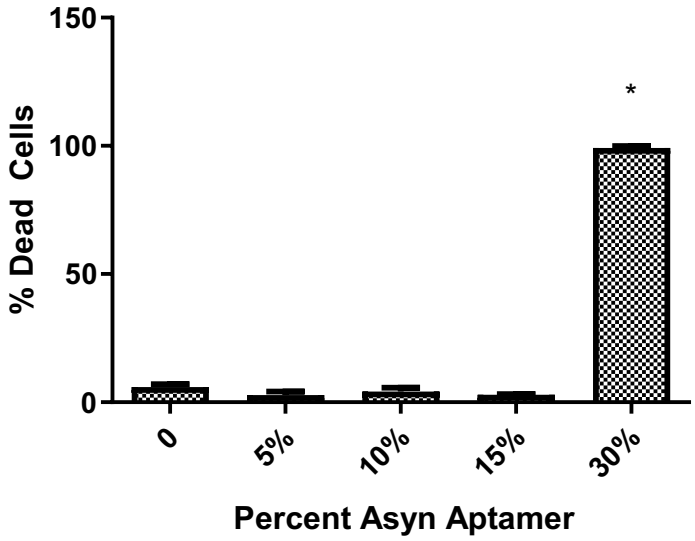

Figure 4: Comparing % Dead cells for the different percent Asyn aptamer groups (0, 5, 10, 15, 30%) where all bars represent the mean % Dead Cells ± SEM. * $p<0.01$

Experiment 1.3

Experimental Treatment groups

To better understand the effect of the asyn aptamer and to determine the influence of elevated percent asyn aptamer in complete media on cell viability, multiple aptamer treatment concentrations were assessed. Experiment 1.3 paralleled that of Experiment 1.2, except that it included a lower range of asyn aptamer concentrations to identify an ideal concentration of this aptamer so that cell death was not promoted. The experimental concentrations were: 0%, 5%, 10%, 15%, 20%, 25%, 30%, plus 30% of a non-binding aptamer (n = 3 per concentration) of the overall complete media solution. Each experimental concentration was assessed in triplicate. The concentration of the asyn aptamer was 25 μM and modified with Cy5 for fluorescent detection purposes. Eight treatment groups comprised 0% asyn aptamer treatment (Control) and varying concentrations of asyn binding aptamer treatment, as well as a 30% non-binding asyn aptamer treatment.

The cellular growth and differentiation procedure was identical to that of Experiment 1.2. Cells were maintained in an incubator at 37˚C and 5% CO_2.Following differentiation, SHSY-5Y cells were treated with the asyn binding aptamer in complete media and incubated at 37˚C and 5% CO_2. The procedure was identical to that of Experiment 1.2 as was the microscopy and Image J analysis.

Results

A one way ANOVA conducted to compare percent dead cells across all treatment groups indicated a treatment effect, $F_{(7,9)} = 5.940$; $p=0.008$. Fishers LSD post-hoc analysis revealed that 0% to 20% asyn aptamer treatment produced significantly fewer ($p<0.01$)

dead cells than did the 25% and 30% asyn aptamer treatments. Also, there was no significant difference in the % dead cells in comparison to the 30% non-binding aptamer treatment group (see Figure 5).

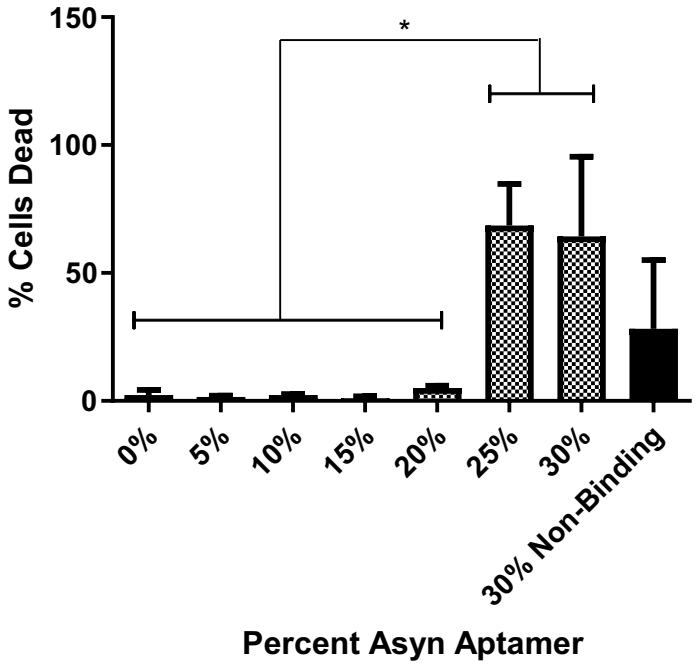

Figure 5: Comparing % Dead cells for the different percent asyn aptamer treatment groups (0, 5, 10, 15, 30%) where all bars represent the mean % Dead Cells ± SEM. *$p<0.05$

Experiment 1.4

Cell growth and Differentiation

A further experiment assessed the long-term changes of asyn protein conformations following transfection with the A53T-eGFP virus. Cells were differentiated using retinoic acid in complete media. For experimental procedures, cells were plated at a concentration of 5 x 10^3 cells/mL in warmed (37˚C) growth medium in a sterile 24-well plate with a coated glass coverslip at the bottom of each experimental well. Otherwise, the procedure was identical to that of Experiment 1.1.

Viral Transfection

Following a week of differentiation, cells were treated with an A53T-eGFP alpha-synuclein virus in DMEM (MOI of 3). The SHSY-5Y cells were incubated with 500uL of the virus solution at 37˚C and 5% CO_2 for 24 hours. Twenty-four hours afterwards, viral solution was removed and replaced with 500uL of warmed complete growth media. Cells were incubated in the complete media at 37˚C and 5% CO_2 for an additional 18 days, during which complete growth media was replaced every 48 hours. The procedural timeline is provided in Figure 6.

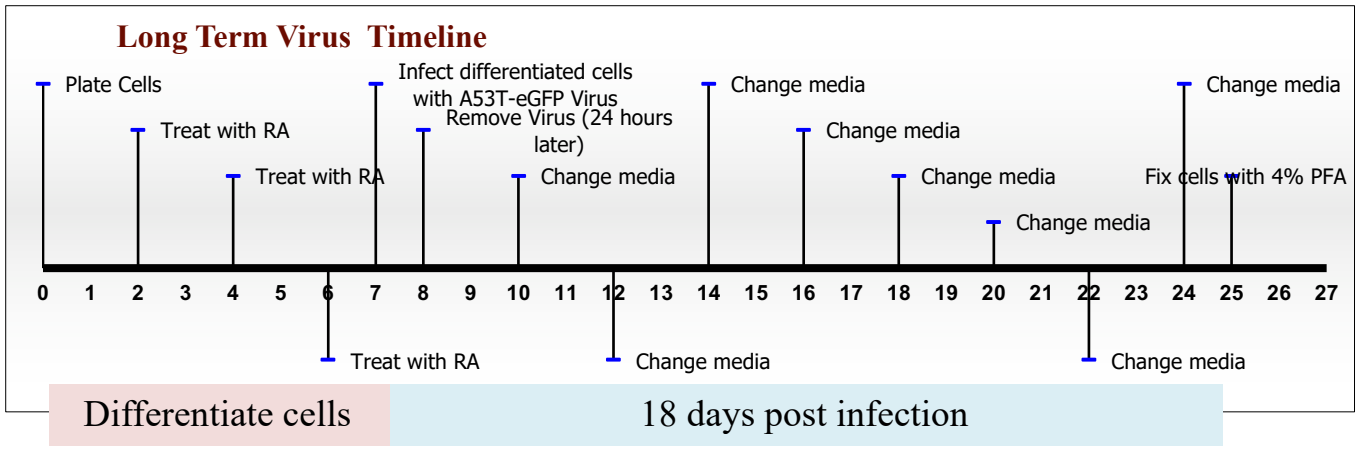

Figure 6: Timeline for Experiment 1.4

Where days are along the X-axis, RA= Retinoic Acid, and PFA= Paraformaldehyde

Fluorescent staining of SHSY-5Y cells

At the desired time, the procedures conducted were identical to those of Experiment 1.1. In addition to staining for pAsyn an additional antibody (filament Asyn (1:1000 Abcam, #ab209538) was used to assess filament asyn protein.

Fluorescent Microscopy

Images were collected using a fluorescence microscope (Zeiss LS560) at 63X. Excitation wavelength for Alexa Fluor 594 was 594nm, while for A53T-eGFP was 488nm; proper filters were chosen to maximize signal and minimize background. Images were assessed using Image J software. To assess the fluorescent images, first channels were split and the red channel was assessed in Image J. Integrated density per area (um^2) for 10-15 cells was assessed by comparing each cell to background integrated density. Three technical replicates were assessed for each coverslip. Relative integrated density was calculated and averaged for each experimental treatment group. Data were analyzed using SPSS Statistics 26 (IBM) and figures were created

using Graph Pad Prism Version 5 (Le Jolla, CA).

Results

Visualizations of the SHSY-5Y cells were prepared to identify the organization and distribution of different asyn conformations. As depicted in Figure 7, the images revealed that pAsyn collected close to the nucleus of cells, whereas filament asyn was found more widely distrubted in the cytosol.

A)

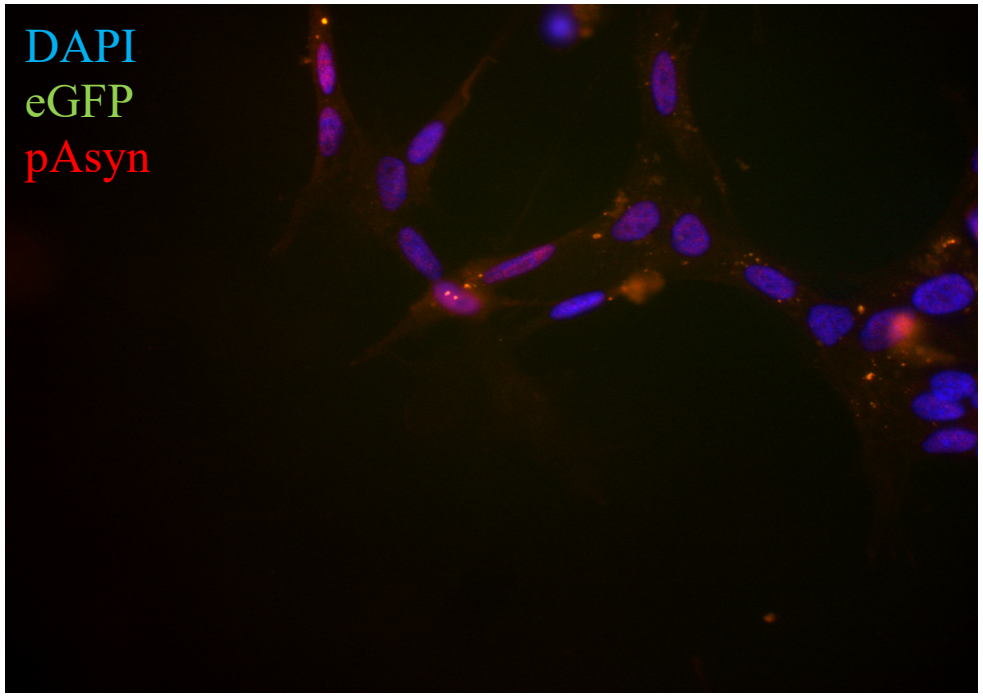

B)

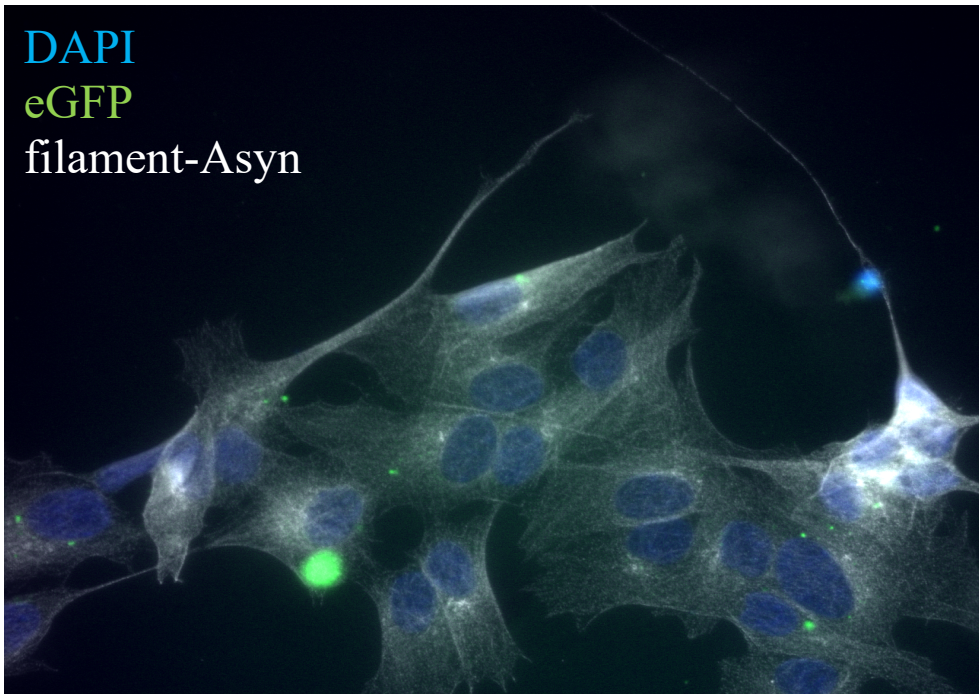

Figure 7: Cell images taken 18 days post infection

Where A) Depicts cells stained with DAPI (Blue), A53Tl-eGFP virus (Green), and pAsyn (pSer129; purple) B) Depicts cells stained with DAPI (Blue), the A53T-eGFP virus (Green), and filament asyn (white)18 days post transfection. Images were taken at 63X using a Zeiss LS560 microscope.

Experiment 1.5

Experimental Treatment groups

To assess the effect of the aptamer on asyn protein expression, three different stock concentrations were evaluated. The aptamer was administered to differentiated SHSY-5Y cells at 10% of the overall complete media solution using 5, 10, or 25 μM stock asyn aptamer concentrations and modified with Cy5 for fluorescent detection purposes. This experiment comprised a 2 (single vs repeated treatment) x 3 (concentrations: 5, 10, and 25 μM) factorial design with two external control conditions. Specifically, the treatments were applied on either a single occasion or on 8 occasions as described earlier. The two control conditions comprised no virus manipulation and one in which a virus was present but no other treatment was administered. Two different asyn protein stains, as described earlier, were assessed on each experimental treatment group, n=3.

Following differentiation, SHSY-5Y cell growth media was changed every 48 hours for 18 days post viral transfection. During the media changes asyn binding aptamer was also administered to the applicable conditions and the plates were incubated at 37˚C and 5% CO_2. Following 18 days of media changes and asyn aptamer treatment(s), cells were fluorescently stained and fluorescent microscopy was conducted as described in Experiment 1.4.

Results

Separate univariate fixed factor ANOVAs were used for each antibody under investigation (two fixed factors). The analysis of the % fluorescent intensity of pAsyn revealed a significant Treatment Concentration x Condition (Single vs Multiple) interaction, $F_{(2,24)} = 103.44$, $p<0.001$. Suggesting that Treatment concentration and Condition combine to have an effect on % fluorescent intensity of pAsyn. The follow-up tests revealed that 25 μM virus + multiple treatment condition produced a greater change in fluorescence than did the single treatment or that of the lower concentrations of asyn aptamer administered repeatedly (see Figure 8a). Furthermore, to assess the influence of the treatment to external controls Dunnett's test was conducted. This test revealed that at the 25 μM concentration % fluorescent change in pAsyn was greater than that apparent in either of the two control conditions.

ANOVA for filament asyn protein indicated that neither the treatment (5, 10, and 25 μM), the treatment condition (single vs multiple), nor the interaction reached statistical significance (as seen in Figure 8b).

A)

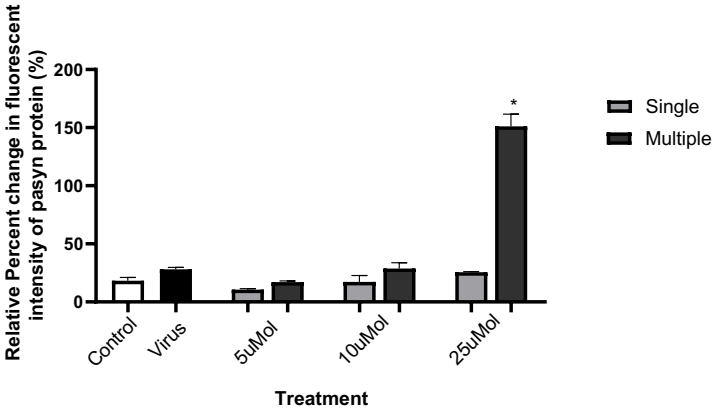

B)

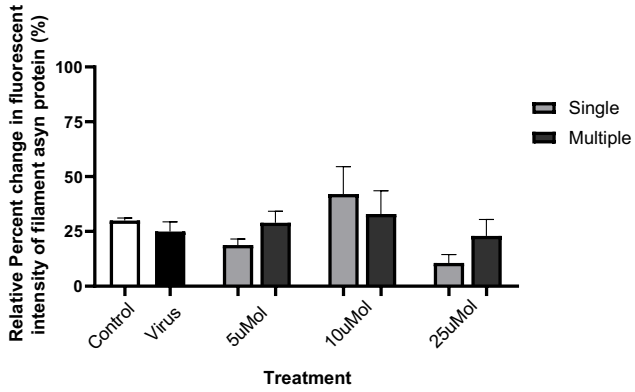

Figure 8: A) Mean Relative Change in Fluorescent intensity of pAsyn protein ± SEM for cells treated with 5μM, 10 μM, and 25 μM Asyn Aptamer B) Mean Relative Change in Fluorescent intensity of Filament Asyn protein ± SEM for cells treated with 5 μM, 10 μM, and 25 μM Asyn Aptamer. * = $p<0.05$

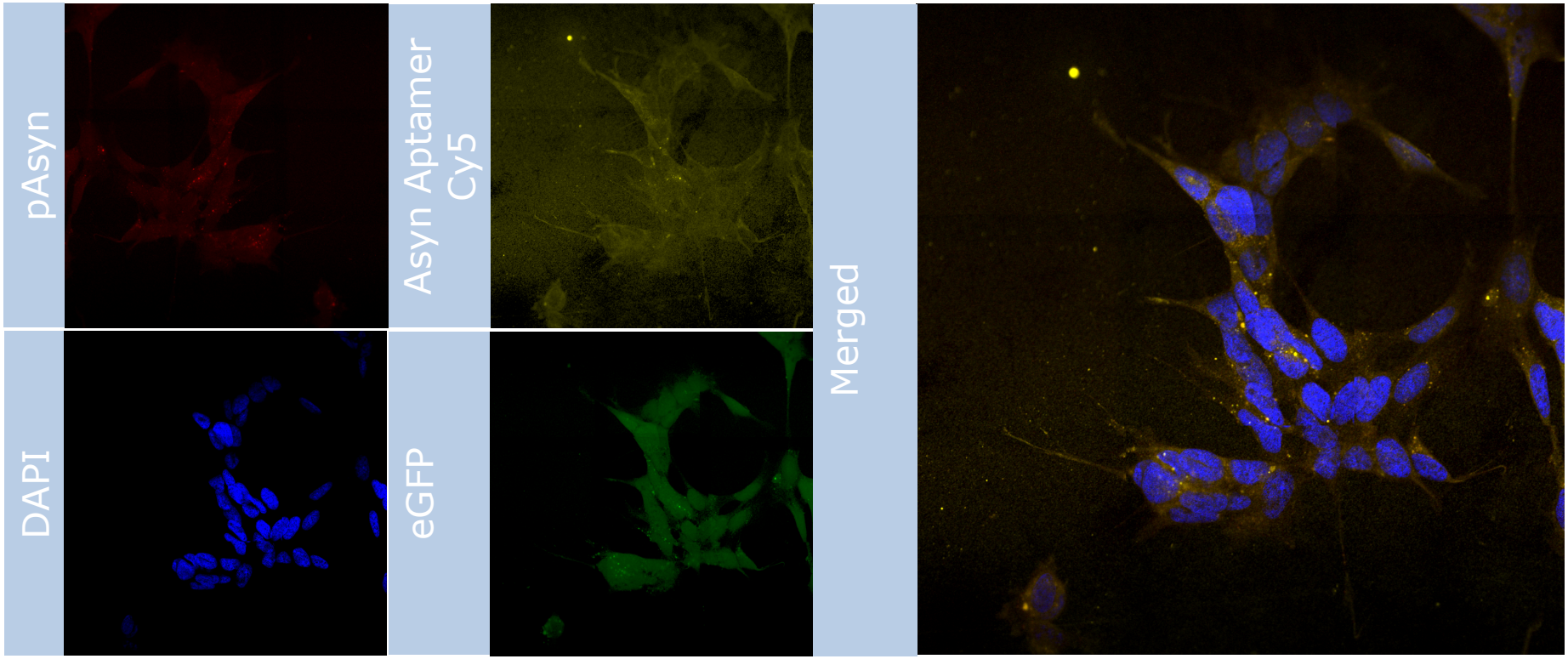

Figure 9: Visualization of virally infected SHSY-5Y cells treated once with 5 μM asyn binding aptamer in an 18 day post infection cellular model. Cells are stained for DAPI, eGFP (A53T virus), Cy5 labelled asyn binding aptamer, pAsyn, and a merged image (shown on the far right).

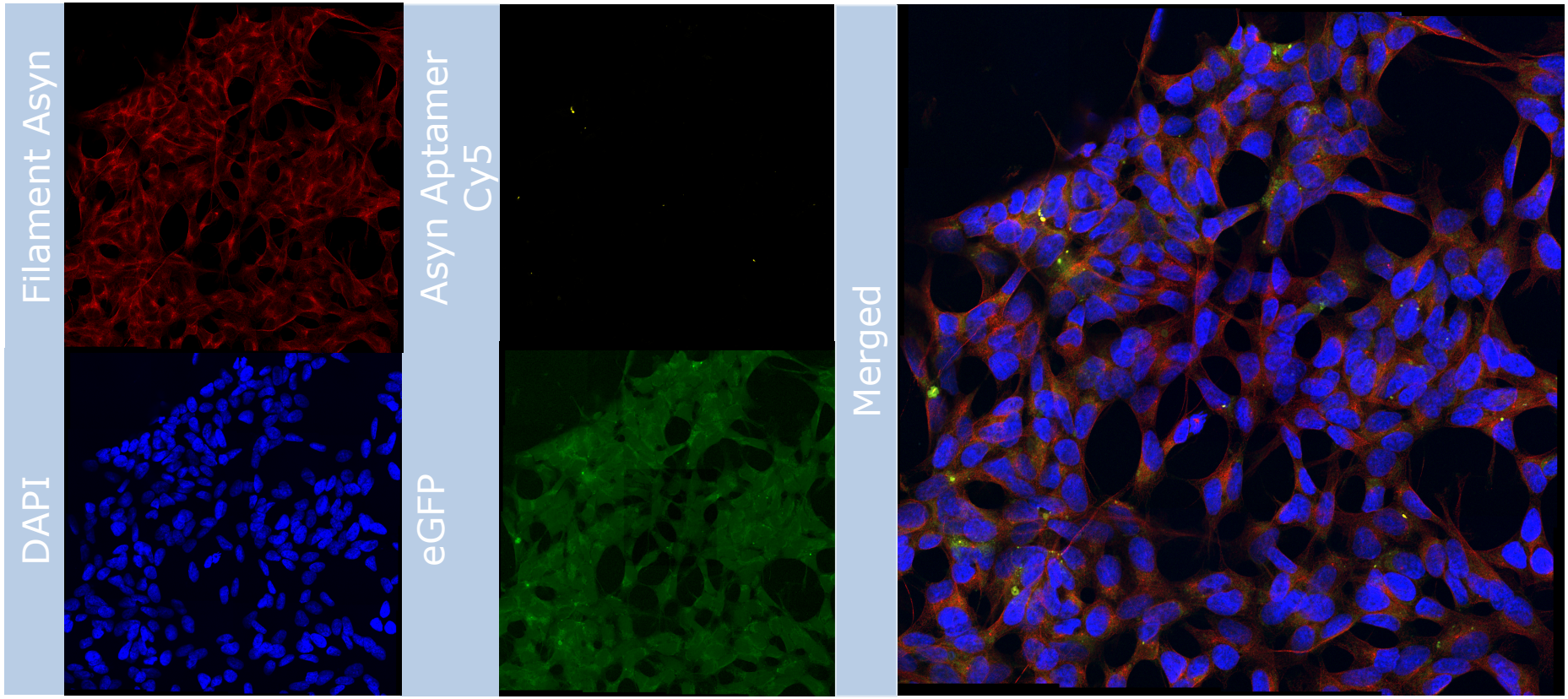

Figure 10 : Visualization of virally infected SHSY-5Y cells treated once with 5 μM asyn binding aptamer in an 18 day post infection cellular model. Cells are stained for DAPI, eGFP (A53T virus), Cy5 labelled asyn binding aptamer, filament asyn, and a merged image (shown on the far right).

Experiment 1.6

Experimental Treatment groups

Experiment 1.6 assessed the influence of the aptamer on asyn protein expression using Western blot analysis to parallel the earlier study using immunofluorescent staining. The asyn aptamer was administered to differentiated SHSY-5Y cells at 10% of the overall complete media solution using 5 μM or 10 μM stock asyn aptamer concentrations and modified as previously described. Six treatment groups were processed for Western blot analysis. The treatments comprised asyn being provided at a concentration of 5 or 10 μM on either a single or multiple occasions as described in the preceding study. As well, a no virus and virus control condition was included in this experiment. Two different Westerns for Asyn (pAsyn Antibody, abcam # 59264) and Oligomer Asyn (Syn33, Sigma Catalog# ABN2265) were performed for each of the treatment groups (n=3 per group for each Western).

Sample Preparation – Western Blot

Once the experimental manipulations had been completed, samples were collected for Western Blot analyses. To this end, all media was removed from each well. Then, 1 mL of sterile PBS was added to each well and a sterile cell scraper was used to collect cells from the bottom of each well. Using a pipette, the lifted cells and 1 mL PBS were deposited into a 15 mL Falcon Tube. This process was repeated twice again. In order to collect enough protein for Western blot techniques, technical triplicates were merged yielding a total of 9 mL of PBS and all possible scraped cells for each sample. All 15 mL falcon tubes were centrifuged at 700G for 10 min at 4°C. Each cellular pellet was kept at -

80°C and the remaining liquid was discarded.

Protein Quantification

In order to prepare each sample for Western blot analysis, proteins were quantified using Pierce's BCA Protein Assay Kit (ThermoFisher, Catalog# 23227) and a 96 well microplate. The kit instructions were followed and sample quantification was determined using a microplate reader (Molecular Devices, Spectra Max 190) and reading at 540nm. Samples were preserved in 5X Loading Buffer in a ratio of 4:1. Samples were prepared to concentrations of 1 ug/uL of protein and then vortexed and heated for 5 min in a heat block set to 105 ºC. After heating, samples were placed on ice for 5 min and stored at -20ºC until processed for Western blot analyses.

Western Blot

For asyn protein detection from cell culture, total protein was determined using a REVERT total protein solution as previously described [67]. Following determination of total protein levels and appropriate washes in tris buffered saline (TBS; pH 7.5; 2 X 5 min each), membranes were blocked for 60 minutes in a TBS solution containing 0.5% fish gelatin (Sigma Catalog # G7041). Membranes were then placed in a 0.5% fish gelatin TBS solution containing either a purified mouse anti-alpha-synuclein (1:2000; Sigma Syn33, Catalog# ABN2265) or an anti-alpha-synuclein (1:1000; Abcam, Catalog # Ab59264), for a period of 90 min in 0.05% fish gelatin in TBS with 0.1% tween. Following incubation in the primary antibody and subsequent washes in TBS-T, membranes were incubated in infrared conjugate directed against the species to which the

primary antibody was raised (Rabbit 800, LI-COR) at a concentration of 1:20 000 in a 0.5% fish gelatin TBS solution containing 0.2% tween and 0.01% SDS. Membranes were washed in TBS to remove any unbound antibody, protein bands were read for 6 min on a Licor Odyssy system at the appropriate wavelength.

Results

Separate ANOVAs were conducted to assess both normalized pAsyn signal and normalized oligomer asyn (Syn33) for the different treatment groups. The 2 concentrations (5 µM or10 µM) x 2 conditions (single vs multiple) ANOVA revealed that the 5 µM dose was significantly lower than that of the 10 µM treatment, $F_{(2,22)} = 4.72$, p=0.024. As well, the Treatment dose x Repeated condition interaction approached statistical significance, $F_{(1,22)} = 3.829$, p=0.068, showing that the effect of the 5 µM dose was prominent in the single treatment condition, whereas this was not apparent with the 10 µM treatment concentration. The Dunnett's test further indicated that the control samples were significantly lower than those in the 10 µM condition as well as the 5µM treatment administered repeatedly. The virus control likewise differed from the 10 µM single and multiple treatment groups. In contrast, the ANOVA comparing normalized Syn33 signal revealed no effect of the asyn aptamer treatment, $F_{(5,18)}= 0.213$ (p=0.952), and likewise no statistically significant differences existed with respect to the Syn33 signal for the different treatment groups (see Figure 11 and 12).

A)

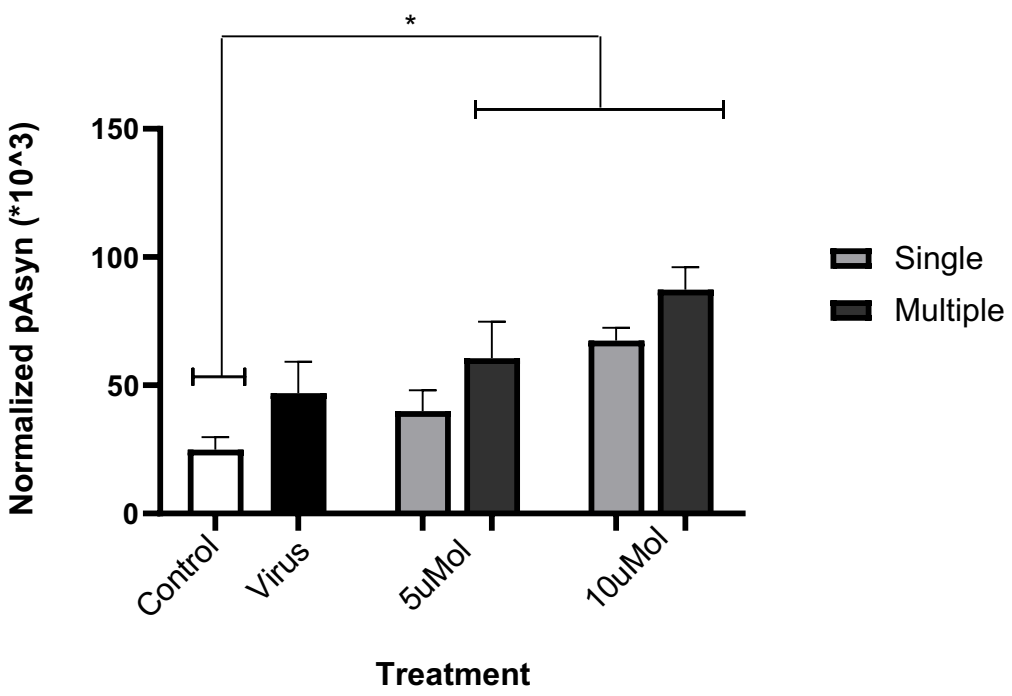

Control	Virus	5 µM Single Apt	5 µM Multi Apt	10 µM Single Apt	10 µM Multi Apt

B)

Figure 11: A) Comparing Normalized (A) pAsyn (pSer129) expression (x 10^3) ± SEM and (B) Representative Blots of differentiated SHSY-5Y cells treated with 5 μM or 10 μM Asyn binding aptamer in a long-term cell culture experiment

A)

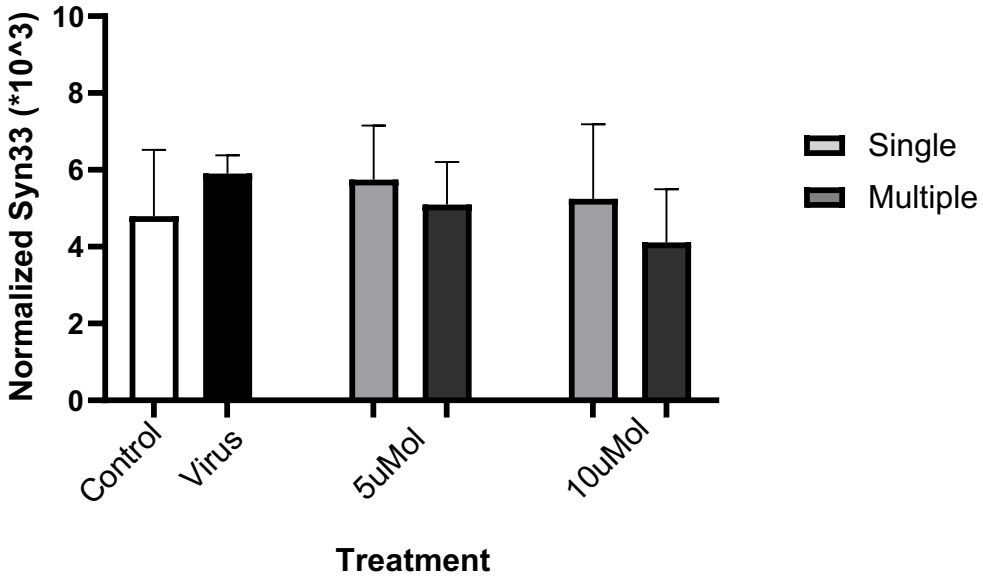

B)

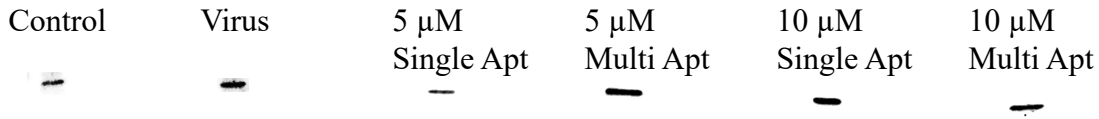

Figure 12 A) Comparing Normalized Oligomer Asyn (Syn33) expression (x10^3) ± SEM and (B) Representative Blots of differentiated SHSY-5Y cells treated with 5 μM or 10 μM Asyn binding aptamer in a long-term cell culture experiment

Discussion:

The 25 μM asyn aptamer dose led to an unexpected, pronounced elevation of pAsyn protein. In fact, this outcome was in the direction opposite to that predicted. It is possible that this effect was a reliable one, but it is equally possible that it was artifactual. Unfortunately, with only 3 samples in each group, a small n bias may have resulted in a unreliable outcome. Accordingly, in subsequent studies only the 5 μM and 10 μM doses were used. Furthermore, in this study the protein quantification used for Western blot analyses was low (1μg/μL), which may have limited the accuracy of the findings. As a result of this low protein yield, potential differences that might have existed between treatment groups could not be detected. Since this procedure is unique and has not previously been evaluated in the context of the present investigation, earlier studies were not available to offer guidance as to best practices.

One of the concerns in using the aptamer, much like any other method to modify functioning, there was the concern that the treatment would actually promote cell death. However, as far as could be determined, this did not materialize given that cell death was no greater using this specific aptamer relative to that produced by a scrambled aptamer variation. Further, it is possible that *in vivo* the aptamer could be broken down by various body organs, immune related responses, or removed by reparative and restorative processes. In the present investigation the aptamer was left in place without being eliminated, the possibility ought to be considered that asyn binding aptamer may have had additive or synergistic effects when administered to cells repeatedly *in vitro*.

Finally, a further limitation of evaluating the aptamer *in vitro* concerned the potential influence of multiple endogenous factors that could not be assessed.

Accordingly, it might be more appropriate to evaluate the actions of the asyn binding aptamer *in vivo*, which was done in the ensuing experiments.

Chapter 3:
Study 2: Distribution of the asyn binding aptamer in vivo

Introduction:

Having investigated the asyn binding aptamer in a cellular model it was of interest to determine whether systemic administration of the asyn aptamer reaches the brain *in vivo*, as well as to determine the longevity of aptamer presence. *In vitro* experiments had suggested that a single treatment with the asyn binding aptamer produced reductions of pAsyn and filament asyn (confirmed by fluorescent intensity staining). Additionally, decreased pAsyn and oligomer asyn were observed (confirmed by Western blot analysis). In contrast, the findings of Experiments 1.5-1.6 suggested that the asyn binding aptamer may have an additive effect when repeatedly administered to SHSY-5Y cells in a cell culture model. These findings suggest that our asyn binding aptamer treatment might not have been effective in isolated cells. Yet, analyses conducted *in vitro* do not have the benefit of peripheral factors that could influence the breakdown of the aptamer. In essence, the model would be best assessed *in vivo* wherein the collective influences on aptamer disposition could be determined.

To introduce this aptamer into a murine model we adopted a delivery vehicle designed to cross the blood-brain-barrier (BBB). In these experiments we employed a previously developed modified liposome as a delivery vehicle [117]. This pegylated liposome has a transferrin receptor aptamer (TRA) modification on the surface that was designed to hijack the transferrin receptors of endothelial cells of the brain. The asyn binding aptamer was loaded into these liposomes using a dialysis procedure.

With this method in hand, a series of experiments assessed the asyn binding aptamer in wildtype mice of the M83 line. This particular line of mice was used since we had planned to subsequently assess the impact of the asyn binding aptamer in transgenic

mice (Chapter 4) and thus it was important to determine the effects in an appropriate wildtype control mouse. Furthermore, in these experiments we evaluated the distribution of the asyn binding aptamer in several brain regions as well as the liver. The liver was selected because it is known to house many transferrin receptors and also because it is the first location in which the asyn binding aptamer will appear following its administration. Of relevance was that this *in vivo* model afforded the opportunity to determine, at least in a preliminary way, the time-course for the asyn binding aptamer's presence.

Materials and Methods:

Experiment 2

Animals and general experimental design

Eighty male B6C3F1/J mice were obtained at 8-10 weeks of age from The Jackson Laboratory, Bar Harbor, ME and were acclimated to the vivarium for 10 days prior to commencing the experiment. All animals were individually housed in standard polypropylene cages (27 x 21 x 14 cm) and maintained on a 12-hour light/ dark cycle with lights on at 08:00 hours. A diet of 2014 Purina mouse chow and water was provided *ad libitum* and room temperature was maintained at ~ 21°C. All procedures were approved by the Carleton University Animal Care Committee in accordance with the guidelines set out by the Canadian Council for Use and Care of Animals in Research.

Experimental Procedure

Animals were assigned to one of three treatment groups: (i) empty liposome (n=16) (ii) 100 uL asyn Aptamer (n=32) (iii) 200uL asyn Aptamer (n=32). On the experimental test day, animals were administered an intraperitoneal (i.p.) injection with the assigned treatment. Animals within each treatment were further separated into one of four conditions in which mice were sacrificed at varying times following treatment (15 min, 30 min, 1 hr, 2 hr). Thus, the design of this experiment comprised a 3 (aptamer dose) x 4 (time between treatment and sacrifice) factorial with either 4 or 8 mice in each of the groups.

Brain extraction

At the prescribed time following aptamer injection mice received an overdose of sodium pentobarbital (48 mg/kg i.p). Animals were then transcardially perfused using 10mL of Phosphate Buffered Saline (0.01M PBS) and brain tissue (motor cortex & midbrain) and liver samples were collected for qPCR. The tissue was immediately frozen upon dissection and stored at -80°C until processing.

DNA Isolation

Genomic DNA was isolated from each sample using a Qiagen DNEasy Blood & Tissue Kit (catalog # 69506). A small piece (~8mg) of each sample was placed in a 1.5mL microcentrifuge tube with 20uL of Proteinase K and 180uL of Buffer ATL. Sample and solutions were vortexed and incubated at 56°C overnight until completely lysed. The following morning, 200uL of Buffer AL and 200uL of 100% Anhydrous Ethanol was added to the microcentrifuge tube and vortexed. The entire mixture was transferred to a DNEasy Mini spin column in a 2mL collection tube. The column was centrifuged at 8000 RPM for 1 min and flow through was discarded. The spin column was placed in a new 2mL collection tube and 500µL of Buffer AW1 was added to the spin column, which was centrifuged for 1 min at 8000 RPM. Flow through was again discarded and the spin column was placed in a new 2mL collection tube and 500µL of Buffer AW2 was added to the spin column. Columns were centrifuged once more for 3.5 min at 17,220 X G. Flow through was discarded and the spin column transferred to a new 1.5mL microcentrifuge tube and 200µL of Buffer AE was added to the center of the spin column membrane. The sample was incubated for 1 min at room temperature (~25°C) and was

centrifuged for 1 min at 8000 RPM. Sample quality and concentrations were determined by absorbance at 280nm and 260nm with a NanoDrop Lite spectrophotometer. Samples were diluted with DEPC-treated water to a concentration of 10 ng/µL

RT-PCR

Samples were stored at -20°C prior to analyses. RT-PCR was conducted on all gDNA samples to determine Cq values using primers designed to detect the asyn aptamer. Five microliters of each gDNA sample were loaded into separate wells in a 96-well PCR plate. Two microliters of 10 mMol forward primers (5'-ATA GTC CCA TCA TTC ATT -3'), 2µL of 10 mMol reverse primers (5'- TGA CAC TTG CTA ATA TCT- 3'), 1µL of DEPC-treated water, and 10 µL Sybr Green Supermix with fluorescein (Bio-Rad Laboratories Inc., Hercules, California) were added to each well. Samples were run in triplicate along with non-template controls. The plate was run on CFX Connect Real-Time PCR Detection System (Bio-Rad) for 30 sec at 90°C, followed by 40 cycles of the following settings: 10 sec at 90°C for denaturing and 40 sec at 60 °C for annealing. The plate was then run at 65°C for 5 sec, then to 95°C for 5 sec, and back to 65°C to generate a melt curve by increasing temperature from 65 °C to 95°C for 5 seconds. All primers were tested for amplification efficiency using the standard curve method, yielding efficiencies over 95%.

Quantification of Aptamer Molecules

A dilution series of known aptamer concentrations was run in triplicate by RT-PCR using the same reactions and equipment stated earlier. The R^2 for the relationship was

determined to be 0.99. The linear relationship between Cq value (y) and concentration (x) was determined to be $y = -1.265ln(x) - 20.871$. Since Cq values were determined for each sample by RT-PCR, the aforementioned equation was used to isolate for *x* and determine the detected concentration of the asyn aptamer within each sample. This concentration was then multiplied by Avogadro's number (6.022×10^{22}) and divided by 200,000 to calculate the number of molecules/ 5 μL.

Results

Figure 12a shows the average Cq values from motor cortex homogenate. The ANOVA revealed a significant Aptamer dose x Time interaction, $F_{(6,68)} = 4.82$, $p<0.001$. Follow-up Tukey's HSD tests of the simple effects comprising this interaction revealed that at 15 min both aptamer doses reduced the Mean Cq value, whereas at 30 min only the 200uL asyn aptamer dose produced such an outcome (p's <0.001). No significant differences were detected 1 or 2 hr after asyn aptamer treatment.

In Figure 12b the average Cq values for midbrain homogenates are shown. The ANOVA revealed a significant interaction between Asyn aptamer dose x Time, $F_{(11,68)} = 7.69$, $p<0.001$. The follow-up tests confirmed that the 100uL and 200uL doses reduced the Cq values throughout ($p<0.001$), except for a less pronounced effect of the 200uL dose 1hr following treatment ($p = 0.077$). In essence, while the interaction was significant, this was primarily accounted for by the single difference (at 1 hr using the 200 uL asyn aptamer) and it is likely that the main effect of treatment was the principal difference between groups.

The average Cq values from liver homogenate are shown in Figure 12c. The ANOVA revealed a significant main effect of the asyn aptamer dose ($F_{(2,17)} = 41.490$, $p<0.001$) as well as a significant interaction of the asyn Aptamer Dose x Time interaction ($F_{(11,68)} = 4.562$, $p<0.001$). The follow-up tests for the simple effects of aptamer dose indicated that the Cq values at both doses were reduced relative to the control (empty liposome) condition at each of the four time points. These follow-up tests also indicated that the magnitude of this difference was less pronounced at 1 hr than at the other times and was greatest at 15 min.

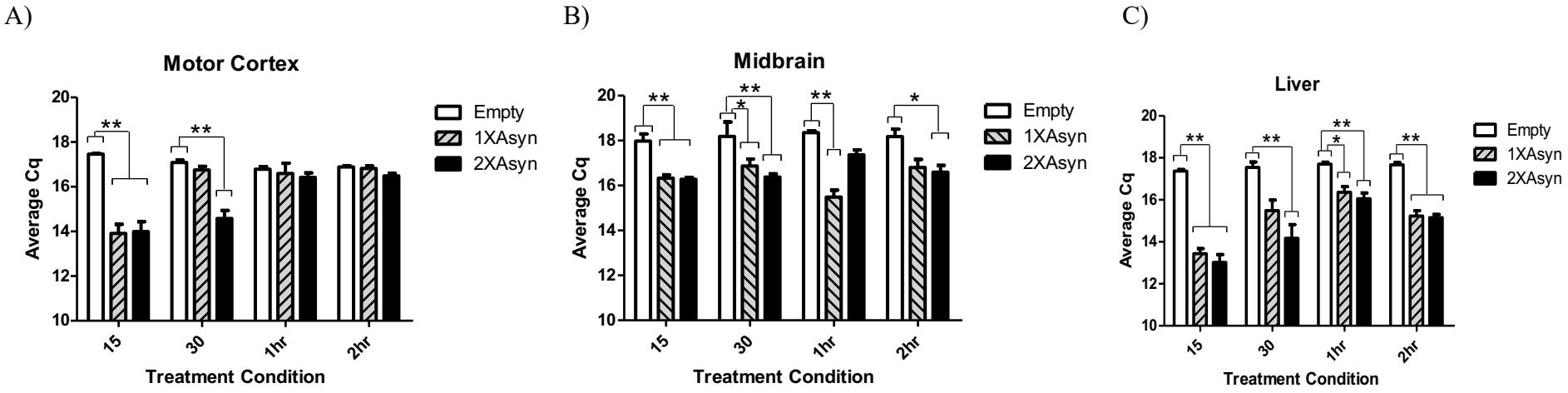

Figure 13: Average Quantification Cycle (Cq) detected for the Asyn Aptamer in (A) Motor Cortex (B) Midbrain (C) Liver for B6C3F1/J male mice treated with 100 µL αSyn Aptamer (1X Asyn) , 200 µL αSyn aptamer (2X Asyn) or a control treatment (empty liposome). All values represent average Cq Values ± SEM. Significant differences determined by Tukey's HSD post-hoc analysis are denoted by *p <0.05; ** p<0.01

In addition to evaluating the Cq values it was of interest to present the actual number of molecules that were present as a result of the experimental treatments. As the number of molecules is derived from the Cq value, the statistical results essentially mirrored one another. This said, ANOVAs were conducted to confirm the Cq findings, (the figures that follow provide asterisks to denote significant between group differences based on these ANOVAs and follow-up tests).

In Figure 13a the average number of molecules of asyn aptamer were calculated and are reported for the motor cortex at all time points (15 mins, 30 mins, 1hr, and 2hr). As seen in Figure 11a, 15 min following treatment with the 100 µL or 200 µL asyn aptamer the number of molecules exceeded that of all other treatment conditions. As well, the number of molecules promoted by 200 µL asyn aptamer treatment 30 min following treatment exceeded that of later time points.

Figure 13b shows the average number of molecules within the midbrain at the various time points. As seen in the Figure, 1 hr following treatment the 100 µL asyn aptamer the number of molecules exceeded that of all other treatment conditions (where, $p<0.01$). At 1 hr following treatment with 100 µL asyn aptamer, the number of molecules of asyn aptamer differed from the 200 µL asyn aptamer treatment at that time and from that seen 15 min following treatment ($p<0.05$).

The average molecules of asyn aptamer in the liver were calculated and are depicted in Figure 13c across all time points. As seen in this Figure 11c 15 min following treatment with 100 µL asyn aptamer the number of molecules differed from that evident at any other time. With the 200 µL asyn aptamer treatment the number of molecules exceeded that detected at the 1 and 2 hr time points ($p<0.01$).

Table 1: Number of Molecules of asyn aptamer/ 5μL for (A) Motor Cortex, (B) Midbrain, and (C) Liver Homogenate at 15 min, 30 min, 1 hr, and 2 hr following treatment with 100 μL of asyn aptamer (1X Asyn Apt) or 200 μL of asyn aptamer (2X Asyn Apt) where numbers represent the average number of molecules for the treatment group.

(A) Motor Cortex Homogenate							
15 mins		30 mins		1hr		2hr	
1X Asyn Apt	2X Asyn Apt	1X Asyn Apt	2X Asyn Apt	1X Asyn Apt	2X Asyn Apt	1X Asyn Apt	2X Asyn Apt
4747722.05	4670857.52	385958.17	2071657.06	456619.45	531184.77	355832.61	463075.94
(B) Midbrain Homogenate							
15 mins		30 mins		1hr		2hr	
1X Asyn Apt	2X Asyn Apt	1X Asyn Apt	2X Asyn Apt	1X Asyn Apt	2X Asyn Apt	1X Asyn Apt	2X Asyn Apt
533121.95	536975.52	395551.40	514941.51	1144744.71	246554.49	455036.12	505264.31
(C) Liver Homogenate							
15 mins		30 mins		1hr		2hr	
1X Asyn Apt	2X Asyn Apt	1X Asyn Apt	2X Asyn Apt	1X Asyn Apt	2X Asyn Apt	1X Asyn Apt	2X Asyn Apt
5759575.67	8778443.72	1452567.46	6130795.08	566531.21	765989.65	1390834.29	1355822.98

A)

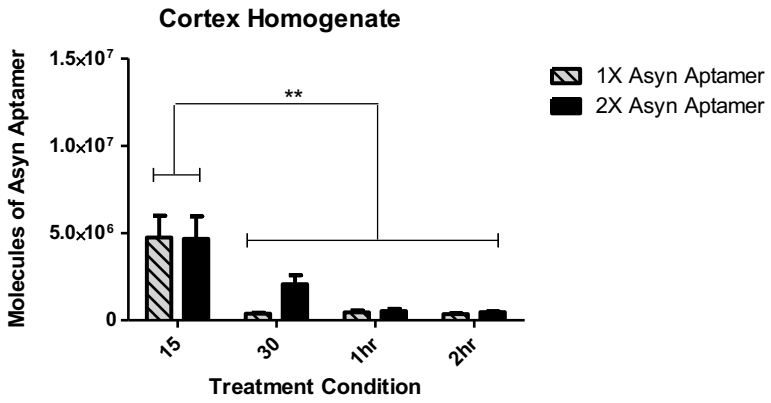

B)

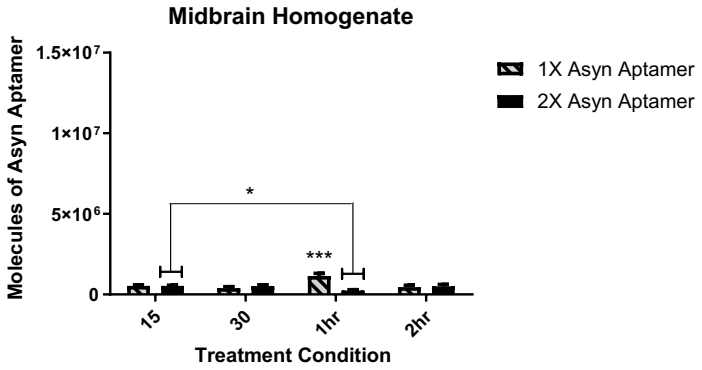

C)

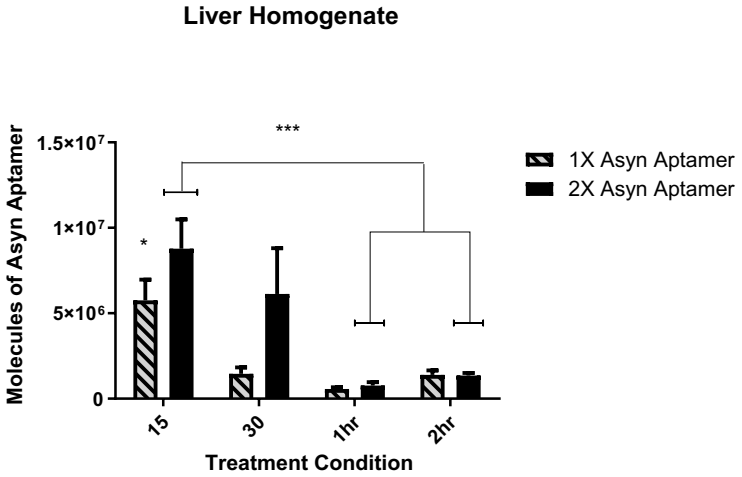

Figure 14: Average Molecules of asyn aptamer/µL calculated in (A) Motor Cortex (B) Midbrain (C) Liver for B6C3F1/J male mice treated with 100 µL asyn aptamer (1X Asyn Apt) or 200 µL asyn aptamer (2X Asyn Apt). All values represent average Molecules of asyn aptamer/μL Values ± SEM. Fishers LSD post-hoc analyses are presented in the figure above. *p <0.05; ** p<0.01

Discussion

A substantial finding from this set of experiments is that our delivery vehicle can transport the asyn binding aptamer across the BBB. One of the major challenges when it comes to developing treatments is that of penetrating the BBB to have disease modifying effects present within the central nervous system.

It is clear from Study 2 that the asyn binding aptamer can be detected in different brain regions and in the liver by RT-PCR. Specifically, immediately following treatment, the highest levels of the asyn aptamer was present in the liver, as predicted given that the aptamer was administered intraperitoneally. Significantly, within 15 minutes of administration the aptamer was detected within the motor cortex and midbrain regions.

One concern of these experiments is that it is uncertain whether the asyn aptamer detected using RT-PCR primers reflects free floating asyn aptamer or that bound to the target. It is possible that the asyn binding aptamer had not yet reached its target and was still free floating, as opposed to the aptamer being bound to its target and functioning as designed. Finally, it is possible that we were unable to fully detect the aptamer that had entered the central nervous system because of natural decomposition processes. The resulting fragmented sequence would not be amplified with the RT-PCR process.

Once again, the absence of information from other studies makes it impossible to determine the generalizability of the present findings. Likewise, it is uncertain how long these brain changes persist. Accordingly, in attempting to develop preclinical models relevant to Parkinson's disease it remains unclear what schedule of treatment would be considered most appropriate.

Chapter 4:
Study 3: Assessing the asyn binding aptamer in vivo

Introduction

Although much is understood regarding the processes leading to Parkinson's disease, as indicated earlier the treatments available are limited to diminishing symptoms of the disorder and often treatment resistance may develop. Moreover, after chronic l-DOPA use dyskinesia may evolve [95]. The value of the asyn aptamer in a treatment capacity is of fundamental importance, particularly if it turns out to be effective when used on a long-term basis, provided that treatment resistance and motor complications do not develop. As a first step in evaluating these possibilities, experiments were undertaken to determine whether PD-like motor features would develop in transgenic mice (Jax, #004479) and whether these indications would be paralleled by pAsyn immunostaining within the motor cortex, possibly reflecting increased Lewy body formation. As well, analyses were performed to determine transgene protein repeats which might reflect the ideal crosses between mouse strains that ought to be used in modeling Parkinson's disease. A final experiment evaluated the influence of the asyn aptamer in modifying cellular signs of PD-like features in a rodent model through Western blot analyses.[1]

[1] *The original intent of this investigation was to parallel Western blot analyses with behavioural studies to determine effectiveness of the asyn binding aptamer in modifying behavioural signs of Parkinson's disease. Unfortunately, this became impossible owing to restrictions stemming from access to research facilities during COVID-19 and due to absence of access to test areas owing to delays in building construction at Carleton University.

Materials & Methods

Experiment 3.1

Subjects and general experimental design

Ninety B6;C3-Tg(Prnp-SNCA*A53T)83Vle/J mice (n = 45 male & n = 45 female) were bred in the Carleton University vivarium. The initial breeding pairs were hemizygous for Tg(SNCA)83Vle and were obtained at 8-12 weeks of age from the Jackson Laboratory (Bar Harbor, ME) and were acclimated to the vivarium for 10 days before breeding. All animals were produced from a planned pairing and were weaned at 3 weeks of age, at which time, a 2mm ear notch was collected and used to determine the genotype. All animals were group-housed (max 4 per home cage) with littermates of the same sex in standard polypropylene cages (27 x 21 x 14 cm) and maintained on a 12 hr light/ dark cycle with lights on at 08:00 hr. A diet of 2014 Purina mouse chow and water was provided *ad libitum* and room temperature was maintained at ~ 21°C. All procedures were approved by the Carleton University Animal Care Committee following recommendations set out by the Canadian Council for Use and Care of Animals in Research.

Apparatus

Noldus Catwalk

The Noldus Catwalk (XT system version 8.0) used to evaluate gait abnormalities was located in a separate room. It consisted of a corridor that directs the free movement of animal in a straight line, a hardened glass walkway that allows the Catwalk to capture each individual footprint, and a high-speed camera to capture the animals motor

movements. All gait analyses were collected in a dark room where the only equipment giving off light was the catwalk equipment and corresponding computer monitor.

Behavioural Procedure

Mice were individually placed on the catwalk and their motor gait was recorded. Each trial comprised a mouse traversing the target region within 5 sec for gait information to be collected. Mice received 3 training trials per day for 5 days prior to the test day. On day 6, the test day, the same procedure was used and the data obtained were statistically analyzed. Between all training and experimental test day sessions all components of the catwalk were wiped clean with 70% ethanol.

Procedure

Animals were assigned to one of five age groups (3, 4, 5, 6, and 7 months old) with 18 mice per age group (n = 18; equal males and females). These groups were further divided based on the three genotypes (i) wildtype (WT) (ii) 1X transgene (1X Tg) which comprised the presence of the asyn transgene band (assessed at genotyping), and (iii) 2X transgene (2X Tg) reflected by a brighter asyn transgene band (assessed at genotyping). This provided a 3 (genotype) x 5 (age) factorial design. However, as a subsequent analysis indicated that there were no significant differences in hemizygous and homozygously dominant animals for the A53T transgene, these mice were pooled in further analyses. Thus, the final design comprised a 2 (genotype) x 5 (age) factorial design.

Brain extraction

Following testing on the Noldus Catwalk animals were taken to a separate room where they received an overdose (0.15mL) of sodium pentobarbital 48 mg/kg, i.p. Ear punch samples of 2mm in diameter were collected for qPCR using a Fine Science Tools ear punch (Catalog #24214-02). The ear punch tissue was stored at -80°C until further processing. Animals were transcardially perfused using 5mL of 0.9% saline (pH 7.2) followed by approximately 50 mL of 4% paraformaldehyde (PFA). Brains were extracted and post-fixed at 4°C in 4% PFA for 24 hours. The following day, brains were placed in a 10% sucrose 0.1M phosphate buffered (PB) solution pH 7.4) on two occasions approximately 6 hr apart and maintained at 4°C between washes. Brains were then placed in a 30% sucrose 0.1M PB solution at 4°C until processing for immunohistochemistry.

DNA Isolation

Genomic DNA was isolated from each 2mm diameter ear punch sample. Crude DNA extraction was accomplished by Qiagen DNEasy Blood and Tissue sample kit (Catalog# 69506). Sample quality and concentrations were determined by absorbance at 280nm and 260nm using a NanoDrop Lite spectrophotometer. Samples were diluted with DEPC-treated water to a concentration of 10 ng/μL.

qPCR

Samples were stored at -20°C until RT-PCR was performed using gDNA samples to determine Cq values with primers designed to detect the alpha-synuclein transgene relative to a mouse transgene. Five µL of each sample was loaded into separate wells of a 96-well PCR plate. Ten µL of Kappa Taqman mastermix, 0.8 µL of 40 mMol Asyn Transgene Forward Primers (5'-TGA CGG GTG TGA CAG CAG TAG -3'), 0.8µL of 40mMol Asyn Transgene Reverse Primers (5'-CAG TGG CTG CTG CAA TG - 3'), 5.8µL of DEPC-treated water, 0.3 µL of 5 µMol Transgene Probe (FAM 5' – CCC TGC TCC CTC CAC TGT CTT – 3') and 0.3 µL of 5 µMol Mouse transgene control probe (HEX 5'– CCA ATG GTC GGG CAC TGC TCA A – 3') were added to each well. The second, separate reaction for the mouse transgene included 0.8 µL of 40 mMol Mouse Transgene Forward Primers (5'- CAC GTG GGC TCC AGC ATT – 3') and 0.8 µL of 40 mMol Mouse transgene reverse primers (5'- TCA CCA GTC ATT TCT GCC TTT G - 3'), 5.8 µL of DEPC-treated water, 0.3 µL of Transgene Probe (FAM 5' – CCC TGC TCC CTC CAC TGT CTT – 3') and 0.3 µL of Mouse transgene control probe (HEX – CCA ATG GTC GGG CAC TGC TCA A – 3') were added to each well. For each of the two single-plex reactions, samples were run in triplicate with non-template controls. The plate was run on CX5 Real-Time PCR Detection System (Bio-Rad) for 3 min at 90°C, followed by 40 cycles of the following settings: 5 sec at 90°C for denaturing and 30 sec at 60 °C for annealing. All primers were tested for amplification efficiency using a standard curve, yielding efficiencies of over 95%.

Immunohistochemistry

Brains were sectioned coronally at 35 um using a Leica CM1900 cryostat (Weztler, Germany). Sections were stored in a 0.1% sodium azide 0.01M PB solution at 4 °C. Following sectioning, brains were stained for phosphorylated asyn protein (1:1000; p-ser129; Abcam Catalog # ab59264). Sections were washed for 3 x 5 min in a 0.2% Triton-X 0.01M phosphate buffered saline (PBS-TX) solution then blocked for 30 min in a 0.3% H_2O_2 PBS-TX solution. These sections were then washed for 3 x 10 min in PBS-TX solution then blocked in a 2% Animal Free Blocker (AFB) (Vector) in PBS-TX solution (blocker solution) for 30 min followed by incubation in primary antibody (rabbit-anti-alpha-synuclein AbCam, 1:1000) for 2 days at room temperature. Sections were then washed for 3 x 5 min in PBS-TX solution and incubated for two hr in secondary antibody (biotinylated goat anti-rabbit IgG Catalog # Ab6721, 1:500) made in blocker solution. Sections were then rinsed for 3 x 10 min in PBS-TX followed by a 1 hr incubation in an avidin-biotinylated complex (ABC Elite Kit; Vector Laboratories). Sections were then washed 3 x 10 min in PBS and exposed to 3,3'-Diaminobenzidine (DAB) reaction containing 30% hydrogen peroxide for visualization of HRP. Sections were washed in PBS 3 x 5 min following DAB exposure. All sections were then slide mounted and dried overnight. Sections were then dehydrated using a series of alcohol and Clearene (Leica Biosystems; Catalog # 3803600) washes and sequentially cover-slipped using Paramount.

Results

Asyn Transgene expression differed significantly across genotypes. A preliminary analysis was conducted to determine differences among genotypes with respect to asyn transgene expression. Seven mice were found to be outliers (± 3 SD from the mean) and were not included in the analyses. As depicted in Figure 15 and confirmed by a one-way ANOVA a significant difference was evident among genotypes with respect to transgene expression, $F_{(2,80)} = 13.510$; $p < 0.01$. Tukey's Post-hoc analyses revealed that WT transgene expression was significantly lower than that of the transgene groups ($p < 0.01$), which did not differ from one another ($p = 0.698$). Since the two transgenic groups did not differ from one another with respect to asyn transgene expression they were pooled for all further analyses.

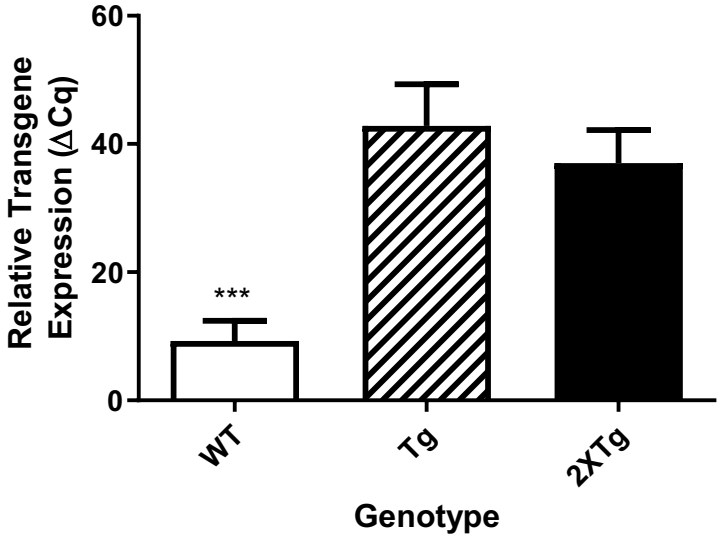

Figure 15: Comparing relative Asyn transgene expression (ΔCq) across genotypes in WT, Tg, and 2XTg in B6;C3-Tg(Prnp-SNCA*A53T)83Vle/J mice. All values represent average ΔCq Values ± SEM. *** $p < 0.01$

PAsyn cellular density significantly increased with age in Tg and WT animals. The cellular density of pAsyn (μm^3) depicted in Figure 15 is reported for wildtype (WT) and pooled transgenic (Tg) mice at 3 to 7 months of age. A 2 (genotype) x 5 (age) ANOVA of pAsyn cellular density revealed a significant effect of age, $F_{(4,78)} = 3.75$ ($p = 0.015$). Tukey's HSD post-hoc analyses indicated that pAsyn cellular density was elevated at 5, 6, and 7 months of age relative to that apparent at 3 months ($p<0.05$). Neither the transgenic manipulation nor the interaction involving this variable was statistically significant.

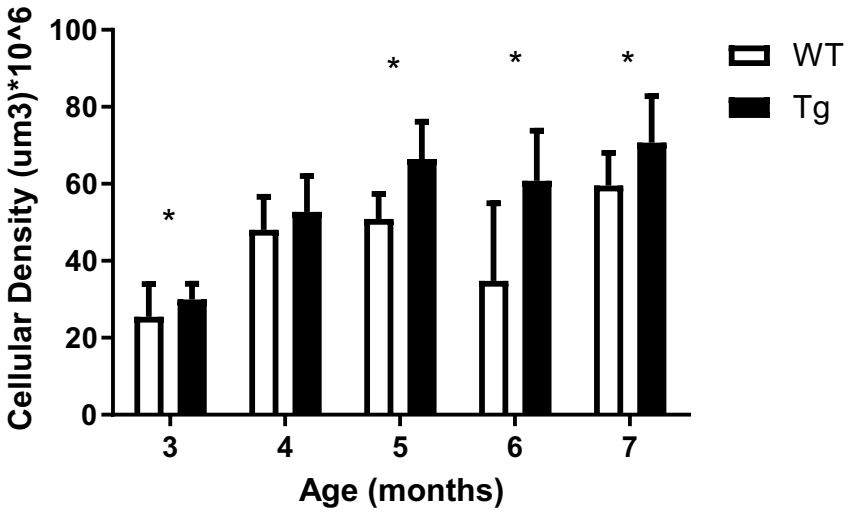

Figure 16: Comparing Asyn Cellular density (μm^3) at different ages (3, 4, 5, 6, and 7 months) in the motor cortex of WT and Tg B6;C3-Tg(Prnp-SNCA*A53T)83Vle/J mice. All values represent average cellular density values ± SEM. * = $p<0.01$ relative to 3-month old animals

The Noldus catwalk provided quantitative data on the run duration (in seconds) of each subject's test trial and the distance between each subject's paws (hind vs front) which is known as the base of support (BOS). A 2 (genotype) x 5 (age) ANOVA was performed for run duration and revealed no significant effects or interactions, as depicted in Figure 17. The BOS revealed a significant effect of age, $F_{(4,78)} = 2.753$ ($p=0.034$). As depicted in Figure 18 a) the front paw base of support increased with age, but Fisher's LSD post-hoc tests indicated that this difference was only statistically significantly between 3 month and 6 month old animals ($p<0.05$). This outcome was not attributable to the inordinately high front paw BOS in wildtype mice as 6 month old Tg mice also exhibited a marked increase in BOS relative to 3 month old animals. A separate 2 (genotype) x 5 (age) ANOVA for the BOS of the hind paws separation revealed no significant effects or interactions.

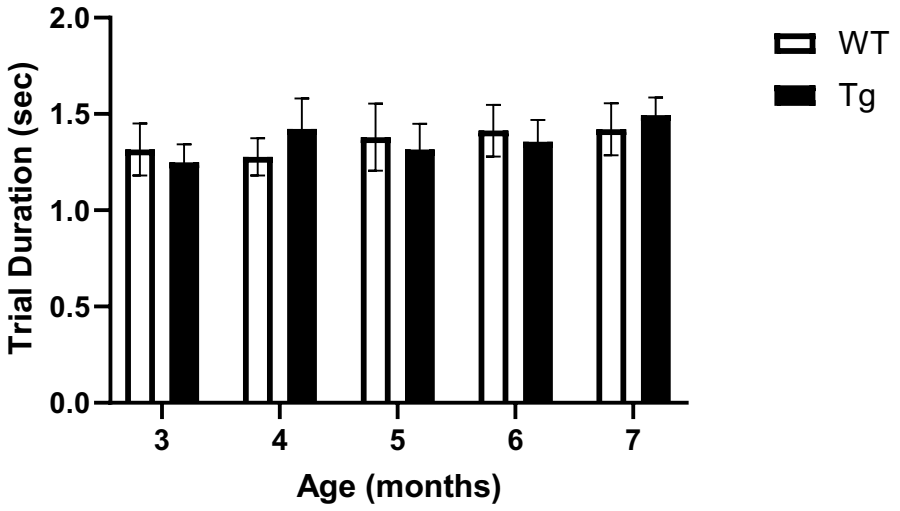

Figure 17: Comparing run duration (in seconds) across ages (3,4,5,6,7 months) for WT and Tg B6;C3-Tg(Prnp-SNCA*A53T)83Vle/J mice. All values represent an average run duration (sec) for each genotype at the specific age indicated ± SEM.

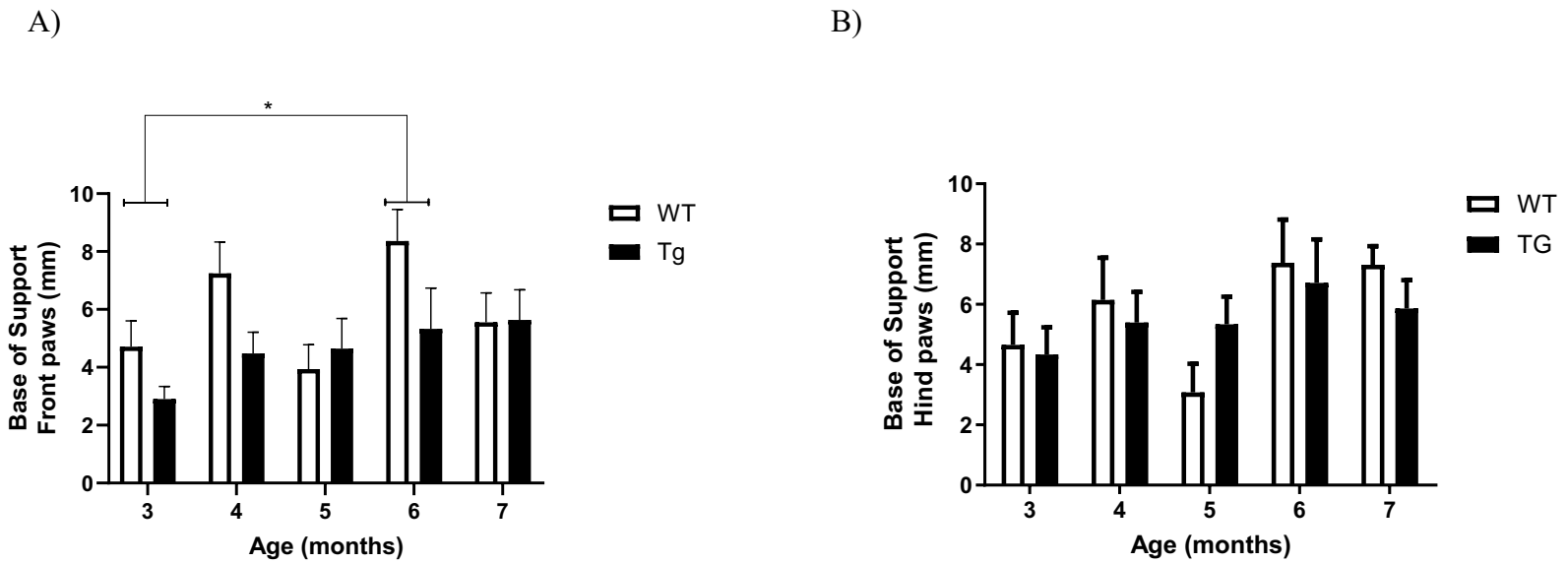

Figure 18: Comparing Base of Support (BOS) across ages (3,4,5,6,7 months) for WT and Tg B6;C3-Tg(Prnp-SNCA*A53T)83Vle/J mice. A) BOS front paws B) BOS hind paws. All values represent an average distance between paws (mm) for each genotype at the specific age indicated. All values represent an average ± SEM. *= $p < 0.05$.

Experiment 3.2

Subjects and general experimental design

Breeding pairs comprising six female mice hemizygous for Tg(SNCA)83Vle (Catalog# 004479) and six male wildtype controls (Catalog# 00101) were obtained at 8-12 weeks of age from The Jackson Laboratory, Bar Harbor, ME. At 10 days following arrival in the laboratory, the female mice B6;C3-Tg(Prnp-SNCA*A53T)83Vle/J mice and the male WT mice were paired for breeding purposes. After weaning, offspring were group-housed (max 4 per home cage) with littermates of the same sex in standard polypropylene cages (27 x 21 x 14 cm) and maintained on a 12 hr light/ dark cycle with lights on at 08:00 hr. A diet of 2014 Purina mouse chow and water was provided *ad libitum* and the room temperature was maintained at ~ 21°C. Of the offspring, both wildtype and hemizygous male mice were weaned at 21 days of age. All procedures were approved by the Carleton University Animal Care Committee and complied with the guidelines set out by the Canadian Council for Use and Care of Animals in Research.

Procedure

At 5 months of age, animals were assigned to one of four experimental groups (i) Control WT (n=12), (ii) Control transgenic mice (n=12), (iii) Transgenic mice that received a single treatment with the asyn binding aptamer (n=12), and (iv) Transgenic mice that received multiple (5) treatments of the asyn aptamer (n=12). Animals in the control treatment groups received a 0.1mL injection of 0.9% saline daily for 5 days. The two treatment groups likewise received a single 0.1mL injection on each of the 5 days between 9:00 hr and 12:00 hr. The single treatment group received the asyn binding

aptamer treatment on the first day followed by saline injections daily on each of the remaining treatment days. Animals in the multiple treatment group received asyn aptamer treatment for each of the 5 consecutive days. All animals were sacrificed by rapid decapitation 7 days following the last injection.

Treatment details

As in the preceding experiments, the asyn aptamer treatment was synthesized and prepared by DeRosa and associates (Chemistry Department, Carleton University). The asyn aptamer was a 66 nucleotide base sequence of single-stranded DNA that had been designed to bind to asyn with high affinity and specificity. The asyn aptamer was modified with a Cy5 label and was encapsulated in a liposome carrier vehicle. As shown previously by Chen et al., the liposome carrier was modified with a DNA transferrin receptor aptamer (TRA) to improve delivery across the BBB [118]. Overall, the aptamer and delivery vehicle consisted of a 38 nanomoles asyn aptamer with 120 nanomoles of transferrin receptor aptamer (TRA). See Table 2 for the specific sequence details.

Table 2: The specific synthesized aptamer sequences used for *in vivo* experiments. Prepared and synthesized by the DeRosa Lab (Carleton University, Ottawa ON).

Name	Sequence (5'→ 3')	Length
ASYN APTAMER -CY5	5' - Cy5- ATA GTC CCA TCA TTC ATT GTA TGG TAC GGC GCG GTG GCG GGT GCG GGG AGA TAT TAG CAA GTG TCA	66
TRA	5' - GAA TTC CGC GTG TGC ACA CGG TCA CAG TTA GTA TCG CTA CGT TCT TTG GTA GTC CGT TCG GGA T	64
SCRAMBLED ASYN APTAMTER	5' - GAT CAT GTA AGT GCG TGA GAG CGA GTA GCT CGA CAC GAA TCA GAA TAC ATT GCC GCT GTG TTA TAA	66

Brain extraction

Following decapitation, brains were extracted and half of the brains from each treatment group was used for Western Blot, and the other half of the brains was used for immunostaining purposes. To collect tissue for Western Blot, brains were quickly excised and placed on a chilled micro-dissecting block that contained slots (0.5mm apart) for single edged razor blades. In this way, after the brain was sliced, micro-punches from coronal sections were taken from the frontal cortex, motor cortex, caudate, and substantia nigra to assess the presence of asyn protein. All region punches were immediately placed on dry ice and stored at -80°C until protein extraction.

The brains collected for immunostaining were post-fixed at 4°C in 4% PFA for 24 hours. The following day brains were placed in a 10% sucrose in 0.1M phosphate-buffered (PB) solution (pH 7.4) twice approximately 6 hours apart and maintained at 4°C between solution changes. Brains were then placed in a 30% sucrose in 0.1M PB solution at 4°C until processing for immunohistochemistry.

Protein Extraction – Western Blot

On the day of extraction, 10 mL of RIPA-like extraction buffer (Fisher, Catalog # P189900) was mixed with one tablet of protease inhibitor cocktail (Roche's Complete Mini EDTA-free cat#1836170). Extraction buffer was added to each sample (150 µL) and brain tissue was sonified. Samples were kept at room temperature for 15 mins and centrifuged for 10 min at 12,000 RPM (13,800G) at 4ºC. The supernatant in each sample tube was removed and the remaining liquid was used to determine protein concentration.

In order to prepare each sample for Western blot analysis, proteins were quantified using Pierce's BCA Protein Assay Kit (ThermoFisher, Catalog# 23227) in a 96 well microplate. Kit instructions were followed and sample quantification was determined using a microplate reader (Molecular Devices, Spectra Max 190) at 540nm.

Samples were preserved in 5X Loading Buffer in a ratio of 4:1. Samples were prepared to concentrations of 10 µg/µL of protein per sample for all brain regions. They were vortexed and heated for 5 min in a heat block set to 105 ºC. After heating, samples were placed on ice for 5 min and stored at -20 ºC until processing for Western blot analyses.

Western Blot

For asyn protein determination, total protein was first determined using a REVERT total protein solution as previously described [67]. Following determination of total protein levels and appropriate washes in tris buffered saline (TBS; pH 7.5; 2 X 5 min each), membranes were blocked for 60 min in a TBS solution containing 0.5% fish gelatin (Sigma). Membranes were then placed in a 0.5% fish gelatin TBS solution

containing either a purified mouse anti-alpha-synuclein (1:2000; Sigma Syn33, Catalog# ABN2265), anti-alpha-synuclein (1:1000; Abcam, Catalog # Ab59264), for a period of 90 min in 0.05% fish gelatin in TBS with 0.1% tween. Following incubation in the primary antibody and subsequent washes in TBS-T, membranes were incubated in infrared conjugate (Rabbit 800, LI-COR) at a concentration of 1:20 000 in a 0.5% fish gelatin TBS solution containing 0.2% tween and 0.01% SDS. Membranes were washed in TBS to remove any unbound antibody, protein bands were read for 6 min on a Licor Odyssy system (ThermoFisher) at the appropriate wavelength.

Results

A one-way ANOVA was conducted for the normalized pAsyn levels within three different brain regions (See Figure 19). These analyses revealed significant treatment effects within the PFC, Caudate, and SNc, F's $_{(3,20)}$ = 4.51, 7.78, and 6.92, p's <0.05, 0.01, 0.01, respectively. Fisher's HSD follow-up tests indicated that within each of the brain regions pAsyn levels were elevated in the control transgenic mice relative to the control wildtype mice. In the PFC, the pAsyn was reduced by the multiple aptamer treatment relative to the control transgenic mice, but this did not occur following a single asyn aptamer treatment. Within both the caudate and SNc, in contrast, the single asyn aptamer treatment reduced pAsyn compared to that evident in the control transgenic mice. In fact, the effects of the single treatment were more pronounced with a single asyn aptamer treatment (not multiple asyn aptamer treatments) in the caudate.

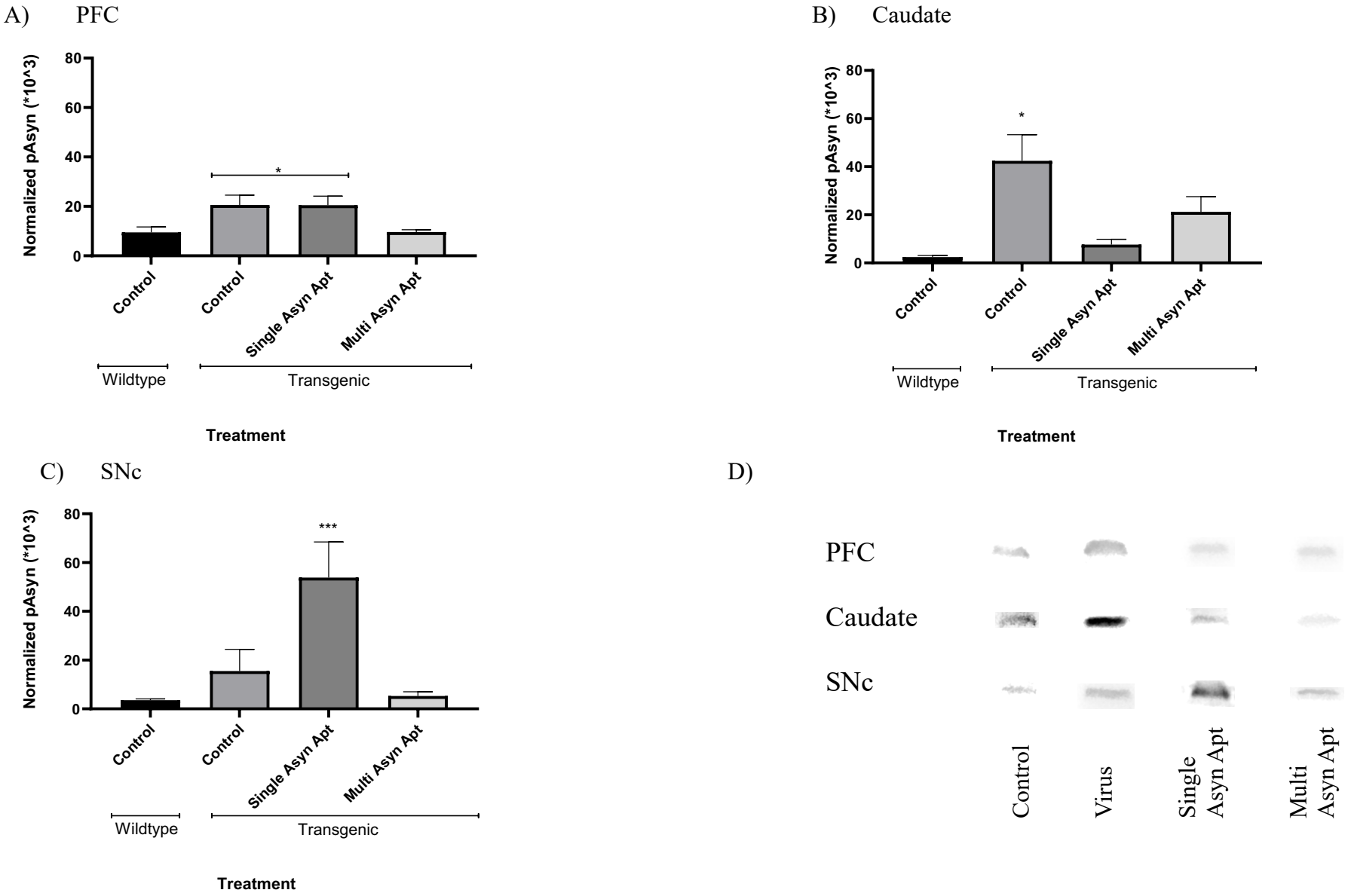

Figure 19: Normalized pAsyn protein levels (x10^3) in the A) Prefrontal cortex (PFC), B) Caudate and C) Substantia Nigra (SNc) and D) representative blots for WT and Tg B6;C3-Tg(Prnp-SNCA*A53T)83Vle/J male mice treated with saline or the asyn binding aptamer (acutely or repeatedly). All values represent an average ± SEM. * denotes that the treatment group(s) are significantly different from all other treatment groups *=$p<0.05$ *** = $p<0.01$

As in the analyses of the pAsyn, a one-way ANOVA was conducted for the normalized Syn33 levels within the three brain regions (See Figure 20). Within the PFC and the Caudate this analysis revealed a significant effect of the treatment, F's $_{(3,20)}$ = 5.35 and 12.40 p's <0.01, and 0.01 respectively. Fisher's HSD follow-up tests indicated that within the PFC a modest non-significant increase in Syn33 levels was evident in the control transgenic mice compared to the control wildtype mice, whereas, in the caudate this difference was statistically significant. Multiple treatments with the asyn aptamer reduced the Syn33 levels relative to the control transgenic mice in both these regions, whereas the single treatment was only effective in reducing Syn33 protein levels in the caudate. In contrast to these brain regions there were no differences between groups within the SNc.

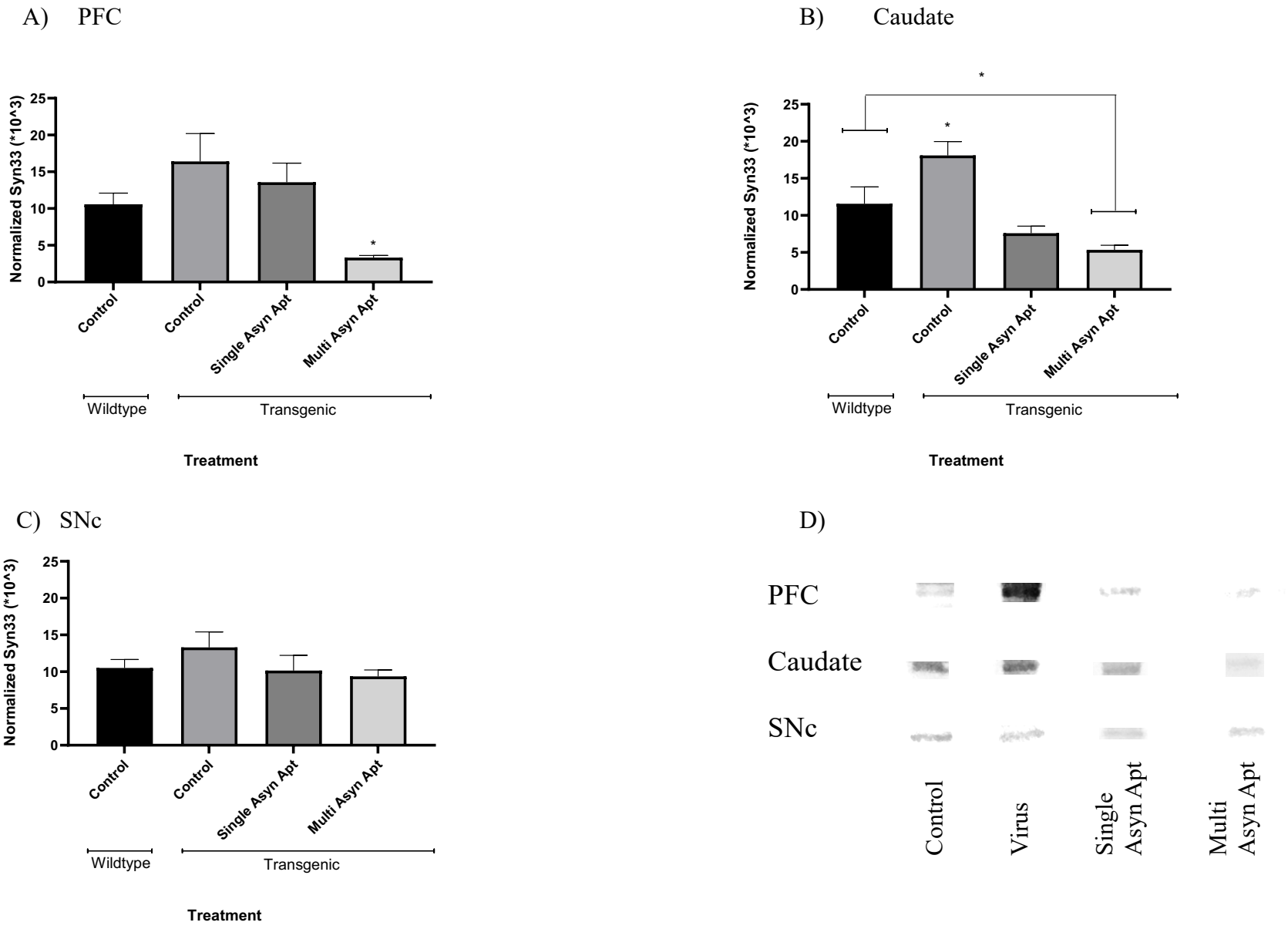

Figure 20: Normalized Syn33 protein levels (x10^3) in the A) Prefrontal cortex (PFC), B) Caudate and C) Substantia Nigra (SNc) and D) representative blots for WT and Tg B6;C3-Tg(Prnp-SNCA*A53T)83Vle/J male mice treated with saline or the asyn binding aptamer (acutely or repeatedly). All values represent an average ± SEM. * = $p<0.05$ *** = $p<0.01$

Discussion

The initial experiments (Experiment 3.1) characterized the transgenic line of mice to determine an appropriate age and therapeutic window for intervention. It was found that there was a significantly different amount of pAsyn when comparing WT to Tg animals at 5 months of age. Additionally, it was determined that there were no statistically different transgene copy numbers among Tg and 2XTg animals and so in further experiments we chose to compare WT vs pooled Tg animals. Based on these experiments it was decided to age the transgenic mice to 5 months and then test the asyn binding aptamer as a treatment to detect changes in toxic asyn species (pAsyn and oligomer asyn (Syn33)) for Experiment 3.2.

There were few significant findings from the catwalk data (trial duration and BOS alterations) and unfortunately it was uncertain whether changes in base of support was due to normal growth with age or were a direct consequence of motor deficits. It is possible that aging the animals beyond 7 months would make the PD phenotype with the atypical motor deficits more apparent. In a subsidiary study (data not shown) in which transgenic animals were observed at 12-14 months of age it was apparent that profound motor deficits occurred in the Tg mice.[2]

The present investigation confirmed that WT mice had lower pAsyn and Syn33 levels than age-matched transgenic animals across all brain regions (PFC, Caudate, and SNc) though these were not always significantly different from one another. The most encouraging finding in this investigation is that animals in the repeated treatment group consistently showed significantly reduced pasyn and oligomer asyn (Syn33) levels

[2] This observation could not be formally quantified owing to restrictions associated with testing during the COVID-19 lockdown.

compared to transgenic control (untreated) mice in all regions apart from in the SNc. Additionally, the repeated treatment group was notably not significantly different from the control WT mice; suggesting the repeated treatment may have rescued these elevated levels of asyn confirmations.

In comparison, the single aptamer treatment group did not reveal many noteworthy changes on asyn protein levels suggesting that multiple treatments with the aptamer may be required to induce substantial protein level changes. Contrary to prediction, the single aptamer treatment in the SNc for pAsyn showed pronounced elevations in pAsyn. This particular Western blot analysis was repeated on 4 separate occasions using the same tissue samples. As such, this outcome could not be attributed to a spurious finding related to the procedure involved. The possibility exists that this finding reflected tissue contamination, although it would be difficult to reconcile why this effect was exclusive to the SNc. Likewise, it could be argued that the increase reflected a compensatory response elicited by an acute challenge, but once more it would be necessary to explain why this action was only present in this single brain region.

Chapter 5: General Discussion

Parkinson's disease has been considered an incurable condition that progresses over the course of several decades, but observable symptoms may not be apparent for several years. In the main, PD symptoms can be diminished by l-DOPA therapy, although its effectiveness diminishes over time, so that within about five years, motor complications reappear [95,96]. Accordingly, alternative strategies have been sought to attenuate symptoms and hopefully to do so for extended times. Similarly, with other treatments, a common theme emerged of worsening motor complications following multiple years of drug therapy [119–123]. In the present investigation, it was possible to visualize the asyn binding aptamer in cells and it was demonstrated *in vitro* that the asyn aptamer did not promote cell death. Furthermore, the aptamer had positive effects in reducing features of PD in a mouse model without apparent immediate adverse effects. After repeated treatments, this novel asyn binding aptamer could reduce levels of pAsyn and oligomer asyn (Syn33) in several brain regions. As mentioned previously, Lewy bodies and Lewy neurites are primarily composed of asyn exhibiting pSer129 post-translational modifications [84,124,125]. This specific modification enhances aggregate formation and reduces degradation [126], whereas its absence increases motor functionality and minimizes aggregate species formation [127]. Thus, the data of the present investigation are consistent with the perspective that the levels of toxic asyn protein may contribute to Parkinsonian symptoms. It remains to be established whether this treatment might also be efficacious in diminishing both motor and non-motor symptoms, whether it could be effective in altering the course of the disorder, and whether tolerance would develop with repeated use.

As much as these findings may facilitate the understanding of mechanisms underlying this neurodegenerative disease, particularly the involvement of the toxic protein asyn, it is undoubtedly necessary to examine in much greater detail the behavioural changes that accompany the molecular variations apparent in transgenic mice. Moreover, it will be essential to evaluate prospectively the long-term benefits of this treatment. Should positive protracted actions be apparent without adverse effects emerging, it might ultimately allow for evaluation of whether the outcomes in mice translate to positive actions in humans.

Despite the potential of aptamers in the treatment of several disorders, this biotechnology has not been widely used. In 2004, the FDA approved pegaptanib sodium, "Macugen", as the first major breakthrough for the clinical use of aptamers [128]. There were indications that Macugen, a vascular endothelial growth factor (VEGF)-binding aptamer, could be used for the treatment of age-related macular degeneration, the leading cause of blindness in people over the age of 50 and has also been shown to promote visual stability in some patients [129]. In addition, there have been indications that an aptamer approach, much like antibody-based manipulations, could potentially be used in cancer immunotherapy [102].

Aptamers are far more appealing than antibodies because of several inherent advantages they possess [130–134]. First, aptamers are selected and synthesized via an *in vitro* process, allowing for a broader range of targets under modifiable conditions. This contrasts with antibodies that are created *in vivo* through much more expensive and complicated procedures involving live animals where their immune system dictates where the antibody interacts. Second, aptamer synthesis reproducibility, limited batch-to-

batch variation, and cost-effective procedures, make aptamers more desirable. Furthermore, the comparative ease of chemical modifications and functionalization variety allows aptamers to be subjected to a greater range of temperature, ionic, and pH environments without being limited to physiological conditions like that of antibodies. Next, aptamers can undergo reversible thermal denaturing and return to their native conformation, allowing for increased stability for extended periods of time. Comparatively, antibodies have a substantially shorter shelf life and often undergo irreversible thermal denaturing when exposed to increased temperature. Finally, aptamers can adopt multiple secondary conformations that contribute to their specific target binding abilities. Conformational adaptations before and after aptamer-target interactions allow aptamers to differentiate between targets and molecules with similar structures without sacrificing their high binding affinity. Due to these unique advantages, aptamers can be utilized as an effective alternative to antibodies in various applications in the areas of drug delivery [135], molecular therapeutics [136], and aptasensor development.

Earlier research attempted to use a similar aptamer approach to develop new diagnostic and therapeutic tools [137]. In particular, this approach was similar to that used by our team to select aptamers for monomeric asyn that could effectively reduce *in vitro* asyn aggregation and target asyn to lysosomal degradation [100,138,139]. This procedure by Zheng *et al*., comprised the design and creation of two different asyn aptamers, F5R1 and F5R2, with respective dissociation constant (K_D) values of 2.40 nM and 3.07 nM [138]. The dissociation constant is a measure of a target concentration in which 50% of aptamers present are bound with the target in an aptamer-target complex [140,141], suggesting that these particular aptamer sequences can readily bind to asyn

monomers and oligomers [138]. Although this may intuitively seem beneficial, in reality, this is problematic since asyn has normal physiological functions. Thus, having the ability to bind to asyn even at low levels might not mimic pathological conditions of PD and could have unintended negative consequences when binding at normal physiological levels of asyn (e.g., by disrupting vesicle release and packaging).

In contrast, the dissociation constant of our asyn binding aptamer was much higher K_D= 70 nM, suggesting that it binds less readily to asyn than the aptamers described earlier [138]. A further advantage of the current procedure stems from the selection process and the design of the asyn aptamer to bind to asyn monomers and prevent fibril formations. In addition, several *in vitro* studies conducted by our collaborators confirmed the specificity and dissociation constants (K_D) of this aptamer when incubated with similar targets to that of asyn (α-synuclein A53T mutant, α-synuclein fibril, β-synuclein, and γ-synuclein) (See Appendix A).

It is important to consider the potential of this unique delivery system in crossing the BBB that consists of endothelial cells that line cerebral capillaries. These cells are fundamental in maintaining the internal microenvironment of the brain and serve as strict regulators of what foreign species can pass through the BBB [142,143]. The large surface area of the brain provides numerous potential exchange sites. This may occur at sites where the barriers are relatively limited, including around the ventricles (e.g., circumventricular organs, such as the organum vasculosum of the lamina terminalis), the median eminence, and the area postrema. As well, both toxins and immune triggers can disrupt BBB functioning, thereby diminishing the integrity of the physical barrier. At the same time, the selective permeability of the BBB poses a significant challenge when

designing therapeutic interventions for brain illnesses since access to the central nervous system is limited [142,143]. There are several routes of entry into the brain through the BBB, including the transcellular pathway directly through the plasma membrane of endothelial cells and the paracellular pathway through channels of adjacent endothelial cells [142,143]. The transcellular pathway employs various modes of diffusion, active transport, and transcytosis to increase the uptake of substances into the brain [142,143]. A variety of different carrier- and receptor-mediated transport systems exist through endothelial cells, resulting in the interest and exploitation of the transferrin receptor to gain access across the BBB [117].

The primary function of transferrin receptors is to mediate the endocytosis of iron into endothelial cells by coupling iron and transferrin [144]. These receptors are present throughout the body; however, the most abundant location of transferrin receptors is along endothelial cells [145]. The fact that transferrin receptors are accessible from the bloodstream has highlighted transferrin receptors as a therapeutic access point for drug delivery. Specifically, DNA and RNA aptamers have been applied as novel delivery approaches [117,118,144]. The initial DNA and RNA mouse transferrin receptor aptamers (TRA) were generated as a way to examine the endocytosis of lysosomal enzymes conjugated with TRA across the BBB [118]. DNA aptamers exhibited greater stability in these *in vitro* investigations relative to the RNA transferrin receptor aptamer [118]. Furthermore, the designed TRA was non-competitive with transferrin-iron complexes, possessed a binding affinity of 0.25 μM, and suggested that TRAs could provide a uniquely effective avenue for transcytosis delivery [118].

Within the field of nanomedicine, liposomes have been used as drug carriers for decades and remains appealing due to their multiple properties as drug delivery vehicles [146–149]. Liposomes are made of multiple phospholipid structures, are ampiphilic, and create an enclosed sphere with two distinct regions when immersed in aqueous solutions [147,148]. The polar phosphate head from groups of phospholipids orient themselves to minimize unfavourable thermodynamic interactions with the solvent, resulting in a hydrophilic core and a lipophilic bilayer that are stabilized through the hydrophobic effect and corresponding van der Waals interactions among its acyl chains. The asyn binding aptamer used in the present investigation was encapsulated in a 20-100 nm liposome and due to its small size was able to penetrate the transferrin receptors.

The asyn aptamer not only demonstrated promising therapeutic potential but could potentially serve as an "aptasensor" for diagnostic purposes. As mentioned earlier, a significant challenge associated with PD is that there is already 60% dopamine neuron loss and 80% dopamine depletion in the SNc at the time of diagnosis [11,27]. As such, having a diagnostic tool able to detect elevated asyn levels far earlier could be a game-changer for early diagnosis and hence disease intervention. Aptasensors function by exploiting aptamers as biorecognition elements to analyze the specific binding event between a target and its selected aptamer. There are several advantages of aptasensors, such as their ability for specific and reproducible detection, continuous data collection, rapid response time, low cost, and ease of experimental preparation, making them inherently attractive for a wide range of experimental procedures [150].

This would certainly require research investments; however, it would be relatively inexpensive and straightforward to print the asyn binding aptamer onto a nitrocellulose

membrane using a Bio dot system. The plasma from animals or patients could be applied to nitrocellulose membrane, which would produce a colour change, indicating whether elevated levels of asyn are present in the blood sample. This method of printing an aptamer onto a nitrocellulose membrane exploits similar mechanisms as pregnancy tests. By developing an asyn aptasensor, an individual showing elevated levels of asyn would be further assessed and monitored for the appearance of other motor and non-motor symptoms related to PD. Of course, this begs the question as to whether early detection of elevated asyn would translate into actionable methods to prevent the development of this neurodegenerative disorder.

Limitations of the present investigation

As much as the data of the present investigation were promising, the number of brain samples assessed was relatively small, and further studies with more samples are clearly called for. Additionally, there was no *a priori* reason to believe that the findings in males and females would be comparable. In fact however, within animal models of other neurodegenerative disorders, such as Alzheimer's disease, very marked sex differences were reported [151]. Of course, this does not imply that this would be the case for Parkinson's disease, but it is known that the disorder occurs more often in males than females, making it that much more important to consider this variable in developing treatment strategies.

In the present investigation, limited attention was devoted to the behavioural changes that accompanied this model of Parkinson's disease and the effects of the aptamer in ameliorating these symptoms. As the disease is typically diagnosed based on behavioural

signs, it is essential for more detailed analyses to be conducted to more closely approximate the diverse behavioural features evident in humans. In considering the usefulness of animal models, it was also suggested that it is necessary to document whether treatments that are effective in humans are also effective in an animal model and ascertain whether treatments that are ineffective in humans are equally ineffective in animals [152]. In the case of the transgenic model used in the present investigation, it is uncertain whether its validity meets these fundamental requirements. The model was selected based on earlier studies that had pointed to the parallel to human pathophysiology that focused on elevated asyn underlying PD [74,115,127,153], but this may not map on nicely to the behavioural profile that accompanies these biological disturbances. As a result, it is still necessary to determine the validity of this model more extensively, and it would be profitable to assess the effectiveness of the aptamer in other PD models.

Unfortunately, this investigation was also unable to accurately develop a dose-response for the asyn aptamer. Given that all *in vivo* experiments had the aptamer administered interperitoneally, it was difficult to determine the exact dose of asyn aptamer that crossed the BBB and the amount that remained in the periphery. Furthermore, it is possible that the amount of aptamer that had been loaded into each liposome varied somewhat, but there was no way of this being determined. This said, this variation would most likely be relatively insignificant in relation to its effects on brain functioning. Relatedly, all mice, irrespective of their weight received a constant dose of the aptamer. The possibility exists that in leaner animals, the amount of asyn aptamer that

reached the brain could differ from that of heavier animals. This possibility cannot be excluded and could be a source of within-group variance.[3]

Now that it has been confirmed that systemic administration of the asyn aptamer reaches the central nervous system, an appropriate next step may be to develop a dose-response curve based on intercranial injections to determine the amount of aptamer in the brain that would be needed to produce meaningful behavioural changes. Of course, treatment in humans would ideally occur through systemic administration. Knowing the approximate ratio of systemically administered aptamer and that which appears in the brain might provide information that will enable the development of procedures appropriate for human trials. This is not to say that the effects in mice are readily translatable to humans but nevertheless provide a reasonable starting point.

Parkinson's disease is often accompanied by cognitive disturbances, sleep disorders, and gastrointestinal disturbances. Thus, it is possible that an aptamer treatment could diminish motor symptoms that accompany Parkinson's disease without necessarily influencing the cognitive or neurovegetative features that so often accompany the disorder [154–156]. Accordingly, it would be advantageous to assess some of these non-motor disturbances and whether they are altered, preferably improved, following administration of the asyn aptamer. Nevertheless, even if the effects of the asyn aptamer were restricted to modifying motor symptoms, this would be highly advantageous and most certainly would enhance the quality of life among patients.

[3] The conditions under which these experiments were conducted were admittedly not ideal. Owing to ongoing construction issues within the laboratories, testing different animal cohorts in varied locations was necessary. On the surface, this might seem trivial, but it is known that even subtle changes within laboratory environments can profoundly influence behavioural outcomes within strains of inbred mice [157].

Summary and conclusions

The underpinnings of Parkinson's disease are fairly well established and methods have been devised to limit symptoms of the disorder. As tolerance develops to the effects of these treatments, alternative therapeutic methods have been sought. The use of aptamers to bind to asyn may be an effective alternative to current drug treatments. The present investigation demonstrated that systemic administration of an asyn aptamer gains access to the brain, where it reduced pAsyn and oligomer asyn following repeated treatments. Accordingly, it may represent an early step in developing a treatment strategy to diminish symptoms of the disorder and could potentially be used as a diagnostic tool to predict the later development of the disorder. Unquestionably, before it can be used in either capacity, considerable research is necessary to evaluate the safety, tolerability, and efficacy of this approach and whether tolerance would develop with sustained use over extended periods of time.

APPENDIX A:

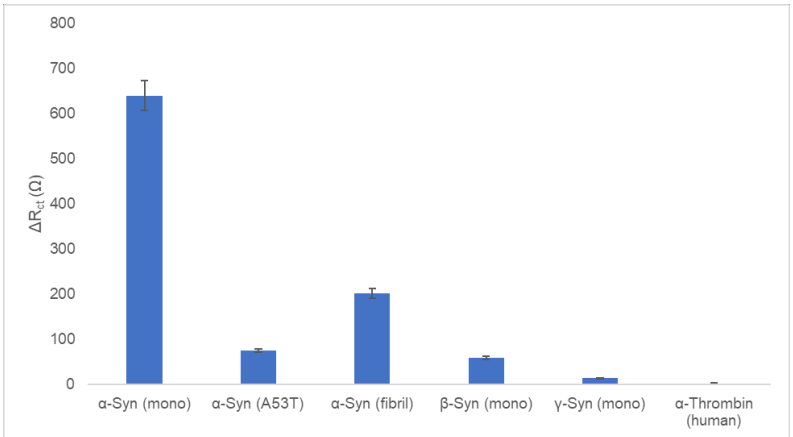

Figure 3. 19: Selectivity of ASYN2 aptasensor in the presence of 1 μM of the respective targets. ASYN2 retained high affinity for monomeric forms of α-synuclein while showing unexpectedly low affinity for the A53T mutant variant.

*(Taken directly from SPENCER BOISJOLI (Chemistry Collaborator) MSc Thesis with permission)

Supplementary Documents:

Approval for AUP # 109155
Use of Adenovirus to overexpress alpha-synuclein in Parkinson's Disease cellular models.
(Experiment 1.1 – 1.6)

Carleton University Biohazards Committee Approval of New Application

The Carleton University Biohazards Committee has examined and approved the biohazards application.
As part of the Tri-Council compliance procedures, research projects must be reviewed and renewed annually and this process is conducted by the Research Office each year during the summer in advance of the August 31st deadline. You will be notified by e-mail in advance of this deadline.

Researcher: Shawn Hayley & Matthew Holahan
Department: Faculty of Science\Neuroscience (Department of)
University: Carleton University
Title of Project: Use of Adenovirus to overexpress immune and Parkinson's disease linked proteins in cellular models.
Start Date: August 01, 2018
Next Renewal Date: August 15, 2019
Expiry Date: August 01, 2021
Funding (if applicable):

Awards File No	Title	Status	
108427	mGluR5 modulation as a neuro-recovery strategy for Parkinson's disease	Active	CORIS Awards

Approval for AUP # 107929
Pharmacokinetics of novel alpha-synuclein aptamers in non-transgenic mice (Experiment 2.1)

Carleton University Animal Care Committee
Ethics Clearance Form: New application

This is to certify that the Carleton University Animal Care Committee has examined the application for ethical clearance. The Committee found the research project to meet the appropriate ethical standards as outlined in the CCAC Guide to the Care and Use of Experimental Animals and policies set up by the Tri-Council, Ethical Review of Research Involving Animals.

Researcher: Matthew Holahan
Department: Faculty of Science\Neuroscience (Department of)

Protocol #: 107929
Title of Project: Pharmacokinetics of novel alpha-synuclein aptamers in non-transgenic mice
Start Date: October 15, 2017
Next Renewal Date: October 15, 2018

Expiry Date: Oct 15, 2018
Awarded Funding (if applicable):

Awards File No	Title	Status	
102314	Utilization of aptamers as therapeutic tools to prevent protein aggregation in Parkinson's disease	Completed	CURO Awards
107734	Pharmokinetic study of alpha synuclein-binding aptamers	Submitted	CURO Awards

All researchers are governed by the following conditions:

Annual review form: You are required to submit an Annual Review Form to the Animal Care Committee at least one month prior to the expiry date. (This can be completed through the Researcher Portal.) Failure to submit the required document will result in the immediate suspension of the project by the Carleton University Research Office. Funded projects will have accounts suspended until the report is submitted and approved.

Amendments: Any changes to the project must be submitted to the Animal Care Committee through an amendment form, available through the Researcher Portal. All changes must be approved prior to the continuance of the research.

Suspension or termination of approval: Failure to conduct the research in accordance with the principles of the CCAC and the Carleton University Animal Care Committee may result in the suspension or termination of the research project.

Approval for AUP # 103009

(Experiment 3.1 & 3.2)

Carleton University Animal Care Committee Ethics Clearance Form: New application

This is to certify that the Carleton University Animal Care Committee has examined the application for ethical clearance. The Committee found the research project to meet the appropriate ethical standards as outlined in the CCAC Guide to the Care and Use of Experimental Animals and policies set up by the Tri-Council, Ethical Review of Research Involving Animals.

Researcher: Matthew Holahan
Department: Faculty of Arts and Social Sciences\Psychology (Department of)

Title of Project: Breeding protocol for alpha-synuclein transgenic mice.
Start Date: May 27, 2015
Next Renewal Date: May 27, 2016

Expiry Date: May 27, 2017
Awarded Funding (if applicable):

Awards File No	Title	Status	
102314	Utilization of aptamers as therapeutic tools to prevent protein aggregation in Parkinson's disease	Active	CURO Awards

All researchers are governed by the following conditions:

Annual review form: You are required to submit an Annual Review Form to the Animal Care Committee at least one month prior to the expiry date. (This can be completed through the Researcher Portal.) Failure to submit the required document will result in the immediate suspension of the project by the Carleton University Research Office. Funded projects will have accounts suspended until the report is submitted and approved.

Amendments: Any changes to the project must be submitted to the Animal Care Committee through an amendment form, available through the Researcher Portal. All changes must be approved prior to the continuance of the research.

Suspension or termination of approval: Failure to conduct the research in accordance with the principles of the CCAC and the Carleton University Animal Care Committee may result in the suspension or termination of the research project.

Approval for AUP #104390

(Experiment 3.1)

Carleton University Animal Care Committee
Ethics Clearance Form: New application

This is to certify that the Carleton University Animal Care Committee has examined the application for ethical clearance. The Committee found the research project to meet the appropriate ethical standards as outlined in the CCAC Guide to the Care and Use of Experimental Animals and policies set up by the Tri-Council, Ethical Review of Research Involving Animals.

Researcher: Matthew Holahan
Department: Faculty of Science\Neuroscience (Department of)

Protocol #: 104390
Title of Project: Longitudinal behavioral and neuropathological assessment of transgenic alpha-synuclein mice
Start Date: April 29, 2016
Next Renewal Date: April 15, 2017

Expiry Date: April 27, 2018
Awarded Funding (if applicable):

Awards File No	Title	Status	
102314	Utilization of aptamers as therapeutic tools to prevent protein aggregation in Parkinson's disease	Active	CURO Awards

All researchers are governed by the following conditions:

Annual review form: You are required to submit an Annual Review Form to the Animal Care Committee at least one month prior to the expiry date. (This can be completed through the Researcher Portal.) Failure to submit the required document will result in the immediate suspension of the project by the Carleton University Research Office. Funded projects will have accounts suspended until the report is submitted and approved.

Amendments: Any changes to the project must be submitted to the Animal Care Committee through an amendment form, available through the Researcher Portal. All changes must be approved prior to the continuance of the research.

Suspension or termination of approval: Failure to conduct the research in accordance with the principles of the CCAC and the Carleton University Animal Care Committee may result in the suspension or termination of the research project.

Approval for AUP # 112227

(Experiment 3.2)

Carleton University Animal Care Committee
Ethics Clearance Form: New application

This is to certify that the Carleton University Animal Care Committee has examined the application for ethical clearance. The Committee found the research project to meet the appropriate ethical standards as outlined in the CCAC Guide to the Care and Use of Experimental Animals and policies set up by the Tri-Council, Ethical Review of Research Involving Animals.

Researcher: Matthew Holahan
Department: Faculty of Science\Neuroscience (Department of)

Protocol #: 112227
Title of Project: Using Asyn Binding Aptamer in 5 month old mice to assess changes in asyn protein following treatment
Start Date: March 02, 2020
Next Renewal Date: September 15, 2020

Expiry Date: August 31, 2020
Awarded Funding (if applicable):

Awards File No	Title	Status	
109555	Utilization of a DNA aptamer to assess the *in vitro* and *in vivo* aggregation properties of alpha-synuclein.	Active	A. CORIS Awards

All researchers are governed by the following conditions:

Annual review form: You are required to submit an Annual Review Form to the Animal Care Committee at least one month prior to the expiry date. (This can be completed through the Researcher Portal.) Failure to submit the required document will result in the immediate suspension of the project by the Carleton University Research Office. Funded projects will have accounts suspended until the report is submitted and approved.

Amendments: Any changes to the project, including additional animals from those approved, must be submitted to the Animal Care Committee through an amendment form, available through the Researcher Portal. All changes must be approved prior to the continuance of the research.

Suspension or termination of approval: Failure to conduct the research in accordance with the principles of the CCAC and the Carleton University Animal Care Committee may result in the suspension or termination of the research project.

References

[1] Merchant KM, Cedarbaum JM, Brundin P, Dave KD, Eberling J, Espay AJ, et al. A Proposed Roadmap for Parkinson's Disease Proof of Concept Clinical Trials Investigating Compounds Targeting Alpha-Synuclein. J Parkinsons Dis 2018:1–31. https://doi.org/10.3233/JPD-181471.

[2] Berg D, Postuma RB, Adler CH, Bloem BR, Chan P, Dubois B, et al. MDS research criteria for prodromal Parkinson's disease. Mov Disord 2015;30:1600–11. https://doi.org/10.1002/mds.26431.

[3] Wong SL, Gilmour H, Ramage-Morin PL. Parkinson's disease: Prevalence, diagnosis and impact. Heal Reports 2014;25:10–4.

[4] Benge JF, Roberts RL, Kekecs Z, Elkins G. Brief Report: Knowledge of, Interest in, and Willingness to Try Behavioral Interventions in Individuals With Parkinson's Disease. Adv Mind Body Med n.d.;32:8–12.

[5] GBD 2016 Parkinson's Disease Collaborators. Global, regional, and national burden of Parkinson's disease, 1990-2016: a systematic analysis for the Global Burden of Disease Study 2016. Lancet Neurol 2018;17:939–53. https://doi.org/10.1016/S1474-4422(18)30295-3.

[6] Dorsey ER, Sherer T, Okun MS, Bloem BR. The Emerging Evidence of the Parkinson Pandemic. J Parkinsons Dis 2018;8:S3–8. https://doi.org/10.3233/JPD-181474.

[7] Kalinderi K, Bostantjopoulou S, Fidani L. The genetic background of Parkinson's disease: current progress and future prospects. Acta Neurol Scand 2016;134:314–26. https://doi.org/10.1111/ane.12563.

[8] Poewe W, Seppi K, Tanner CM, Halliday GM, Brundin P, Volkmann J, et al. Parkinson disease. Nat Rev Dis Prim 2017;3:17013. https://doi.org/10.1038/nrdp.2017.13.

[9] Gazewood JD, Richards DR, Clebak K. Parkinson disease: an update. Am Fam Physician 2013;87:267–73.

[10] Postuma RB, Berg D, Adler CH, Bloem BR, Chan P, Deuschl G, et al. The new definition and diagnostic criteria of Parkinson's disease. Lancet Neurol 2016;15:546–8. https://doi.org/10.1016/S1474-4422(16)00116-2.

[11] Dauer W, Przedborski S. Parkinson's disease: mechanisms and models. Neuron 2003;39:889–909.

[12] Carlsson A, Lindqvist M, Magnusson T. 3,4-Dihydroxyphenylalanine and 5-hydroxytryptophan as reserpine antagonists. Nature 1957;180:1200. https://doi.org/10.1038/1801200a0.

[13] Bedarf JR, Hildebrand F, Goeser F, Bork P, Wüllner U. Das Darmmikrobiom bei der Parkinson-Krankheit. Nervenarzt 2019;90:160–6. https://doi.org/10.1007/s00115-018-0601-6.

[14] Mukherjee A, Biswas A, Das SK. Gut dysfunction in Parkinson's disease. World J Gastroenterol 2016;22:5742. https://doi.org/10.3748/wjg.v22.i25.5742.

[15] Schapira AH V, Chaudhuri KR, Jenner P. Non-motor features of Parkinson disease. Nat Rev Neurosci 2017;18:435–50. https://doi.org/10.1038/nrn.2017.62.

[16] Ferrer I. Neuropathology and Neurochemistry of Nonmotor Symptoms in Parkinson's Disease. Parkinsons Dis 2011;2011:1–13. https://doi.org/10.4061/2011/708404.

[17] Prell T. Structural and Functional Brain Patterns of Non-Motor Syndromes in Parkinson's Disease. Front Neurol 2018;9. https://doi.org/10.3389/fneur.2018.00138.

[18] Jankovic J. Parkinson's disease: clinical features and diagnosis. J Neurol Neurosurg Psychiatry 2008;79:368–76. https://doi.org/10.1136/jnnp.2007.131045.

[19] Magrinelli F, Picelli A, Tocco P, Federico A, Roncari L, Smania N, et al. Pathophysiology of Motor Dysfunction in Parkinson's Disease as the Rationale for Drug Treatment and Rehabilitation. Parkinsons Dis 2016;2016:1–18. https://doi.org/10.1155/2016/9832839.

[20] Mazzoni P, Shabbott B, Cortes JC. Motor Control Abnormalities in Parkinson's Disease. Cold Spring Harb Perspect Med 2012;2:a009282–a009282. https://doi.org/10.1101/cshperspect.a009282.

[21] Bridi JC, Hirth F. Mechanisms of α-Synuclein Induced Synaptopathy in Parkinson's Disease. Front Neurosci 2018;12. https://doi.org/10.3389/fnins.2018.00080.

[22] Postuma RB, Berg D, Stern M, Poewe W, Olanow CW, Oertel W, et al. MDS clinical diagnostic criteria for Parkinson's disease. Mov Disord 2015;30:1591–601. https://doi.org/10.1002/mds.26424.

[23] Gibb WR, Lees AJ. The relevance of the Lewy body to the pathogenesis of idiopathic Parkinson's disease. J Neurol Neurosurg Psychiatry 1988;51:745–52. https://doi.org/10.1136/jnnp.51.6.745.

[24] Marsili L, Rizzo G, Colosimo C. Diagnostic Criteria for Parkinson's Disease: From James Parkinson to the Concept of Prodromal Disease. Front Neurol

2018;9:156. https://doi.org/10.3389/fneur.2018.00156.

[25] Goetz CG, Tilley BC, Shaftman SR, Stebbins GT, Fahn S, Martinez-Martin P, et al. Movement Disorder Society-sponsored revision of the Unified Parkinson's Disease Rating Scale (MDS-UPDRS): Scale presentation and clinimetric testing results. Mov Disord 2008;23:2129–70. https://doi.org/10.1002/mds.22340.

[26] Riederer P, Wuketich S. Time course of nigrostriatal degeneration in parkinson's disease. A detailed study of influential factors in human brain amine analysis. J Neural Transm 1976;38:277–301. https://doi.org/10.1007/BF01249445.

[27] Cheng H-C, Ulane CM, Burke RE. Clinical progression in Parkinson disease and the neurobiology of axons. Ann Neurol 2010;67:715–25. https://doi.org/10.1002/ana.21995.

[28] Schapira AHV. Neurobiology and treatment of Parkinson's disease. Trends Pharmacol Sci 2009;30:41–7. https://doi.org/10.1016/j.tips.2008.10.005.

[29] Cookson MR, Hardy J, Lewis PA. Genetic neuropathology of Parkinson's disease. Int J Clin Exp Pathol 2008;1:217–31.

[30] Wakabayashi K, Tanji K, Odagiri S, Miki Y, Mori F, Takahashi H. The Lewy body in Parkinson's disease and related neurodegenerative disorders. Mol Neurobiol 2013;47:495–508. https://doi.org/10.1007/s12035-012-8280-y.

[31] Volpicelli-Daley LA, Gamble KL, Schultheiss CE, Riddle DM, West AB, Lee VM-Y. Formation of α-synuclein Lewy neurite-like aggregates in axons impedes the transport of distinct endosomes. Mol Biol Cell 2014;25:4010–23. https://doi.org/10.1091/mbc.E14-02-0741.

[32] McKeith IG, Galasko D, Kosaka K, Perry EK, Dickson DW, Hansen LA, et al.

Consensus guidelines for the clinical and pathologic diagnosis of dementia with Lewy bodies (DLB): report of the consortium on DLB international workshop. Neurology 1996;47:1113–24. https://doi.org/10.1212/wnl.47.5.1113.

[33] Braak H, Braak E. Pathoanatomy of Parkinson's disease. J Neurol 2000;247 Suppl:II3-10. https://doi.org/10.1007/PL00007758.

[34] Vekrellis K, Xilouri M, Emmanouilidou E, Rideout HJ, Stefanis L. Pathological roles of α-synuclein in neurological disorders. Lancet Neurol 2011;10:1015–25. https://doi.org/10.1016/S1474-4422(11)70213-7.

[35] Noyce AJ, Lees AJ, Schrag A-E. The prediagnostic phase of Parkinson's disease. J Neurol Neurosurg Psychiatry 2016;87:871–8. https://doi.org/10.1136/jnnp-2015-311890.

[36] Rietdijk CD, Perez-Pardo P, Garssen J, van Wezel RJA, Kraneveld AD. Exploring Braak's Hypothesis of Parkinson's Disease. Front Neurol 2017;8. https://doi.org/10.3389/fneur.2017.00037.

[37] Braak H, Tredici K Del, Rüb U, de Vos RA., Jansen Steur EN., Braak E. Staging of brain pathology related to sporadic Parkinson's disease. Neurobiol Aging 2003;24:197–211. https://doi.org/10.1016/S0197-4580(02)00065-9.

[38] Visanji NP, Brooks PL, Hazrati L-N, Lang AE. The prion hypothesis in Parkinson's disease: Braak to the future. Acta Neuropathol Commun 2013;1:2. https://doi.org/10.1186/2051-5960-1-2.

[39] Vasili E, Dominguez-Meijide A, Outeiro TF. Spreading of α-Synuclein and Tau: A Systematic Comparison of the Mechanisms Involved. Front Mol Neurosci 2019;12. https://doi.org/10.3389/fnmol.2019.00107.

[40] Ordonez DG, Lee MK, Feany MB. α-synuclein Induces Mitochondrial Dysfunction through Spectrin and the Actin Cytoskeleton. Neuron 2018;97:108-124.e6. https://doi.org/10.1016/j.neuron.2017.11.036.

[41] Prots I, Grosch J, Brazdis R-M, Simmnacher K, Veber V, Havlicek S, et al. α-Synuclein oligomers induce early axonal dysfunction in human iPSC-based models of synucleinopathies. Proc Natl Acad Sci 2018;115:7813–8. https://doi.org/10.1073/pnas.1713129115.

[42] Braak H, Alafuzoff I, Arzberger T, Kretzschmar H, Del Tredici K. Staging of Alzheimer disease-associated neurofibrillary pathology using paraffin sections and immunocytochemistry. Acta Neuropathol 2006;112:389–404. https://doi.org/10.1007/s00401-006-0127-z.

[43] Braak H, Del Tredici K. Neuropathological Staging of Brain Pathology in Sporadic Parkinson's disease: Separating the Wheat from the Chaff. J Parkinsons Dis 2017;7:S71–85. https://doi.org/10.3233/JPD-179001.

[44] Kumari P, Ghosh D, Vanas A, Fleischmann Y, Wiegand T, Jeschke G, et al. Structural insights into α-synuclein monomer–fibril interactions. Proc Natl Acad Sci 2021;118:e2012171118. https://doi.org/10.1073/pnas.2012171118.

[45] Kordower JH, Chu Y, Hauser RA, Freeman TB, Olanow CW. Lewy body–like pathology in long-term embryonic nigral transplants in Parkinson's disease. Nat Med 2008;14:504–6. https://doi.org/10.1038/nm1747.

[46] Kordower JH, Chu Y, Hauser RA, Olanow CW, Freeman TB. Transplanted dopaminergic neurons develop PD pathologic changes: A second case report. Mov Disord 2008;23:2303–6. https://doi.org/10.1002/mds.22369.

[47] Kurowska Z, Englund E, Widner H, Lindvall O, Li J-Y, Brundin P. Signs of Degeneration in 12–22-Year Old Grafts of Mesencephalic Dopamine Neurons in Patients with Parkinson's Disease. J Parkinsons Dis 2011;1:83–92. https://doi.org/10.3233/JPD-2011-11004.

[48] Del Tredici K, Rüb U, De Vos RAI, Bohl JRE, Braak H. Where does parkinson disease pathology begin in the brain? J Neuropathol Exp Neurol 2002;61:413–26. https://doi.org/10.1093/jnen/61.5.413.

[49] King E, Thomas A. Systemic Inflammation in Lewy Body Diseases. Alzheimer Dis Assoc Disord 2017;31:346–56. https://doi.org/10.1097/WAD.0000000000000211.

[50] WHO. Neurological disorders: a public health approach. Neurol Disord Public Heal Challenges 2006:40–110. https://doi.org/10.1037/e521482010-002.

[51] Brooks DJ. Imaging approaches to Parkinson disease. J Nucl Med 2010;51:596–609. https://doi.org/10.2967/jnumed.108.059998.

[52] Young CB, Reddy V, Sonne J. Neuroanatomy, Basal Ganglia. 2020.

[53] DeLong MR, Alexander GE, Georgopoulos AP, Crutcher MD, Mitchell SJ, Richardson RT. Role of basal ganglia in limb movements. Hum Neurobiol 1984;2:235–44.

[54] Calabresi P, Picconi B, Tozzi A, Ghiglieri V, Di Filippo M. Direct and indirect pathways of basal ganglia: a critical reappraisal. Nat Neurosci 2014;17:1022–30. https://doi.org/10.1038/nn.3743.

[55] Ghiglieri V, Calabrese V, Calabresi P. Alpha-Synuclein: From Early Synaptic Dysfunction to Neurodegeneration. Front Neurol 2018;9.

https://doi.org/10.3389/fneur.2018.00295.

[56] Hikosaka O, Kim HF, Amita H, Yasuda M, Isoda M, Tachibana Y, et al. Direct and indirect pathways for choosing objects and actions. Eur J Neurosci 2019;49:637–45. https://doi.org/10.1111/ejn.13876.

[57] E. Fernandez-Espejo and I. Liste. Cell-based Replacement Therapies for Parkinson's Disease. Cortico-Subcortical Dyn. Park. Dis., 2009, p. 405–31. https://doi.org/10.1007/978-1-60327-252-0.

[58] McGregor MM, Nelson AB. Circuit Mechanisms of Parkinson's Disease. Neuron 2019;101:1042–56. https://doi.org/10.1016/j.neuron.2019.03.004.

[59] Deleidi M, Gasser T. The role of inflammation in sporadic and familial Parkinson's disease. Cell Mol Life Sci 2013;70:4259–73. https://doi.org/10.1007/s00018-013-1352-y.

[60] Cannon JR, Greenamyre JT. Gene-environment interactions in Parkinson's disease: specific evidence in humans and mammalian models. Neurobiol Dis 2013;57:38–46. https://doi.org/10.1016/j.nbd.2012.06.025.

[61] Litteljohn D, Mangano E, Clarke M, Bobyn J, Moloney K, Hayley S. Inflammatory mechanisms of neurodegeneration in toxin-based models of Parkinson's disease. Parkinsons Dis 2010;2011:713517. https://doi.org/10.4061/2011/713517.

[62] Noyce AJ, Bestwick JP, Silveira-Moriyama L, Hawkes CH, Giovannoni G, Lees AJ, et al. Meta-analysis of early nonmotor features and risk factors for Parkinson disease. Ann Neurol 2012;72:893–901. https://doi.org/10.1002/ana.23687.

[63] Jagmag SA, Tripathi N, Shukla SD, Maiti S, Khurana S. Evaluation of Models of

Parkinson's Disease. Front Neurosci 2016;9. https://doi.org/10.3389/fnins.2015.00503.

[64] Siegel GJ, Agranoff BW, Albers RW et al. Basic neurochemistry: molecular, cellular and medical aspects. 6th ed. Philadelphia: Lippincott-Raven; 1999.

[65] Klein C, Westenberger A. Genetics of Parkinson's disease. Cold Spring Harb Perspect Med 2012;2:a008888. https://doi.org/10.1101/cshperspect.a008888.

[66] Goedert M, Spillantini MG, Del Tredici K, Braak H. 100 years of Lewy pathology. Nat Rev Neurol 2013;9:13–24. https://doi.org/10.1038/nrneurol.2012.242.

[67] Rudyk C, Dwyer Z, Hayley S, CLINT membership. Leucine-rich repeat kinase-2 (LRRK2) modulates paraquat-induced inflammatory sickness and stress phenotype. J Neuroinflammation 2019;16:120. https://doi.org/10.1186/s12974-019-1483-7.

[68] Lev N, Roncevic D, Roncevich D, Ickowicz D, Melamed E, Offen D. Role of DJ-1 in Parkinson's disease. J Mol Neurosci 2006;29:215–25. https://doi.org/10.1385/jmn:29:3:215.

[69] Stefanis L. -Synuclein in Parkinson's Disease. Cold Spring Harb Perspect Med 2012;2:a009399–a009399. https://doi.org/10.1101/cshperspect.a009399.

[70] Kruger R, Kuhn W, Leenders KL, Sprengelmeyer R, Muller T, Woitalla D, et al. Familial parkinsonism with synuclein pathology: Clinical and PET studies of A30P mutation carriers. Neurology 2001;56:1355–62. https://doi.org/10.1212/WNL.56.10.1355.

[71] Spillantini MG, Goedert M. Neurodegeneration and the ordered assembly of α-synuclein. Cell Tissue Res 2018;373:137–48. https://doi.org/10.1007/s00441-017-

2706-9.

[72] Maries E, Dass B, Collier TJ, Kordower JH, Steece-Collier K. The role of α-synuclein in Parkinson's disease: insights from animal models. Nat Rev Neurosci 2003;4:727–38. https://doi.org/10.1038/nrn1199.

[73] Ikeuchi T, Kakita A, Shiga A, Kasuga K, Kaneko H, Tan C-F, et al. Patients Homozygous and Heterozygous for SNCA Duplication in a Family With Parkinsonism and Dementia. Arch Neurol 2008;65:514. https://doi.org/10.1001/archneur.65.4.514.

[74] Spillantini MG, Schmidt ML, Lee VM-Y, Trojanowski JQ, Jakes R, Goedert M. α-Synuclein in Lewy bodies. Nature 1997;388:839–40. https://doi.org/10.1038/42166.

[75] Volpicelli-Daley LA, Standaert DG. Invisible Killers. Mov Disord 2016;31:44. https://doi.org/10.1002/mds.26465.

[76] Gracia P, Camino JD, Volpicelli-Daley L, Cremades N. Multiplicity of α-Synuclein Aggregated Species and Their Possible Roles in Disease. Int J Mol Sci 2020;21. https://doi.org/10.3390/ijms21218043.

[77] Xu L, Bhattacharya S, Thompson D. On the ubiquity of helical α-synuclein tetramers. Phys Chem Chem Phys 2019;21:12036–43. https://doi.org/10.1039/c9cp02464f.

[78] Ruf VC, Nübling GS, Willikens S, Shi S, Schmidt F, Levin J, et al. Different Effects of α-Synuclein Mutants on Lipid Binding and Aggregation Detected by Single Molecule Fluorescence Spectroscopy and ThT Fluorescence-Based Measurements. ACS Chem Neurosci 2019;10:1649–59.

https://doi.org/10.1021/acschemneuro.8b00579.

[79] Dettmer U. Rationally Designed Variants of α-Synuclein Illuminate Its *in vivo* Structural Properties in Health and Disease. Front Neurosci 2018;12. https://doi.org/10.3389/fnins.2018.00623.

[80] Alam P, Bousset L, Melki R, Otzen DE. α-synuclein oligomers and fibrils: a spectrum of species, a spectrum of toxicities. J Neurochem 2019;150:522–34. https://doi.org/10.1111/jnc.14808.

[81] Blauwendraat C, Heilbron K, Vallerga CL, Bandres-Ciga S, von Coelln R, Pihlstrøm L, et al. Parkinson's disease age at onset genome-wide association study: Defining heritability, genetic loci, and α-synuclein mechanisms. Mov Disord 2019;34:866–75. https://doi.org/10.1002/mds.27659.

[82] Anderson JP, Walker DE, Goldstein JM, de Laat R, Banducci K, Caccavello RJ, et al. Phosphorylation of Ser-129 Is the Dominant Pathological Modification of α-Synuclein in Familial and Sporadic Lewy Body Disease. J Biol Chem 2006;281:29739–52. https://doi.org/10.1074/jbc.M600933200.

[83] Covy JP, Yuan W, Waxman EA, Hurtig HI, Van Deerlin VM, Giasson BI. Clinical and pathological characteristics of patients with Leucine-rich repeat kinase-2 mutations. Mov Disord 2009;24:32–9. https://doi.org/10.1002/mds.22096.

[84] Fujiwara H, Hasegawa M, Dohmae N, Kawashima A, Masliah E, Goldberg MS, et al. alpha-Synuclein is phosphorylated in synucleinopathy lesions. Nat Cell Biol 2002;4:160–4. https://doi.org/10.1038/ncb748.

[85] Taguchi K, Watanabe Y, Tsujimura A, Tanaka M. Expression of α-synuclein is regulated in a neuronal cell type-dependent manner. Anat Sci Int 2019;94:11–22.

https://doi.org/10.1007/s12565-018-0464-8.

[86] Logan T, Bendor J, Toupin C, Thorn K, Edwards RH. α-Synuclein promotes dilation of the exocytotic fusion pore. Nat Neurosci 2017;20:681–9. https://doi.org/10.1038/nn.4529.

[87] Fitzgerald E, Murphy S, Martinson HA. Alpha-Synuclein Pathology and the Role of the Microbiota in Parkinson's Disease. Front Neurosci 2019;13. https://doi.org/10.3389/fnins.2019.00369.

[88] Calo L, Wegrzynowicz M, Santivañez-Perez J, Grazia Spillantini M. Synaptic failure and α-synuclein. Mov Disord 2016;31:169–77. https://doi.org/10.1002/mds.26479.

[89] Garcia-Reitböck P, Anichtchik O, Bellucci A, Iovino M, Ballini C, Fineberg E, et al. SNARE protein redistribution and synaptic failure in a transgenic mouse model of Parkinson's disease. Brain 2010;133:2032–44. https://doi.org/10.1093/brain/awq132.

[90] Teravskis PJ, Covelo A, Miller EC, Singh B, Martell-Martínez HA, Benneyworth MA, et al. A53T Mutant Alpha-Synuclein Induces Tau-Dependent Postsynaptic Impairment Independently of Neurodegenerative Changes. J Neurosci 2018;38:9754–67. https://doi.org/10.1523/JNEUROSCI.0344-18.2018.

[91] Nemani VM, Lu W, Berge V, Nakamura K, Onoa B, Lee MK, et al. Increased expression of alpha-synuclein reduces neurotransmitter release by inhibiting synaptic vesicle reclustering after endocytosis. Neuron 2010;65:66–79. https://doi.org/10.1016/j.neuron.2009.12.023.

[92] Alabi AA, Tsien RW. Perspectives on Kiss-and-Run: Role in Exocytosis,

Endocytosis, and Neurotransmission. Annu Rev Physiol 2013;75:393–422. https://doi.org/10.1146/annurev-physiol-020911-153305.

[93] Bartels T, Ahlstrom LS, Leftin A, Kamp F, Haass C, Brown MF, et al. The N-terminus of the intrinsically disordered protein α-synuclein triggers membrane binding and helix folding. Biophys J 2010;99:2116–24. https://doi.org/10.1016/j.bpj.2010.06.035.

[94] Stolzenberg E, Berry D, Yang D, Lee EY, Kroemer A, Kaufman S, et al. A Role for Neuronal Alpha-Synuclein in Gastrointestinal Immunity. J Innate Immun 2017;9:456–63. https://doi.org/10.1159/000477990.

[95] Jankovic J, Aguilar LG. Current approaches to the treatment of Parkinson's disease. Neuropsychiatr Dis Treat 2008;4:743–57. https://doi.org/10.2147/ndt.s2006.

[96] The Lancet Neurology. Building on 50 years of levodopa therapy. Lancet Neurol 2016;15:1. https://doi.org/10.1016/S1474-4422(15)00349-X.

[97] Birkmayer W. Hornykiewicz O. [The L-3,4-dioxyphenylalanine (DOPA)-effect in Parkinson-akinesia]. Wien Klin Wochenschr 1961;73:787–8.

[98] Connolly BS, Lang AE. Pharmacological Treatment of Parkinson Disease. JAMA 2014;311:1670. https://doi.org/10.1001/jama.2014.3654.

[99] Hauser RA, LeWitt PA, Comella CL. On demand therapy for Parkinson's disease patients: Opportunities and choices. Postgrad Med 2021:1–7. https://doi.org/10.1080/00325481.2021.1936087.

[100] Ruscito A, DeRosa MC. Small-Molecule Binding Aptamers: Selection Strategies, Characterization, and Applications. Front Chem 2016;4.

https://doi.org/10.3389/fchem.2016.00014.

[101] Tuerk C, Gold L. Systematic evolution of ligands by exponential enrichment: RNA ligands to bacteriophage T4 DNA polymerase. Science (80-) 1990;249:505–10. https://doi.org/10.1126/science.2200121.

[102] Zhou G, Wilson G, Hebbard L, Duan W, Liddle C, George J, et al. Aptamers: A promising chemical antibody for cancer therapy. Oncotarget 2016;7:13446–63. https://doi.org/10.18632/oncotarget.7178.

[103] Xicoy H, Wieringa B, Martens GJM. The SH-SY5Y cell line in Parkinson's disease research: a systematic review. Mol Neurodegener 2017;12:10. https://doi.org/10.1186/s13024-017-0149-0.

[104] Biedler JL, Helson L, Spengler BA. Morphology and growth, tumorigenicity, and cytogenetics of human neuroblastoma cells in continuous culture. Cancer Res 1973;33:2643–52.

[105] Xie H, Hu L, Li G. SH-SY5Y human neuroblastoma cell line: *in vitro* cell model of dopaminergic neurons in Parkinson's disease. Chin Med J (Engl) 2010;123:1086–92.

[106] Takahashi T, Deng Y, Maruyama W, Dostert P, Kawai M, Naoi M. Uptake of a neurotoxin-candidate, (R)-1,2-dimethyl-6,7-dihydroxy-1,2,3,4-tetrahydroisoquinoline into human dopaminergic neuroblastoma SH-SY5Y cells by dopamine transport system. J Neural Transm Gen Sect 1994;98:107–18.

[107] Shipley MM, Mangold CA, Szpara ML. Differentiation of the SH-SY5Y Human Neuroblastoma Cell Line. J Vis Exp 2016. https://doi.org/10.3791/53193.

[108] Agholme L, Lindström T, Kågedal K, Marcusson J, Hallbeck M. An *in vitro* model

for neuroscience: differentiation of SH-SY5Y cells into cells with morphological and biochemical characteristics of mature neurons. J Alzheimers Dis 2010;20:1069–82. https://doi.org/10.3233/JAD-2010-091363.

[109] Kovalevich J, Langford D. Considerations for the use of SH-SY5Y neuroblastoma cells in neurobiology. Methods Mol Biol 2013;1078:9–21. https://doi.org/10.1007/978-1-62703-640-5_2.

[110] Påhlman S, Ruusala AI, Abrahamsson L, Mattsson ME, Esscher T. Retinoic acid-induced differentiation of cultured human neuroblastoma cells: a comparison with phorbolester-induced differentiation. Cell Differ 1984;14:135–44.

[111] Ross RA, Spengler BA, Biedler JL. Coordinate morphological and biochemical interconversion of human neuroblastoma cells. J Natl Cancer Inst 1983;71:741–7.

[112] Encinas M, Iglesias M, Liu Y, Wang H, Muhaisen A, Ceña V, et al. Sequential treatment of SH-SY5Y cells with retinoic acid and brain-derived neurotrophic factor gives rise to fully differentiated, neurotrophic factor-dependent, human neuron-like cells. J Neurochem 2000;75:991–1003.

[113] Henrich MT, Geibl FF, Lee B, Chiu W-H, Koprich JB, Brotchie JM, et al. A53T-α-synuclein overexpression in murine locus coeruleus induces Parkinson's disease-like pathology in neurons and glia. Acta Neuropathol Commun 2018;6:39. https://doi.org/10.1186/s40478-018-0541-1.

[114] Polymeropoulos MH. Mutation in the -Synuclein Gene Identified in Families with Parkinson's Disease. Science (80-) 1997;276:2045–7. https://doi.org/10.1126/science.276.5321.2045.

[115] Luk KC, Lee VM-Y. Modeling Lewy pathology propagation in Parkinson's

disease. Parkinsonism Relat Disord 2014;20 Suppl 1:S85-7. https://doi.org/10.1016/S1353-8020(13)70022-1.

[116] Lashuel HA, Overk CR, Oueslati A, Masliah E. The many faces of α-synuclein: from structure and toxicity to therapeutic target. Nat Rev Neurosci 2013;14:38–48. https://doi.org/10.1038/nrn3406.

[117] McConnell EM, Ventura K, Dwyer Z, Hunt V, Koudrina A, Holahan MR, et al. In Vivo Use of a Multi-DNA Aptamer-Based Payload/Targeting System To Study Dopamine Dysregulation in the Central Nervous System. ACS Chem Neurosci 2019;10:371–83. https://doi.org/10.1021/acschemneuro.8b00292.

[118] Chen CB, Dellamaggiore KR, Ouellette CP, Sedano CD, Lizadjohry M, Chernis GA, et al. Aptamer-based endocytosis of a lysosomal enzyme. Proc Natl Acad Sci U S A 2008;105:15908–13. https://doi.org/10.1073/pnas.0808360105.

[119] Freitas ME, Hess CW, Fox SH. Motor Complications of Dopaminergic Medications in Parkinson's Disease. Semin Neurol 2017;37:147–57. https://doi.org/10.1055/s-0037-1602423.

[120] Parkinson Study Group CALM Cohort Investigators. Long-term effect of initiating pramipexole vs levodopa in early Parkinson disease. Arch Neurol 2009;66:563–70. https://doi.org/10.1001/archneur.66.1.nct90001.

[121] Bressman S, Saunders-Pullman R. When to Start Levodopa Therapy for Parkinson's Disease. N Engl J Med 2019;380:389–90. https://doi.org/10.1056/NEJMe1814611.

[122] PD Med Collaborative Group, Gray R, Ives N, Rick C, Patel S, Gray A, et al. Long-term effectiveness of dopamine agonists and monoamine oxidase B

inhibitors compared with levodopa as initial treatment for Parkinson's disease (PD MED): a large, open-label, pragmatic randomised trial. Lancet (London, England) 2014;384:1196–205. https://doi.org/10.1016/S0140-6736(14)60683-8.

[123] Olanow CW, Watts RL, Koller WC. An algorithm (decision tree) for the management of Parkinson's disease (2001): treatment guidelines. Neurology 2001;56:S1–88. https://doi.org/10.1212/wnl.56.suppl_5.s1.

[124] Nishie M, Mori F, Fujiwara H, Hasegawa M, Yoshimoto M, Iwatsubo T, et al. Accumulation of phosphorylated alpha-synuclein in the brain and peripheral ganglia of patients with multiple system atrophy. Acta Neuropathol 2004;107:292–8. https://doi.org/10.1007/s00401-003-0811-1.

[125] Sato H, Arawaka S, Hara S, Fukushima S, Koga K, Koyama S, et al. Authentically Phosphorylated -Synuclein at Ser129 Accelerates Neurodegeneration in a Rat Model of Familial Parkinson's Disease. J Neurosci 2011;31:16884–94. https://doi.org/10.1523/JNEUROSCI.3967-11.2011.

[126] Smith WW, Margolis RL, Li X, Troncoso JC, Lee MK, Dawson VL, et al. Alpha-synuclein phosphorylation enhances eosinophilic cytoplasmic inclusion formation in SH-SY5Y cells. J Neurosci 2005;25:5544–52. https://doi.org/10.1523/JNEUROSCI.0482-05.2005.

[127] Lee K-W, Chen W, Junn E, Im J-Y, Grosso H, Sonsalla PK, et al. Enhanced phosphatase activity attenuates α-synucleinopathy in a mouse model. J Neurosci 2011;31:6963–71. https://doi.org/10.1523/JNEUROSCI.6513-10.2011.

[128] Proske D, Blank M, Buhmann R, Resch A. Aptamers—basic research, drug development, and clinical applications. Appl Microbiol Biotechnol 2005;69:367–

74. https://doi.org/10.1007/s00253-005-0193-5.

[129] Zampros I, Praidou A, Brazitikos P, Ekonomidis P, Androudi S. Antivascular Endothelial Growth Factor Agents for Neovascular Age-Related Macular Degeneration. J Ophthalmol 2012;2012:1–12. https://doi.org/10.1155/2012/319728.

[130] Jayasena SD. Aptamers: an emerging class of molecules that rival antibodies in diagnostics. Clin Chem 1999;45:1628–50.

[131] Dollins CM, Nair S, Sullenger BA. Aptamers in immunotherapy. Hum Gene Ther 2008;19:443–50. https://doi.org/10.1089/hum.2008.045.

[132] Song S, Wang L, Li J, Fan C, Zhao J. Aptamer-based biosensors. TrAC Trends Anal Chem 2008;27:108–17. https://doi.org/10.1016/j.trac.2007.12.004.

[133] Song K-M, Lee S, Ban C. Aptamers and Their Biological Applications. Sensors 2012;12:612–31. https://doi.org/10.3390/s120100612.

[134] Tombelli S, Minunni M, Mascini M. Analytical applications of aptamers. Biosens Bioelectron 2005;20:2424–34. https://doi.org/10.1016/j.bios.2004.11.006.

[135] McGinely NL, Plumb JA, Wheate NJ. DNA-based aptamer fails as a simultaneous cancer targeting agent and drug delivery vehicle for a phenanthroline-based platinum(II) complex. J Inorg Biochem 2013;128:124–30. https://doi.org/10.1016/j.jinorgbio.2013.07.021.

[136] Brody EN, Gold L. Aptamers as therapeutic and diagnostic agents. J Biotechnol 2000;74:5–13. https://doi.org/10.1016/s1389-0352(99)00004-5.

[137] Tsukakoshi K, Harada R, Sode K, Ikebukuro K. Screening of DNA aptamer which binds to α-synuclein. Biotechnol Lett 2010;32:643–8.

https://doi.org/10.1007/s10529-010-0200-5.

[138] Zheng Y, Qu J, Xue F, Zheng Y, Yang B, Chang Y, et al. Novel DNA Aptamers for Parkinson's Disease Treatment Inhibit α-Synuclein Aggregation and Facilitate its Degradation. Mol Ther - Nucleic Acids 2018;11:228–42. https://doi.org/10.1016/j.omtn.2018.02.011.

[139] McKeague M, McConnell EM, Cruz-Toledo J, Bernard ED, Pach A, Mastronardi E, et al. Analysis of *In Vitro* Aptamer Selection Parameters. J Mol Evol 2015;81:150–61. https://doi.org/10.1007/s00239-015-9708-6.

[140] Jing M, Bowser MT. Methods for measuring aptamer-protein equilibria: a review. Anal Chim Acta 2011;686:9–18. https://doi.org/10.1016/j.aca.2010.10.032.

[141] Kastritis PL, Bonvin AMJJ. On the binding affinity of macromolecular interactions: daring to ask why proteins interact. J R Soc Interface 2013;10:20120835. https://doi.org/10.1098/rsif.2012.0835.

[142] Abbott NJ, Patabendige AAK, Dolman DEM, Yusof SR, Begley DJ. Structure and function of the blood-brain barrier. Neurobiol Dis 2010;37:13–25. https://doi.org/10.1016/j.nbd.2009.07.030.

[143] Abbott NJ, Rönnbäck L, Hansson E. Astrocyte-endothelial interactions at the blood-brain barrier. Nat Rev Neurosci 2006;7:41–53. https://doi.org/10.1038/nrn1824.

[144] Pardridge WM. Drug transport across the blood–brain barrier. J Cereb Blood Flow Metab 2012;32:1959–72. https://doi.org/10.1038/jcbfm.2012.126.

[145] Jefferies WA, Brandon MR, Hunt S V, Williams AF, Gatter KC, Mason DY. Transferrin receptor on endothelium of brain capillaries. Nature n.d.;312:162–3.

https://doi.org/10.1038/312162a0.

[146] Bangham AD, Standish MM, Watkins JC. Diffusion of univalent ions across the lamellae of swollen phospholipids. J Mol Biol 1965;13:238–52. https://doi.org/10.1016/s0022-2836(65)80093-6.

[147] Pattni BS, Chupin V V, Torchilin VP. New Developments in Liposomal Drug Delivery. Chem Rev 2015;115:10938–66. https://doi.org/10.1021/acs.chemrev.5b00046.

[148] Gao W, Hu C-MJ, Fang RH, Zhang L. Liposome-like Nanostructures for Drug Delivery. J Mater Chem B 2013;1. https://doi.org/10.1039/C3TB21238F.

[149] Sercombe L, Veerati T, Moheimani F, Wu SY, Sood AK, Hua S. Advances and Challenges of Liposome Assisted Drug Delivery. Front Pharmacol 2015;6:286. https://doi.org/10.3389/fphar.2015.00286.

[150] Sassolas A, Blum LJ, Leca-Bouvier BD. Electrochemical Aptasensors. Electroanalysis 2009;21:1237–50. https://doi.org/10.1002/elan.200804554.

[151] Abd-Elrahman KS, Albaker A, de Souza JM, Ribeiro FM, Schlossmacher MG, Tiberi M, et al. Aβ oligomers induce pathophysiological mGluR5 signaling in Alzheimer's disease model mice in a sex-selective manner. Sci Signal 2020;13:eabd2494. https://doi.org/10.1126/scisignal.abd2494.

[152] Anisman H, Matheson K. Stress, depression, and anhedonia: caveats concerning animal models. Neurosci Biobehav Rev 2005;29:525–46. https://doi.org/10.1016/j.neubiorev.2005.03.007.

[153] Volpicelli-Daley LA, Luk KC, Patel TP, Tanik SA, Riddle DM, Stieber A, et al. Exogenous α-synuclein fibrils induce Lewy body pathology leading to synaptic

dysfunction and neuron death. Neuron 2011;72:57–71. https://doi.org/10.1016/j.neuron.2011.08.033.

[154] Wang Y-X, Zhao J, Li D-K, Peng F, Wang Y, Yang K, et al. Associations between cognitive impairment and motor dysfunction in Parkinson's disease. Brain Behav 2017;7:e00719. https://doi.org/10.1002/brb3.719.

[155] Poletti M, Frosini D, Pagni C, Baldacci F, Nicoletti V, Tognoni G, et al. Mild cognitive impairment and cognitive-motor relationships in newly diagnosed drug-naive patients with Parkinson's disease. J Neurol Neurosurg Psychiatry 2012;83:601–6. https://doi.org/10.1136/jnnp-2011-301874.

[156] Domellöf ME, Elgh E, Forsgren L. The relation between cognition and motor dysfunction in drug-naive newly diagnosed patients with Parkinson's disease. Mov Disord 2011;26:2183–9. https://doi.org/10.1002/mds.23814.

[157] Crabbe JC, Wahlsten D, Dudek BC. Genetics of mouse behavior: interactions with laboratory environment. Science 1999;284:1670–2. https://doi.org/10.1126/science.284.5420.1670.